Evaluation of Building Wireless Performance for Indoor Networks with Device-to-device Communication and Extremely Large Aperture Arrays

Jixuan Lin

Department of Electronic and Electrical Engineering

University of Sheffield

Supervisors: Prof. Jie Zhang, Prof. Lee Ford

This thesis is submitted for the approval of the

Doctor of Philosophy

September 2023

This thesis is dedicated to my beloved parents. Without their unconditional love, encouragement and support, I would not be the person I am today.

Acknowledgements

First of all, I would like to thank my supervisor, Prof. Jie Zhang, for his consistent guidance. He has not only helped me with my research, but has been educating me on how to become an independent person. I will always remember what he taught me. I am also thankful to my second supervisor, Prof. Lee Ford. He provided me a lot of valuable advice for my academic training.

I would like to thank Dr. Jiliang Zhang and Dr. Haonan Hu. They were always there to help me every time I had a question. Their passion for academics has deeply influenced me.

I would also like to thank Mr. Yan Jiang, Mr. Zeyang Li, Mr Songjiang Yang and Mr. Gang Yu. Their encouragement and support for me help me complete my PHD studies. Hope you all have a wonderful future!

Abstract

The performance of indoor wireless networks is affected by the indoor wireless propagation environment. If wireless networks are deployed in unsuitable rooms or buildings, the performance of the network will be significantly constrained. This issue will become increasingly acute because the data traffic demand is predicted to boost by up to 1000× in the next decade with over 80% occurring indoors. To solve this looming problem, future indoor wireless networks should actively provide guidance on the design and construction of future wireless-friendly buildings instead of passively adapting to the built environment.

To design and construct wireless-friendly buildings, building wireless performance (BWP), an intrinsic building property used to measure the wireless-friendliness of buildings to wireless networks, must be evaluated to provide quantitative guidance for architects. However, the existing concept of BWP is still in its infancy, and the related research is not comprehensive. The existing theoretical system related to the BWP evaluation lacks sufficient evaluation metrics and corresponding evaluation methods to deal with different indoor network architectures and various indoor communication requirements. Therefore, to promote the perfection of the BWP evaluation theoretical system, this thesis investigates the BWP evaluation based on several wireless networks that are likely to be widely deployed in indoor scenarios in the beyond 5G (B5G) and even 6G era.

Firstly, the first systematic BWP evaluation approach for indoor D2D networks is proposed. Considering that room walls can block out-of-room interference to improve the SINR and coverage performance, a metric named blockage gain was proposed for the BWP evaluation. The blockage gain is defined as the spatially averaged coverage probability (SACP) improvement due to the out-of-room interference blockage by the room walls. The

theoretical upper and lower bounds of SACP are derived, and the empirical formulas for the fast calculation of the SACP and the blockage gain are obtained by function fitting based on them. The results indicate that the impacts of building layouts and building materials on the blockage gain can be decoupled. Moreover, numerical results show that well-designed rooms can improve the SACP of the indoor D2D network by at least 0.1.

Secondly, a BWP evaluation approach for indoor extremely large aperture array (ELAA) networks is proposed. Considering that the performance of indoor ELAA systems is impacted by indoor blockages, the achievable power gain is adopted as the BWP evaluation metric to measure the impact of indoor blockages on the total power received by the user from the ELAA. Then, an algorithm to calculate the achievable power gain for an arbitrary building layout and placement of indoor blockages is proposed. The BWP evaluation approach was applied for an example room, and a room modification scheme was provided for a higher BWP. Numerical results show that the room modification scheme can achieve a 13% spatially averaged power gain improvement compared with the original building design.

Thirdly, D2D relay technology is combined with indoor ELAA networks to enhance the coverage of the ELAA in indoor scenarios, and a BWP evaluation approach based on such indoor relay-assisted ELAA network is proposed. The coverage rate is adopted as the metric for the BWP evaluation and an algorithm to obtain the coverage rate with arbitrary building layouts is provided. Numerical results show that only a very low transmit power is required for D2D relays to provide a sufficient coverage rate, and in this case, increasing the number of potential relays can achieve a higher coverage rate than increasing the transmit power of relays. By analyzing the impact of building layouts on the spatially averaged coverage rate, it is illustrated that the loss of spatially averaged coverage rate due to unsuitable building design exceeds 34%, which demonstrates that the performance of indoor wireless networks will suffer a great loss in unsuitable buildings.

List of publications

Submitted

J. Lin, H. Hu, J. Zhang, J. Zhang “Evaluation of Building Wireless Performance for Indoor Device-to-Device Networks," has been submitted as the major revision response to *IEEE Transactions in Vehicular Technology* on Sep. 3rd, 2023. (Chapter 3)

J. Lin, H. Hu, J. Zhang, J. Zhang “Building Wireless Performance Evaluation for Indoor Extremely Large Aperture Array Networks," has been submitted to *IEEE Wireless Communication Letters* on Jun. 18th, 2023. (Chapter 4)

Table of contents

List of figures

List of tables

Abbreviations

AoV Angle of View

AR Aspect Ratio

B5G Beyond Fifth Generation

BPP Binomial Point Process

BS Base Station

BWP Building Wireless Performance

CB Conjugate Beamforming

CDF Cumulative Distribution Function

CSI Channel State Information

D2D Device-to-Device

EB Exabytes

EE Energy Efficiency

ELAA Extremely Large Aperture Array

5G Fifth Generation

IG Interference Gain

IoT Internet of Things

LEP Logarithmic Eigenvalue Product

LES Logarithmic Eigenvalue Summation

LoS Line-of-Sight

MBS Macro Base Station

MIMO Multi-Input-Multi-Output

MMSE Minimum Mean Square Error

mmWave Millimeter Wave

NLoS Non-line-of-sight

PDF Probability Density Function

PG Power Gain

PGFL Probability Generating Functional

PMF Probability Mass Function

PPP Poisson Point Process

QoS Quality of Service

RMS Root Mean Square

SACP Spatially Averaged Coverage Probability

SBS Small Base Station

SCN Small Cell Network

SE Spectral Efficiency

6G Sixth Generation

SINR Signal-to-noise-plus-interference-Ratio

SIR Signal-to-interference Ratio

SNR Signal-to-noise Ratio

2D Two-Dimensional

3D Three-dimensional

UE User Equipment

VR Visibility Region

URA Uniform Rectangular Array

ZF Zero Forcing

Chapter 1

Introduction

Overview

The performance of indoor wireless networks is inevitably affected by the building environment. The performance will be severely constrained if wireless networks are deployed in unsuitable buildings. To address this problem fundamentally, buildings should be designed and constructed based on wireless network requirements. This idea has led to the birth of the conceptions of wireless-friendly buildings and building wireless performance (BWP). This thesis focuses on the evaluation of BWP based on several wireless networks that are likely to be widely deployed in indoor scenarios in the future.

In this chapter, the background of the research is introduced first. Then, the motivations and contributions are discussed. Finally, the structure of the thesis is presented.

1.1 Background

1.1.1 Requirements of B5G communications

The development of wireless communication technologies and the proliferation of wirelessly connected devices has provided convenience to people's daily lives and changed people's lifestyle. This change has resulted in a significant growth in the demand for wireless

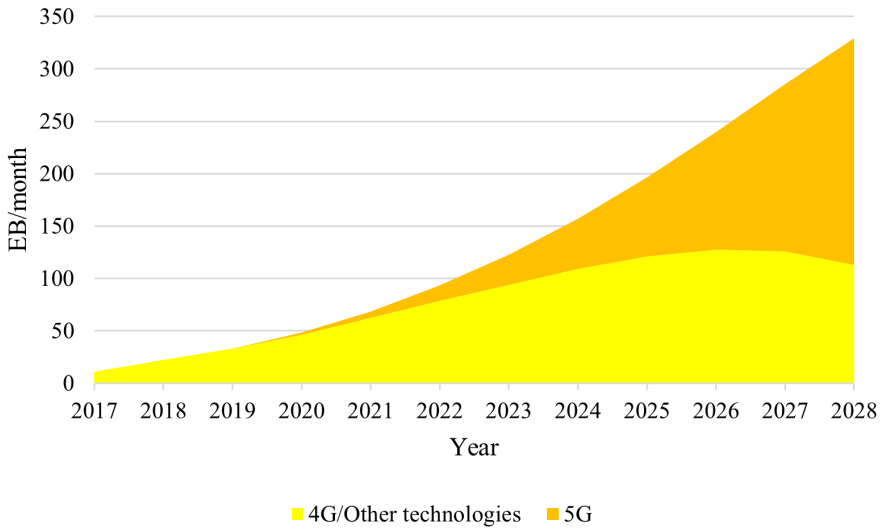

Fig. 1.1 Global mobile data traffic growth trend by Ericsson [Source: Ericsson mobility report, June 2023].

communications, bringing new challenges for the upcoming beyond fifth-generation (B5G) wireless communication systems.

The mobile data traffic has been experiencing a tremendous growth recently as the wireless communication system gradually evolves from 5G to the beyond 5G (B5G) era. According to Ericsson's statistics [2], global mobile data traffic has already reached 93 exabytes (EB) per month in 2022 and is predicted to reach 329 EB per month by 2028, achieving a 3.5-fold increase in the next five years as shown in Fig. 1.1. On the other hand, the total number of connected devices grew from 14.2 billion in 2017 to 23.5 billion in 2022 and is predicted to grow to 45.7 billion in the next five years, as shown in Fig. 1.2. This exponential growth trend illustrates the growing demand for mobile data traffic, which will be increasingly challenging to meet with conventional wireless communication technologies.

A range of emerging wireless communication applications also place more diverse requirements on B5G wireless communication systems [3]. For instance, virtual reality, augmented reality and holographic teleconferencing demand not only high data rates, with a downlink peak rate over 1 Tbit/s, but also a latency less than 0.1 ms for real-time voices. Additionally, the tactile Internet of Things (IoT) require massive connectivity between a large number of densely deployed sensors and devices. In intelligent driving scenarios,

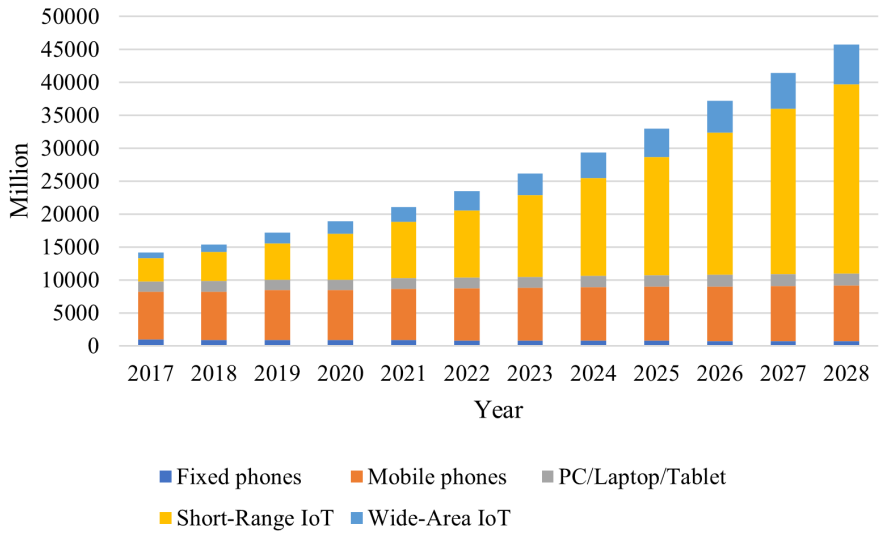

Fig. 1.2 Trends in the number of connectable devices globally by Ericsson [Source: Ericsson mobility report, June 2023].

which involve applications such as path planning, obstacle detection, vehicle monitoring and emergency rescue control, both high data rate, low latency and massive connectivity should be provided in high-speed mobility scenarios [4]. Compared with conventional wireless technologies, the B5G wireless communication system is demanded to provide multi-dimensional Quality of Services (QoS) for mobile users.

Consequently, wireless communication systems in the B5G era should not only meet the increasing demand for mobile data traffic, but also provide more multidimensional wireless communication performance. To satisfy these requirements, new paradigms of wireless communication networks should be investigated.

1.1.2 Indoor wireless networks

Wireless communication in indoor scenarios cannot be ignored in satisfying the requirements of B5G communication systems, since is estimated that over 80% mobile data traffic occurs indoors [5]. In recent years, the Covid-19 pandemic has also raised awareness of the importance of living and working at home and the reliance on indoor wireless communications. Additionally, some emerging technologies, such as smart factories and remote

surgery, should be applied indoors in the future, bringing a higher demand for indoor wireless communications.

Facing the increasing indoor wireless communication demand, the wireless communication industry has begun to focus on indoor scenarios. Compared to the 2G/3G era when indoor wireless communication services were provided by outdoor base stations (BSs), small BSs are deployed indoors from 4G to complement outdoor-to-indoor communications. In the 5G/B5G era, more dense small cell networks (SCNs) and device-to-device (D2D) networks are deployed indoors to provide higher indoor coverage and capacity. Based on this trend, the deployment and application of wireless networks will focus more on indoor scenarios in the future.

Compared to outdoor scenarios, indoor wireless communication has the following main characteristics: 1) indoor space is usually enclosed and small in size, so signals are usually transmitted in short range; 2) the coverage of indoor wireless networks is constrained by walls and ceilings with high penetration loss; 3) a large number of scatters are distributed densely indoors, and the reflection and scattering of wireless signals lead to more complex multi-path effects [6]. These characteristics determine that the indoor wireless environment is complex and studying indoor wireless networks is difficult.

The B5G era has brought new challenges to indoor wireless communications. To increase the capacity of wireless networks, B5G requires the utilization of broader spectrum resources, which triggers the employment of the millimeter wave (mmWave) from sub-6GHz to 300GHz [7]. However, mmWave has a weak radio wave diffraction ability and severe penetration loss. When mmWave is used for wireless signal propagation, the signals will be blocked by a large number of indoor blockages, and receivers cannot receive signals with sufficient power.

1.1.3 Wireless-friendly buildings and BWP

The performance of in-building wireless networks highly depends on the indoor wireless environment because the propagation of wireless signals is significantly impacted by the indoor wireless environment. Building materials determine the penetration loss and the reflection coefficient. Building layouts and indoor blockage placements determine whether

the connection between transmitters and receivers are line-of-sight (LoS) or non-line-of-sight (NLoS) link. The distribution of scatters affects the multi-path propagation of signals, further impacting the channel gain. Thus, if indoor wireless networks are deployed in unsuitable rooms or buildings, the performance of indoor wireless networks will be constrained by buildings, and indoor wireless networks cannot provide sufficient QoS to meet the growing demand for indoor mobile communications.

To break through this constraint, future indoor wireless networks should actively provide guidance on building design and construction instead of passively adapting to the built environment. Based on this idea, future buildings can be designed and constructed to be wireless-friendly to indoor wireless networks to achieve a higher indoor wireless network performance. We can envision that the demand for wireless communication will be as important a criterion in building design as water, gas, and electricity supply in the future.

To guide the design of such type of wireless-friendly buildings, the concept of BWP has been proposed to quantitatively measure how buildings are wireless-friendly to indoor wireless networks [8]. BWP is an intrinsic property of buildings which is determined by building layouts and building materials. In the process of building design, architects can first design the basic structure of the building based on the requirements of building owners. Then, architects can modify and optimize the building under design by evaluating and analyzing the BWP iteratively to finally design a wireless-friendly building.

1.2 Motivations and contributions

1.2.1 Motivations

As introduced above, designing and constructing wireless-friendly buildings will be an important way to satisfy the explosively growing indoor wireless communication demand. BWP evaluation is the primary task in designing wireless-friendly buildings, as architects need a quantitative metric to identify which building design is more wireless-friendly to indoor wireless networks. However, the existing theoretical system of BWP evaluation is only in its infancy, and the related research is still not comprehensive. As a result, architects

cannot evaluate BWP for buildings comprehensively, and cannot design wireless-friendly buildings.

The existing theoretical system of BWP evaluation only consider SCNs for BWP evaluation. Buildings designed based on the existing theoretical system of BWP evaluation are only wireless-friendly to SCNs but not wireless-friendly to other indoor wireless network types. Various network types have different key performance indicators and main factors affecting the performance. It is not feasible to evaluate BWP for all types of networks with single BWP metric and evaluation approach. This requires evaluation approaches for different types of networks. Accordingly, architects can use these evaluation approaches together to conduct a more comprehensive BWP evaluation for buildings and design buildings that are wireless-friendly for more types of networks. Therefore, this is the main motivation of this thesis, i.e., to propose BWP evaluation approaches for more types of indoor wireless networks to complete the existing theoretical system of BWP evaluation.

Besides, existing studies have made some progress in BWP evaluation of building materials [9, 10], but BWP evaluation considering building layout still lacks. Thus, this thesis mainly evaluate BWP from the perspective of building layouts.

Firstly, as an important part of IoT, D2D technology is expected to be widely exploited in indoor scenarios to provide services such as smart home or smart factories. In D2D networks, devices should be equipped with specific functions, so D2D receivers should associate with intended transmitters to achieve functions. The specific association mechanism distinguishes the performance of indoor D2D networks from SCNs considered in existing BWP evaluation works. Thus, BWP evaluation approaches for indoor D2D networks are essential.

Then, extremely large aperture arrays (ELAAs) are envisioned to be integrated into large indoor structures, such as walls of stadiums or shopping malls, to provide higher data rate, area throughput, and coverage performance than massive multi-input-multi-output (MIMO) systems [11]. However, the performance of ELAA systems mainly depends on the visibility regions (VRs) of users and the spatial dimension of the array [12]. VRs are determined by indoor blockages and the array dimension is constrained by indoor space. Hence, we should consider indoor ELAA systems in the BWP evaluation.

As two key technologies of B5G and 6G, D2D networks and ELAA systems are likely to be deployed indoors to serve indoor mobile users simultaneously. ELAA systems influenced by indoor blockages can rely on D2D relays to enlarge the coverage region. The performance of both indoor ELAA systems and indoor D2D relays is impacted by building layouts. It is necessary to consider the signal cooperative transmission achieved by these two types of networks and evaluate the BWP based on such indoor relay-assisted ELAA networks.

1.2.2 Contributions

The main objectives of this thesis is to propose BWP metrics and evaluation approaches for networks that will be widely deployed in indoor scenarios in the future. Our work enable BWP evaluation applicable to more indoor network types and extend the application range of the existing theoretical system of BWP evaluation. Architects can design buildings that are wireless-friendly to more types of indoor wireless networks. To achieve this aim, the contributions of this thesis can be summarized as follows.

- **Chapter 3: BWP evaluation for indoor D2D networks**

  A BWP evaluation approach has been proposed for indoor D2D networks, filling the gap of indoor D2D networks in the existing theoretical system of BWP evaluation. A new metric, blockage gain, was created to measure BWP for indoor D2D networks, which is defined as the spatially averaged coverage probability (SACP) improvement due to the out-of-room blockage effect by rooms. Additionally, the theoretical upper and lower bounds of the SACP have been derived and the empirical formulas of SACP and blockage gain have been obtained with the derived upper and lower bounds by function fitting. The empirical formulas can help architects to quickly compute the BWP.

- **Chapter 4: BWP evaluation for indoor ELAA networks**

  The first BWP evaluation approach for indoor ELAA networks has been proposed. The achievable power gain was adopted as the primary metric fot BWP evaluation.

An algorithm to calculate the achievable power gain for an arbitrary building layout and indoor blockage placement was provided. The algorithm can effectively avoid the high computational complexity by incorporating the ELAA as an entirety into the calculation. In addition, a specific building layout was provided as an example to show the process of the BWP evaluation and building design optimization. The modification scheme can achieve a 13% improvement in the achievable power gain.

- **Chapter 5: BWP evaluation with joint consideration of indoor ELAA networks and D2D communication**

  The first indoor relay-assisted ELAA network architecture was proposed, where D2D relays are utilized to enhance the coverage performance of ELAAs in indoor scenarios. The BWP evaluation approach for this type of network has been proposed with the coverage rate as the BWP metric. An algorithm calculating the coverage rate of the indoor relay-assisted ELAA network with an arbitrary building layout has been proposed based on the Monte Carlo method.

1.3 Structure of the thesis

The content of this thesis is organized as follows.

Chapter 1 introduces the background of the research and the concepts of wireless-friendly buildings and BWP. The motivations and the contributions are also summarized in this chapter.

Chapter 2 reviews relevant technical concepts and related researches from three aspects. Firstly, contents related to the D2D technology, including both D2D direct communication and D2D relay communication, are reviewed. Then, the concepts of massive MIMO and ELAA are introduced and related works are reviewed. Finally, works related to BWP evaluation are reviewed.

Chapter 3 presents a BWP evaluation approach for indoor D2D networks. The indoor D2D network model and the metric for the BWP evaluation are shown firstly. Then, the SACP is derived for both the indoor scenario and the open space scenario. Based on the

derived SACPs, the empirical formulas for the SACP of the general scenario and the blockage gain is obtained. Finally, the numerical results are obtained and analyzed.

Chapter 4 presents a BWP evaluation approach for indoor ELAA networks. The concept of the achievable power gain, which is the metric for the BWP evaluation, is introduced and defined firstly. An approach to calculate the achievable power gain is presented, which includes the basic principle and the process of the approach. Then, based on an example building for the evaluation, how to evaluate the BWP of a specific building layout and how to optimize the building layout with the BWP as the reference are presented. The numerical results section shows the effect of utilizing the proposed BWP evaluation approach to improve the performance of the indoor ELAA network.

Chapter 5 presents an indoor relay-assisted ELAA network model and the BWP evaluation approach for this type of network where the coverage rate is adopted as the metric. Then, the approach to obtain the coverage rate is introduced. Finally, the relationship between the building layout and the performance of the proposed network is analyzed in numerical results.

Chapter 6 summarizes the main research outcomes and the conclusions obtained from the research. Meanwhile, potential future works are presented.

Chapter 2

State of the art and research challenges

Overview

In this chapter, relevant technologies and related researches are reviewed from three aspects. Firstly, contents related to the D2D technology, including both D2D direct communication and D2D relay communication, are reviewed. Then, the concept and related works of massive MIMO and ELAA are introduced. Finally, works related to BWP evaluation are reviewed.

2.1 D2D technology

2.1.1 D2D direct communication

With the increasing demand of mobile communications, the traditional cellular mode, where all data must be transmitted through macro BSs (MBSs) or small BSs (SBSs), has become inefficient. When a large amount of mobile data needs to be transmitted, it is burdensome to the cellular network even though sometimes the transmitter and the receiver are physically close to each other. To deal with this issue, D2D technology was proposed and has received a lot of attention from academia and industry. D2D communications enable direct data transmission between the transmitter and the receiver while BSs are only responsible for the communication control or even allow mobile users (MUs) control the communication system autonomously [13–15]. D2D technology not only reduces the heavy burden at BSs, but also

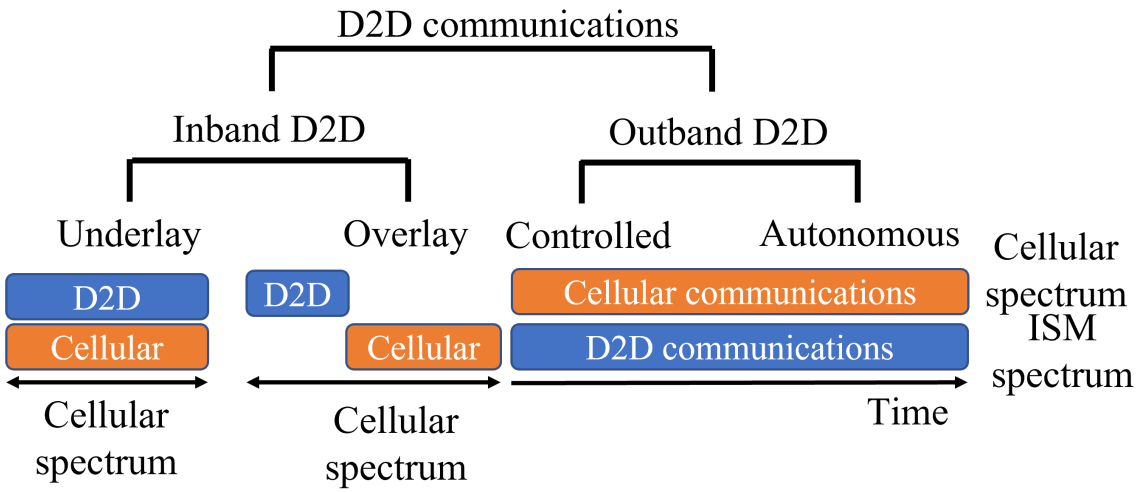

Fig. 2.1 The classification of D2D communications.

improves the spectral and energy efficiencies and provides higher connectivity and lower delay.

Generally, D2D communications can be categorized into two main categories based on the way of spectrum reuse: inband D2D communication and outband D2D communication, as shown in Fig. 2.1. Inband D2D communications operate in the licensed band of the cellular mobile networks, while outband D2D communications operate in the unlicensed band. The advantage of using the licensed band is that the communication can be controlled in cellular systems, resulting in a more stable D2D connection and controlled interference. However, applying D2D to the licensed band may cause interference to cellular users. Thus, the application of D2D to the unlicensed band has also been considered for a lower cellular interference and lower cost. But the communication in the unlicensed band is uncontrollable which imposes limitations on the QoS.

Inband D2D communication can be further classified into underlay and overlay D2D communications. In underlay D2D communication, the base station, cellular users and D2D users share the same radio resources. In overlay D2D communication, D2D communication is assigned dedicated radio resources. In contrast, the underlay mode can improve the spectral efficiency (SE) by spectrum reuse but leads to a high interference, while the overlay reduces interference by assigning dedicated spectrum to D2D communication but the SE is lower. In

the inband D2D communication, the most important problem is the interference between the cellular communications and D2D communications. To solve this problem, two common methods are resource allocation [16–18] and power control [19–21].

On the other hand, outband D2D communication can be classified based on whether the communication is controlled by BSs or not into controlled outband D2D communications [22] and autonomous outband D2D communications [23]. In controlled outband D2D communications, cellular BSs undertake functions such as radio resources assignment, power control, and mode selection for D2D users. In this type of systems, BSs control the whole system to reduce conflicts caused by users. In autonomous outband D2D communications, the channel access and interference management are controlled at the user side. In this control system, nodes are autonomous, leading to the rapid adaptation and decision making of dynamic systems.

With the proliferation of intelligent household devices, D2D communication is widely employed in indoor scenarios. In indoor scenarios, the work [24] investigated the D2D resources allocation problem considering human bodies as main indoor blockages to reduce the interference in an enclosed region. The authors developed a robust system to analyze the side effect of human bodies by the self-blockage model. With the proposed model, a closed expression of the signal-to-noise-plus-interference-ratio (SINR) coverage probability was derived. Then, an algorithm to enhance system throughput and reduce interference was proposed. In the work [25], a SINR-based device association vector algorithm for the maximum network connectivity has been proposed. The algorithm can achieve the maximum network connectivity by discovering the neighbors and the corresponding D2D link based on the sum rate and SINR. In addition, considering the impact of the dynamic variation of the signal-to-interference ratio (SIR) caused by random movement of indoor objectives, the probability density function (PDF) of SIR of communicating D2D pairs in the random movement has been obtained and the time-dependent behavior of SIR in D2D environments has been analyzed [26].

2.1.2 D2D relay communication

D2D technology allows direct transmission of information between two adjacent devices. With this feature, some devices in areas where direct links are unavailable due to location constraints can receive information from BSs or other devices via some devices as relays. Through D2D relays, the coverage range of the wireless network can be expanded to provide better QoS for users [27]. Besides, the transmit power of D2D users can be reduced through multi-hop relaying, so the interference between D2D and cellular networks can be solved in relay-assisted transmission.

D2D relaying has two main advantages. Firstly, relays can use existing D2D nodes directly without deploying additional nodes, resulting in a very low cost of D2D relay deployment. Secondly, users can easily select the suitable relay node from a large number of deployed devices. In contrast, potential relays are not controlled by operators, users may not be able to find a relay node at any time due to the movement of potential relays. In addition, relay-assisted transmission may lead to information security issues.

According to the relay protocol, D2D relays can be classified into three main categories: amplify-and-forward relays, decode-and-forward relays and quantized-and-forward relays. For amplify-and-forward relays, the received power of relay devices is simply amplified and forwarded to the target device. Low complexity is the advantage since there is nearly no signal processing. But amplify-and-forward relays can amplify noise and interference, leading to a performance reduction. This type of relays will be more effective when the SINR is high. Decode-and-forward relays should decode the received signal before modulating and transmitting the signal. This type of relays has high communication capacity, but the complexity and energy consumption is also high. Quantized-and-forward relays quantize and compress the received information and then forward it to the destination. Quantized-and-forward relays can reduce bit error rate by setting the quantization level flexibly.

In the work [28], the achievable system capacity of a multi-hop D2D system has been analyzed over Rayleigh fading channels. By jointly considering the spatial density of nodes in both D2D and cellular systems and the number of relay hops, the achievable transmission capacity of decode-and-forward relays has been analyzed. It has been concluded from the

work [28] that the relay-assisted transmission can effectively improve the capacity of D2D systems, but the improvement is not obvious when the number of relay hops is high. In addition, the coverage probability and the SE of D2D relay assisted cellular networks have been analyzed and compared in both mmWave scenarios and microwave scenarios [29]. The results show that a higher coverage can be achieved in microwave scenarios because D2D links can be established in NLoS conditions and in mmWave scenarios, blockages can effectively block interference to improve the coverage performance and SE.

The relay selection problem with dynamic blockages has been investigated [30]. The authors developed a probabilistic model for relay selection considering the movement of user equipment (UE) and blockages. By utilizing the information from a MIMO radar connected to the BS, the probability that the link is blocked by the dynamic blockage in 3-D space was analyzed, and a strategy was developed to find the best relay which can maximize the expected data rate.

2.2 ELAA technology

2.2.1 Massive MIMO networks

The application of multiple antennas, so called MIMO technology, as a mainstream SE improvement approach, has been extensively studied in recent years [31]. The directional beam was introduced to allow more aggressive frequency reuse. At present, mainstream MIMO technologies can be divided into three categories, e.g., single user MIMO, multiuser MIMO, and massive MIMO.

For the single user MIMO, a BS adopting an antenna array transmits signal to a UE equipped with multiple antennas. In this way, the diversity gain and multiplexing gain can be achieved to benefit the system capacity [32]. The multiuser MIMO has two essential advantages. Firstly, the multiuser MIMO has better adaptability to complex channel environments and is less sensitive to channels due to the higher diversity gain, multiplexing gain and spatial resolution of MIMO system. Secondly, multiuser MIMO systems allow the single antenna UE to access the system [32]. Correspondingly, multiuser MIMO systems also have

significant disadvantages. On the one hand, the complicated signal processing scheme should be considered by the BS and UEs. On the other hand, the downlink transmission requires that the channel state information (CSI) must be known by both the transmitter and receiver. With the development of mmWave communication and signal processing technologies, the BS has the preconditions to be equipped with a huge number of antenna elements, and massive MIMO technology came into being.

For the massive MIMO system, the number of antenna elements at the BS is much larger than the number of antenna elements equipped by UEs. The linear signal processing technologies can be applied by the transceivers, which enables the scalable characteristic of the massive MIMO system [31]. With the assumption of unlimited numbers of antenna elements, the authors in [33] analyzed the effect on the pilot contamination. Meanwhile, the results in [33] indicated that the increasing number of antenna elements can effectively eliminate the uncorrelated noise and fast fading. For a mightily long time, academia believed that even the number of antennas tends to be infinite, the coherent interference caused by pilot contamination will lead to the limitation of system capacity. However, in [34], the authors prove that the massive MIMO system capacity can be improved without bound. The authors applied multicell minimum mean square error (MMSE) precoding strategy and considered large-scale fading variations over antenna arrays. The results indicated that the capacity of the massive MIMO system can be increased with the increasing number of antenna elements, even the pilot contamination exists. In order to provide more favorable support for the application of massive MIMO, many channel models based on measurement have been proposed. In [35], the authors provided the measurement data in the 2.6 GHz frequency range with the large-scale antenna arrays. By analyzing the measurement data, authors extended the cluster-based COST 2100 stochastic channel model, which considered the VRs and the visibility gains. To explore the potential of massive MIMO in practice, the authors in [36] designed a measurement campaign with different shapes and apertures antenna arrays. The results shown that the system performance can be proved with the aperture increases, when the user density is high. Meanwhile, the channel resolvability is observed at the user side.

In general, the massive MIMO system can effectively improve the throughput and coverage performance of the wireless communication system. Under various channel environments, compared with conventional MIMO systems, massive MIMO can still stably provide diversity gain, spatial multiplex gain and spatial resolution to benefit the system capacity. Meanwhile, relevant measurements and theoretical results show that combined with mmWave technology, massive MIMO systems can significantly improve the SE [31].

2.2.2 ELAA technology

Compared with massive MIMO systems, ELAAs have larger array dimensions, usually from hundreds to thousands of antenna elements [11]. The larger array size means that the benefits of massive MIMO systems mentioned in the previous subsection, such as SE, diversity gain and throughput, can be further enhanced in ELAA systems. These benefits can effectively deal with the increasing indoor mobile communication demand, and it has been envisioned that ELAAs could be integrated into large indoor structures, such as walls of stadium or shopping malls [11, 12]. This is the fundamental purpose of studying indoor ELAA networks.

In indoor scenarios, users are usually in the near-field of ELAAs. In this case, some important far-field propagation assumptions are invalid, such as the plane wavefront assumption and the spatial stationarity. Typically, the Rayleigh distance is used to to distinguish the near field from the far field of antenna arrays [37]. Rayleigh distance Z is given by

$$Z = \frac{2D^2}{\lambda}, \tag{2.1}$$

where D is the maximum linear dimension of the ELAA measured by length units, and λ is the wavelength of the transmitted signal. It can be observed from the equation that with the increase of the array size, the Rayleigh distance of the array also increases, and users are more likely to be in the near field of the array. For instance, if an ELAA has a size of 4 m $\times$ 4 m and operates at the carrier frequency of 2.5 GHz, the Rayleigh distance of the ELAA is 133.34 m. Most buildings will be smaller than this distance in plan size. If the size

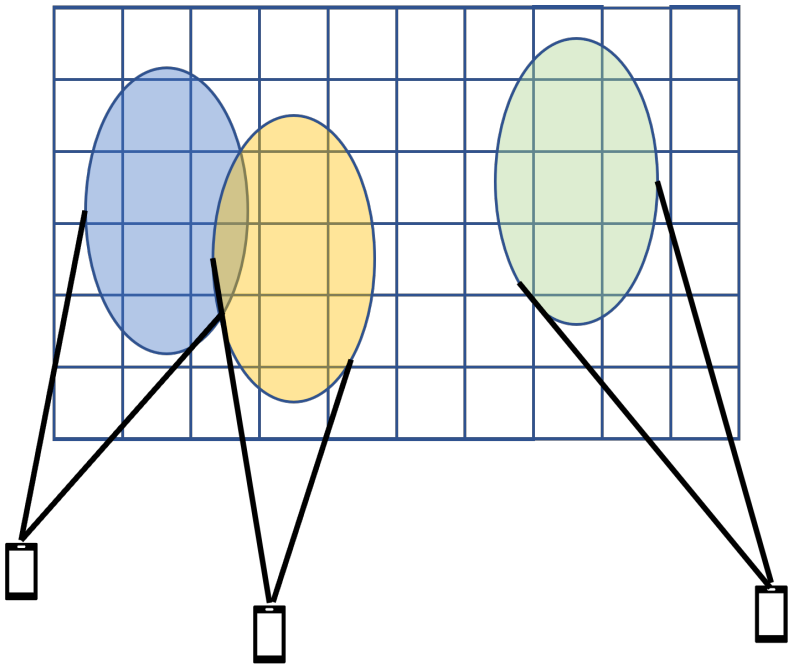

Fig. 2.2 An example of an ELAA system where different users have different VRs due to the spatial non-stationarity.

of the ELAA is further increased or the ELAA transmits signals with mmWave, the Rayleigh distance will be higher and indoor users will more likely be in the near-field of the ELAA.

The spatial non-stationarity is a crucial feature, which is the main difference from massive MIMO systems [12]. The spatial non-stationarity states that when the array size becomes extremely large, the distances between the user terminal and different portions of the array vary significantly, and the user terminal receives distinct powers from different array portions and even view different array portions with different channel paths. In some cases, the user terminal can only receive power from a portion of the array, while the power from other array portions can hardly be received due to the long propagation distance and the rapid power attenuation. The array portion that provide most of the user's received power is called VR.

There are works exploiting the impact of the spatial non-stationarity on the performance of ELAA systems. Authors of the work [36] undertook an experimental measurement by measuring the received power of an ELAA from terminals. The measurement results show that there exists a considerable variation of the average received power across the array, which exceeds 10 dB. From the theoretical derivation aspect, the authors of the work [38] proposed

a simple spatial non-stationary channel model, and the SINRs of conjugate beamforming (CB) and zero forcing (ZF) precoders were derived and analyzed with the proposed channel model. It is illustrated by their results that compared with stationary channels, the SINR loss can be as high as 15 dB for small VRs. However, this model only treats the non-stationarities as a binary form without considering the long-term fading variations of visible antenna elements. The work [39] investigated the uplink performance of ELAA systems by considering VRs. The authors proposed an ELAA system architecture based on the subarray and derived the tight closed-form uplink SE approximations.

Channel estimation for ELAA systems should also consider the spatial non-stationarity. The work [40] proposed two non-stationary channel estimation methods based on the subarray-wise and scatter-wise channel proporties facing the subarrays and scatters in the wireless environment with ELAAs. In the channel estimation methods, the ELAA is divided into small subarrays and the multi-path channel is modelled with the last-hop scatterers. The results show that the subarray-wise method can achieve a high accuracy with low complexity and the scatter-wise method can accurately identify most mapping between scatters and subarrays.

In addition, considering that the power transmitted by the user concentrate on the user's VR, the authors of the work [41] proposed a distributed processing scheme to overcome the huge computational complexity brought by the signal processing of a large number of antenna elements in ELAA systems. By distributing the processing to small and disjoint subarrays, the computational burden of the centralized processing can be effectively reduced by the proposed distributed receiver architecture.

On the other hand, due to the spatial non-stationarity, the power received by the user terminal from some antenna elements of the ELAA may be significantly larger than that from other antenna elements, which means that activating all antennas simultaneously is not energy-efficient. Thus, the work [42] derived a closed-form energy efficiency (EE) of the ELAA systems and proposed an antenna selection scheme. The scheme can determine the optimal number of serving antennas by an iterative method to maximize the EE.

2.3 BWP evaluation

2.3.1 Conventional methods evaluating indoor wireless network performance

Indoor wireless communications becomes increasingly significant because of the growing demand for indoor wireless communications. Evaluating the performance of wireless networks in indoor scenarios can help indoor wireless networks optimize the configuration and parameters to meet indoor mobile data traffic demand. However, indoor wireless propagation environment is complex and dynamic, and it is expensive and time consuming to evaluate network performance based on a series of measurements. Thus, some general mathematical models are required to assist in evaluating indoor wireless network performance. Commonly used methods include indoor propagation channel models, random blockage models and LoS probability analysis, etc.

Indoor propagation channel models can be classified into two categories: stochastic modelling (empirical models) and deterministic modelling [43]. Stochastic modelling describes the channel by obtaining the probability distribution of electromagnetic field intensity in different indoor scenarios from a large amount of measurement data. Path loss models [44], One slope model [45], COST231 Indoor Model [46] and WINNER II project [47] all belong to the stochastic models family. Stochastic modelling can achieve high accuracy in general indoor scenarios, but in some specific scenarios, the accuracy of the channel parameters is reduced [48]. For instance, in office environments, there are various sizes for different offices and different offices are built of diverse materials (brick, concrete, mud, wood etc.), and stochastic modelling cannot effectively operate in all of these environments.

In contrast, deterministic modelling is one outstanding alternative approach to model indoor propagation channels in wider varying scenarios. In deterministic modelling, full wave solutions can obtain the channel parameters for a specific indoor scenario by simulating the whole indoor wireless propagation environment and analyze the spatial distribution of electromagnetic fields [49–52]. Although full wave solutions can achieve high accuracy in specific scenarios, the high computational complexity limits their application.

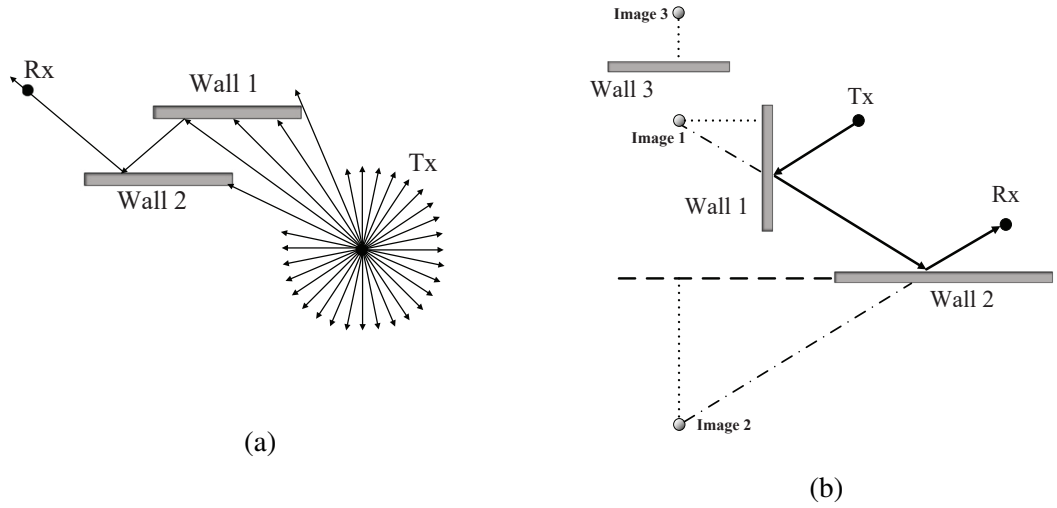

Fig. 2.3 A comparison between ray-tracing and ray-launching: (a) Ray-launching, (b) Ray-tracing.

Ray-tracing and ray-launching plays an extraordinarily important role in indoor propagation models as they can achieve a high accuracy with a lower computational complexity compared with full wave solutions [53–57]. Unlike the full wave solutions that calculate the distribution of the electromagnetic field intensity within the full space, ray-tracing and ray-launching only need to simulate signal propagation paths by rays to calculate the multi-path propagation characteristic, which greatly reduces the computational complexity and ensures the accuracy of the channel parameters. Although the basic ideas are similar, the principles of ray-tracing and ray-launching are different. As shown in Fig. 2.3, in the ray-launching, the transmitter emits a large number of rays and looks for rays that can reach the receiver to determine the signal propagation paths. In the ray-tracing, the signal propagation paths are determined by the image of the transmitter and receiver on the reflective surface of the object. In contrast, ray-tracing can further reduce the computational complexity.

For the indoor network performance evaluation, the work [58] proposed a method to optimize indoor antennas deployment to obtain a higher indoor coverage performance based on the ray-tracing algorithm. By ray-tracing simulation, an approach using passive reflectors to enhance the indoor coverage of mmWave systems has been proposed [59].

Then, indoor blockages, including walls, furniture and human bodies, is a non-negligible problem in indoor wireless communications, since indoor blockages can block communication links between transmitters and receivers and reduce the received power significantly. With the arrival of the 5G era and the application of mmWave communication, this problem becomes more severe because of the weak radio wave diffraction ability and severe penetration loss. Facing this problem, a number of random blockage models have been proposed.

Generally, when walls are used as the main blockages in an indoor wireless environment, walls can be assumed to be line segments or straight lines with no thickness but with penetration loss. For instance, in the work [1], the authors proposed four random wall generation methods for the indoor blockage modelling based on the stochastic geometry, as shown in Fig. 2.4. In these methods, the location (i.e., the location of the center point of a wall), orientation, wall spacing and length of walls are usually mainly considered parameters and some of them follow a specific probability distribution to generate randomly deployed walls in indoor scenarios. For each proposed method, the authors of the work [1] provided the analytical expression of the average power attenuation and the SIR approximations. Their numerical results show that for different wall generation methods, the average attenuation is the same but the SIR performance varies.

On the other hand, when considering human bodies as the primary blockage in indoor scenarios, human bodies are generally assumed to be cylinders. For instance, the authors of the work [60] established a 3-dimensional (3D) SCN model considering human body blockage to analyze the impact of the BS height, the BS density and the density of indoor blockages on the downlink coverage probability of the indoor SCN. In this work, human bodies are modelled as cylinders and their locations follow the Poisson point process (PPP).

With random blockage models, the performance of indoor wireless networks can be evaluated and analyzed more accurately. The authors of the work [61] derived the closed-form expression of the distribution of SIR and outage probability of the neighborhood small cell network by the random blockage model. In the work [62], the performance of indoor SCNs was evaluated by modelling the spatial distribution of interior walls and integrating

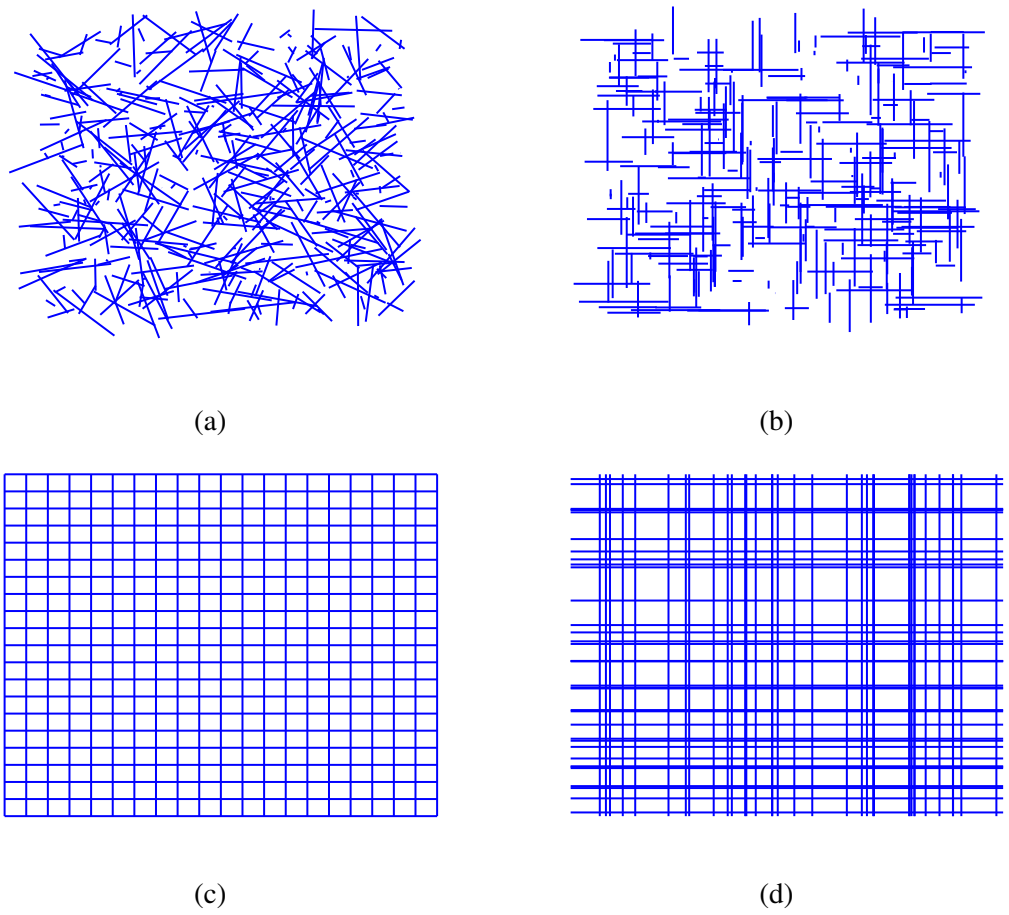

(a) (b)

(c) (d)

Fig. 2.4 Four random wall generation methods [1].

the wall penetration loss into the indoor path-loss model. In addition, the probability mass function (PMF) of the number of walls penetrated by the signal was derived with with three types of wall distribution models [63].

LoS probability models can distinguish between LoS and NLoS propagation in indoor wireless networks, enabling the evaluation of indoor network performance more accurate and convenient. In indoor scenarios, the signal propagation is affected by indoor blockages, resulting in high energy loss, especially in the mmWave band. In this case, the energy received by the BS or users in the network mainly comes from the LoS links. On the other hand, because of the complex indoor wireless propagation environment, the NLoS links have many reflection and refraction paths, resulting in long root mean square (RMS) delay spread and severe inter-symbol interference. It is crucial to consider the LoS probability in the evaluation of indoor network performance.

The indoor LoS probability models include empirical models and plan-based models. Empirical models are generally derived from fitting functions to the real measurement data [64, 47]. These models are simple and convenient to use, but they are limited by specific environments, resulting in difficulty in extending them to scenarios with different characteristics. Plan-based models are obtained according to specific building layouts and use specific propagation environment information to improve accuracy [65, 66].

Some works have applied the LoS probability model for indoor network performance evaluation. In the work [65], a novel model computing the LoS probability with an arbitrary building consisting rectangular rooms and corridors has been proposed. With the LoS probability model, the coverage rate of the indoor SCN is evaluated. The work [67] proposed a LoS probability computing model for typical buildings in the 3-D space. The proposed model is used to compute the coverage rate of a one-tier dense homogeneous network in a building.

2.3.2 BWP evaluation

Unlike the conventional approaches of optimizing the network configuration and parameters based on the building for a higher indoor network performance, the proposal of the concepts

of wireless-friendly buildings and BWP offers a new perspective for indoor wireless networks: to improve indoor network performance by modifying the building itself, including building layouts and materials [8]. The potential limits imposed by buildings on indoor wireless networks will sooner or later become a significant bottleneck to indoor network performance improvement by conventional approaches. But evaluating and modifying buildings can fundamentally address this constraint.

Existing studies related to the BWP evaluation mainly focus on two aspects: building layouts and building materials, which are two main architectural factors that affect the performance of indoor wireless networks.

Firstly, from the perspective of building layouts, the initial two metrics for the BWP evaluation were proposed: power gain (PG) and interference (IG) [68, 69]. These two metrics were defined by comparing the desired signal power or interference signal power in the in-building scenario and the open space scenario where there exists no signal blockages, respectively. The SINRs in the in-building scenario and the open space scenario can be respectively denoted by

$$\gamma_{\mathrm{B}} = \frac{P_{\mathrm{B}}}{I_{\mathrm{B}} + \delta^2}, \quad \gamma_{\mathrm{O}} = \frac{P_{\mathrm{O}}}{I_{\mathrm{O}} + \delta^2}, \tag{2.2}$$

where P_{B} and P_{O} are received signal power in two scenarios, I_{B}, I_{O} are interference signal power in two scenarios, respectively, and δ^2 is the thermal noise power. Then the PG and IG can be defined as

$$g_{\mathrm{P}} \triangleq \frac{P_{\mathrm{B}}}{P_{\mathrm{O}}}, \quad g_{\mathrm{I}} \triangleq \frac{I_{\mathrm{O}} + \delta^2}{I_{\mathrm{B}} + \delta^2}, \tag{2.3}$$

respectively. These two metric can extract the impact of the building from the indoor wireless network performance and can be used to measure the wireless performance of the building itself. The work [68, 69] play a seminal role in subsequent studies of BWP evaluation.

Then, based on the work [68, 69], the authors of [70] proposed a more tractable approach to calculate the PG and IG with a partition-based path gain model. The approach enables the PG and the IG to capture the impact of both building materials and the building layout on indoor wireless network performance.

Meanwhile, from the perspective of building materials, in the literature [9], a multi-path model for an indoor single-user LoS MIMO system considering wall reflection was constructed. A closed-form ergodic capacity was derived. Then, the wireless-friendliness of building materials was defined based on the indoor spatially averaged capacity, and the corresponding evaluation method was proposed. According to the numerical results, the relative permittivity and thickness of wall material have significant impact on the indoor capacity.

The work [10] integrate the antenna array in building material to avoid negative visual and weight impact of antenna arrays, and presented a method to evaluate the wireless performance of such antenna arrays integrated building materials by ray-tracing model. In the proposed approach, the spatially averaged capacity was adopted as the metric for the performance evaluation of the integrated material. By optimizing the conductivity, permittivity, thickness and integration depth of the material, the spatially averaged capacity of the integrated material achieved an improvement.

In the work [71], the authors considered indoor BSs equipped with MIMO antenna arrays deployed in the vicinity of a wall. The asymptotic expression of lower-bound network capacity was derived and it is revealed that the impact of the BS transmit power and that of the wall material properties on the capacity can be decoupled. By leveraging this conclusion, the logarithmic eigenvalue summation (LES) and logarithmic eigenvalue product (LEP) and the upper-bound outage probability are defined as three new metric for the fast calculation of the BWP of building materials.

Chapter 3

BWP evaluation for indoor D2D networks

Overview

Indoor D2D communication becomes increasingly essential with the proliferation of intelligent household devices. For higher indoor D2D network performance, future buildings should be designed friendly to indoor D2D networks. Towards this end, a BWP evaluation approach for indoor D2D networks is proposed in this chapter. Firstly, a new performance metric named blockage gain is created for the BWP evaluation. To obtain the blockage gain, the SACP in the indoor and the open space scenarios are derived, respectively. Then, empirical formulas for the fast calculation of the SACP and the blockage gain are obtained. Results show that the impacts of building layouts and building materials on the blockage gain can be decoupled. Moreover, numerical results show that well-designed rooms can improve the SACP of the indoor D2D network, which theoretically proves that designing wireless-friendly buildings benefits indoor D2D network performance.

3.1 Introduction

D2D communication is considered a critical technology of the B5G mobile communication networks. It can avoid the heavy network load by establishing direct communication links between adjacent devices without the assistance of BSs [13, 72, 73]. With the proliferation of intelligent household devices, D2D technology is widely employed in indoor scenarios

as an important part of the IoT to provide services such as smart homes or smart factories [24, 25, 74]. Since the data traffic demand is predicted to boost by up to 1000× in the next decade and over 80% occurs indoors [75], indoor D2D networks are required to provide higher performance, such as coverage and throughput.

Enhancing indoor D2D network performance requires designing and constructing wireless-friendly buildings, because buildings determine the indoor propagation environment, thus influencing the performance of in-building D2D networks [8]. Conventional methods studying indoor wireless networks all aim to evaluate indoor network performance and optimize network configurations with existing buildings, including indoor propagation channel models [54–56], random blockage modeling [1, 61, 62], and LoS probability analysis [65, 67]. However, improving network performance with network configuration optimization is becoming challenging because wireless channel capacity is approaching the Shannon limit with the development of communication techniques [76, 77]. To deal with the growing data traffic demand, migrating from optimizing network configuration to optimizing building design is necessary.

To design and construct wireless-friendly buildings, it is essential to quantitatively evaluate the wireless-friendliness of building layouts and building materials, generally referred to as BWP [8]. The purpose of BWP is to provide architects with a numerical reference to guide building design. By iteratively optimizing the building under design with the BWP improvement as the feedback, architects can design wireless-friendly buildings. Thus, evaluating the BWP for indoor D2D networks is necessary since it can guide architects to design wireless-friendly buildings for higher indoor D2D network performance.

3.1.1 Related works and motivations

There is a lack of the BWP evaluation approach for indoor D2D networks in the existing theoretical system of BWP evaluation, which results in the inability to design a wireless-friendly building for indoor D2D networks at this stage. Existing related works mainly focus on indoor SCNs. For instance, the work [78] investigated the impact of building story height on the coverage probability and SE of a multi-story indoor SCN, where the user associates to

the nearest BS. In [68, 69], two metrics, i.e., power gain and interference gain, were defined to measure the impact of building layouts on indoor wireless networks with an idealistic model, where the user can associate to all BSs which are deployed with a infinitely high density and infinitesimal cell sizes. However, devices in D2D networks should be equipped with specific functions, so D2D receivers should associate with intended transmitters to achieve functions [79, 80]. Due to the specific association mechanism, the probability distribution of association distances of D2D networks is different from that of SCNs. As a result, the signal, interference, and SINR received by D2D receivers are distinct from SCN users. This network performance difference results in that wireless-friendly buildings designed based on the existing theoretical system of BWP evaluation are not wireless-friendly to indoor D2D networks. Therefore, BWP should be evaluated for indoor D2D networks instead of only for SCNs, enabling buildings to be evaluated more comprehensively.

BWP can also be evaluated for building materials. The work [9] considered an indoor single-user LoS MIMO system with wall reflection. The indoor spatially averaged capacity of the network is employed as the metric to measure the wireless-friendliness of building materials. In [10], antenna arrays are integrated into walls, and a method to evaluate the wireless performance of the integrated building materials was proposed based on the ray-tracing model. Based on the model proposed by [68, 69], the authors of [70] analyzed the impact of wall penetration loss, which is determined by building materials. Existing related works investigated the impacts of building layouts or building materials on indoor wireless network performance, respectively. However, the impacts of them on network performance have not been considered simultaneously, and the relationship between them has not been discussed.

Coverage probability is essential for D2D networks because it determines whether D2D links are stable and the device functions can be successfully achieved, and it can be used as the metric of BWP evaluation. Existing coverage analyses for D2D networks are undertaken in outdoor environments, but the impact of the finite non-isotropic indoor region on the D2D network coverage performance has not been considered. Coverage probability is usually studied using stochastic geometry. In related works, the work [80] derived the

outage probability for a D2D underlying cellular network where devices are assumed to be distributed by PPP in a cell, modeled by a finite circle region. Only the interference transmitted within the finite area is considered in this work. In [81], D2D users located in a finite circular region receive the desired signal from the intended transmitter and interference from both the unmanned aerial vehicle as a flying BS and other D2D users distributed by PPP over an infinite area, and the coverage probability of the reference D2D user is derived. In [82], a fixed number of cache-enabled devices are modeled as binomial point process (BPP) in a finite circular region, and the coverage probability is derived when the target device associates with the k-th closest device for the cached content. These works obtain the coverage probability within a circular finite area. However, buildings or rooms usually have non-isotropic shapes, and this feature has not been discussed in the existing works. Meanwhile, indoor wireless networks are usually impacted by external interference power, which is attenuated due to the wall blockage. However, attenuated interference power from outside the finite area has not been discussed in the existing work.

We summarize the main motivations of our work as follows: 1) The BWP evaluation approach for indoor D2D networks is still absent; 2) Existing BWP-related works have not considered the impacts of building layouts and building materials simultaneously, and the relationship between them has been discussed in existing works; 3) the coverage probability of indoor D2D networks should be calculated within a finite non-isotropic region and consider the impact of the blocked external interference power, which has not been analyzed in exiting works.

3.1.2 Contributions

In this paper, we study the BWP evaluation for indoor D2D networks following stochastic geometry. The main contributions of this paper are summarized as follows:

- We propose the first systematic BWP evaluation approach for indoor D2D networks, which fills the gap of indoor D2D networks in the existing theoretical system of BWP evaluation. Considering that room walls can block out-of-room interference to improve the SINR and coverage performance, we create a new BWP evaluation metric, blockage

gain, to evaluate the wireless-friendliness of buildings. The blockage gain is defined as the SACP improvement due to the out-of-room interference blockage by the room walls. Results reveal that the maximal blockage gain can be achieved when the product of the room area and the interfering device density is a specific value. The maximal blockage gain is determined by the room aspect ratio (AR). In this case, the SACP of the indoor D2D network can be improved by at least 0.1 compared with the open space scenario.

- We investigate the relationship between the impacts of building layouts and building materials on BWP evaluation for indoor D2D networks. Results show that the impacts of building materials and layouts on the blockage gain can be decoupled. The decoupling allows architects to improve the BWP from the perspective of building materials or building layouts separately.

- To obtain the blockage gain, we propose an approach to calculate the SACP within a finite non-isotropic region, considering the impact of the attenuated external interference power. To calculate the SACP, we analytically derived the theoretical upper and lower bounds achieved by the different wall penetration loss, and we obtain the empirical formulas for the SACP in general scenarios with the help of the theoretical upper and lower bounds. Monte Carlo simulations validate the analytical results and the empirical formula.

3.2 System model

The system model is presented in this section. Since rooms are the most basic units of a building, building layouts can be determined by the sizes of rooms or corridors constituting the building. Accordingly, BWP evaluation can be performed for each room in the building, and then wireless-friendly buildings can be designed by jointly optimizing the size of each room based on their BWPs. Thus, we focus on the BWP evaluation for a single room in this chapter. To ensure the function achievement, we consider the case where the D2D transmitter

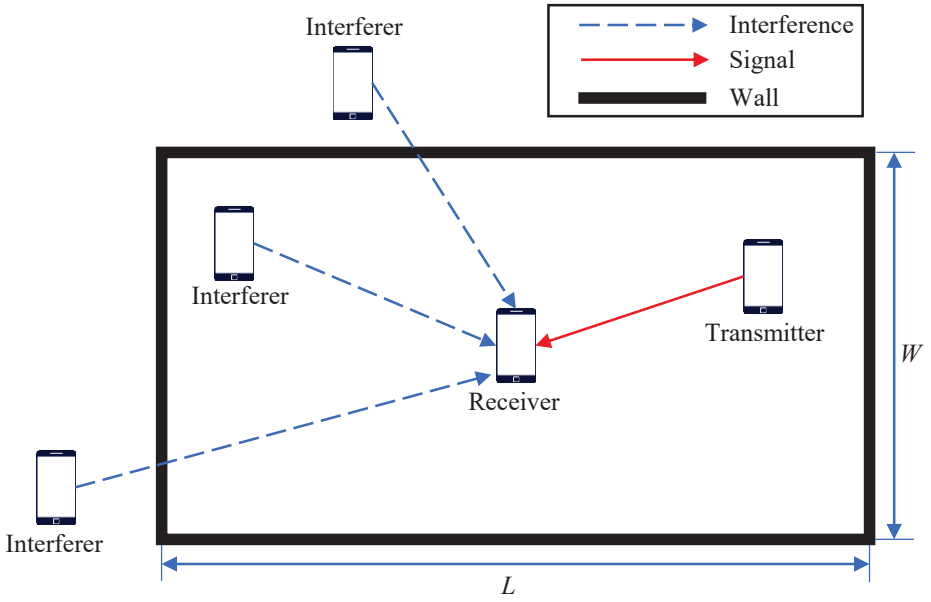

Fig. 3.1 The system model of a rectangular room with the size $L(\mathrm{m}) \times W(\mathrm{m})$, where a D2D network is deployed.

and receiver are both in the same room. In this case, the room can block out-of-room interference and improve the SINR and coverage performance.

From the aspect of building layouts, the out-of-room interference blockage effect by the room is mainly determined by the room's shape and size. Since the rectangle is the basic shape of rooms [68, 69, 63], we consider a rectangular room with the size of $L(\mathrm{m}) \times W(\mathrm{m}) \times H(\mathrm{m})$, as shown in Fig. 3.1. For analytical simplicity, we assume that all devices are at the same height, and we thus neglect the room height H and define the room under evaluation as a 2-dimensional (2D) plane region, which is denoted by $\mathbb{B}$. In this case, the building layout can be determined by rooms' area, given by $A = LW$, and rooms' AR, which is $\mathrm{AR} = W/L$ without loss of generality. On the other hand, wall penetration loss, denoted by β, is the main factor influencing the out-of-room interference blockage effect by the room walls from the aspect of building materials. The thickness and electromagnetic properties of the material determine wall penetration loss. For simplicity, we ignore the thickness as assumed in [65, 67] because the wall thickness influences the room size and complicates the analysis. β is defined to be within the range of $[0, 1]$, and in this paper, we mainly describe the wall penetration loss in decibel as $\beta_{\mathrm{dB}} = -10\log_{10}(\beta)$.

Based on the specific association mechanism of D2D networks, the receiver should associate to a specific transmitter, forming a D2D pair. Accordingly, we consider a D2D pair and a number of interfering devices in our model. We assume that the transmitter $\mathbf{v}_\mathrm{t}$ and the receiver $\mathbf{v}_0$ in the D2D pair are both uniformly distributed in $\mathbb{B}$, and R_t denotes the distance between them. All interfering devices are assumed to be distributed as a PPP Φ of the intensity λ over the infinite area. Interfering devices distributed inside the room region $\mathbb{B}$ are denoted by $\Phi_\mathrm{in} = \Phi \cap \mathbb{B}$, and those distributed outside $\mathbb{B}$ are denoted by $\Phi_\mathrm{out} = \Phi \setminus \Phi_\mathrm{in}$. The locations of interfering devices are represented as $\mathbf{v}_i$ for $i \in \Phi_\mathrm{in}$ and $\mathbf{v}_j$ for $j \in \Phi_\mathrm{out}$. We define R_i and R_j as the distance between the receiver and interfering devices of Φ_in and Φ_out, respectively.

We consider the path-loss and small-scale fading for the wireless channel. For the path-loss, we adopt the log-distance model with the path-loss exponent α. The small-scale fading is assumed as Rayleigh fading with average unit power. The channel fading gains of the wireless channel from the transmitter, interfering devices inside the room, and interfering devices outside the room are respectively denoted by g_t, g_i and g_j. Random variables g_t, g_i and g_j are independent and follow the exponential distribution with mean 1. Hence, the received signal power from $\mathbf{v}_\mathrm{t}$ is defined as $P_\mathrm{r} = P g_\mathrm{t} R_\mathrm{t}^{-\alpha}$, where P is the transmit power of each device. By denoting σ^2 as the thermal noise power, the received SINR in general scenarios can be defined as

$$\mathrm{SINR_G} = \frac{P g_\mathrm{t} R_\mathrm{t}^{-\alpha}}{I_\mathrm{in} + I_\mathrm{out} + \sigma^2} = \frac{g_\mathrm{t} R_\mathrm{t}^{-\alpha}}{\sum_{i\in\Phi_\mathrm{in}} g_i R_i^{-\alpha} + \beta \sum_{j\in\Phi_\mathrm{out}} g_j R_j^{-\alpha} + \hat{n}}, \tag{3.1}$$

where $I_\mathrm{in} = P\sum_{i\in\Phi_\mathrm{in}} g_i R_i^{-\alpha}$ is the cumulative interference power from interfering devices inside the room, and $I_\mathrm{out} = P\beta \sum_{j\in\Phi_\mathrm{out}} g_j R_j^{-\alpha}$ is the attenuated interference power from interfering devices outside the room with the wall blockage. $\hat{n} \triangleq \sigma^2/P$ is the normalized noise power.

Then, we measure the performance of indoor D2D networks with the metric SACP. The SACP is the averaged coverage probability with a given receiver's location within the

evaluated room, and it is given by

$$\mathscr{P}_{\mathrm{G}} = \mathbb{E}_{\mathbf{v}\in\mathbb{B}}\left[\mathscr{P}_{\mathrm{G},\mathbf{v}}\right], \tag{3.2}$$

where $\mathscr{P}_{\mathrm{G},\mathbf{v}}$ is the coverage probability when the receiver $\mathbf{v}_0$ is at the location $\mathbf{v}$. $\mathscr{P}_{\mathrm{G},\mathbf{v}}$ is defined as the probability that the SINR of the receiver is higher than the SINR threshold τ, and it is given by

$$\mathscr{P}_{\mathrm{G},\mathbf{v}} = \mathbb{P}\left\{\mathrm{SINR}_{\mathrm{G}} \geq \tau | \mathbf{v}_0 = \mathbf{v}\right\}. \tag{3.3}$$

There exist theoretical upper and lower bounds on the SINR and SACP of indoor D2D networks determined by wall penetration loss. On the one hand, when β_{dB} is assumed to be able to approach infinity, the out-of-room interference can be completely blocked by walls approximately. In this case, the receiver only receives intra-room interference; the SINR and SACP can reach the theoretical upper bound. On the other hand, when we assume that β_{dB} can reach 0 dB, the out-of-room interference power can be received without attenuation, and the SINR and SACP can reach the theoretical lower bound. We refer to these idealistic scenarios that achieve the theoretical upper and lower bound as the indoor and open space scenarios. We denote the SINR these two scenarios by

$$\mathrm{SINR}_{\mathrm{I}} = \frac{g_{\mathrm{t}} R_{\mathrm{t}}^{-\alpha}}{\sum_{i\in\Phi_{\mathrm{in}}} g_i R_i^{-\alpha} + \hat{n}}, \tag{3.4}$$

$$\mathrm{SINR}_{\mathrm{O}} = \frac{g_{\mathrm{t}} R_{\mathrm{t}}^{-\alpha}}{\sum_{m\in\Phi} g_m R_m^{-\alpha} + \hat{n}}. \tag{3.5}$$

Similarly, we have the SACP in these two scenarios as $\mathscr{P}_{\mathrm{I}}$ and $\mathscr{P}_{\mathrm{O}}$. For notational simplicity, we represent the SINRs and SACPs in the general scenario, the indoor scenario and the open space scenario as $\mathrm{SINR}_{\mathrm{s}}$ and $\mathscr{P}_{\mathrm{s}}$ for $s \in \{G, I, O\}$, respectively.

Based on these three scenarios, we can create a new metric, the blockage gain denoted by G_{B}, as the primary BWP evaluation metric for indoor D2D networks. Blockage gain is defined as the SACP improvement due to the out-of-room interference by the room. Since the room in the open space scenario has no blockage effect on out-of-room interference, we

employ the SACP in the open space scenario as the benchmark, and define the blockage gain as

$$G_{\mathrm{B}} = \mathscr{P}_{\mathrm{G}} - \mathscr{P}_{\mathrm{O}}. \tag{3.6}$$

Since $\mathscr{P}_{\mathrm{I}}$ is the theoretical upper bound of $\mathscr{P}_{\mathrm{G}}$, the blockage gain has the upper bound given by $\mathscr{P}_{\mathrm{G}} - \mathscr{P}_{\mathrm{I}}$.

3.3 Performance analysis

Since the shape of the room is non-isotropic, the boundary of the finite region is not uniform in all directions. To calculate the SACP in general scenarios, intra-room interference and attenuated out-of-room interference should be calculated separately, depending on the non-uniform room boundary. This makes that our results highly complex, reducing the efficiency of the BWP evaluation and the building design. Hence, we analytically derive the theoretical upper and lower bounds of the SACP and rely on them to obtain the SACP and the blockage gain by function fitting. In this section, we first derive the PDF of the distance between the reference receiver $\mathbf{v}_0$ and any device uniformly deployed in $\mathbb{B}$, which follows the assumption of the specific association. Then, the analytical results of $\mathscr{P}_{\mathrm{I}}$ and $\mathscr{P}_{\mathrm{O}}$ can be obtained with the derived PDF.

3.3.1 PDF of indoor communication link distance

The coverage probability $\mathscr{P}_{\mathrm{s},\mathbf{v}}$ given by (3.3) can be further derived as

$$\mathscr{P}_{\mathrm{s},\mathbf{v}} = \int_0^\infty \mathbb{P}\left\{\mathrm{SINR}_{\mathrm{s}} \geq \tau | \mathbf{v}, R_{\mathrm{t}} = r\right\} f_{R_{\mathrm{t}}}\left(r|\mathbf{v}_0 = \mathbf{v}\right) \mathrm{d}r. \tag{3.7}$$

The function $f_{R_{\mathrm{t}}}(r|\mathbf{v}_0 = \mathbf{v})$ is the conditional probability distribution of the distance R_{t} when the receiver $\mathbf{v}_0$ is located at $\mathbf{v}$. For notational simplicity, we denote the PDF $f_{R_{\mathrm{t}}}(r|\mathbf{v}_0 = \mathbf{v})$ as $f_{R_{\mathrm{t}}}(r|\mathbf{v})$. Similarly, the conditional coverage probability $\mathbb{P}\left\{\mathrm{SINR}_{\mathrm{s}} \geq \tau | \mathbf{v}, R_{\mathrm{t}} = r\right\}$ is simplified as $\mathscr{P}_{\mathrm{s},\mathbf{v},r}$.

Table 3.1 Array D_k and θ_k

k	Array D_k	Array θ_k
1	$L-x$	$\arctan\left(\frac{W-y}{L-x}\right)$
2	$W-y$	$\arctan\left(\frac{L-x}{W-y}\right)$
3	$W-y$	$\arctan\left(\frac{x}{W-y}\right)$
4	x	$\arctan\left(\frac{W-y}{x}\right)$
5	x	$\arctan\left(\frac{y}{x}\right)$
6	y	$\arctan\left(\frac{x}{y}\right)$
7	y	$\arctan\left(\frac{L-x}{y}\right)$
8	$L-x$	$\arctan\left(\frac{y}{L-x}\right)$

The distribution of the distance between two uniformly distributed nodes within a finite region has been studied in the last decade. The most popular method of these studies is first deriving the cumulative distribution function (CDF) of the distance and then obtaining the PDF by differentiating. The derivation of the CDF requires the analytical results of the intersection area between a circle, which has the reference receiver as the center and the distance as the radius, and the region where the two nodes are deployed. Depending on the radius and the relative position of the center within the region, the shape of the intersection is usually irregular and differs significantly [83]. Hence, some related works should rely on algorithms to obtain the PDF in different types of deployment regions, such as [83] and [84]. In this chapter, we only carry out analysis in a rectangular region and provide an approach inspired by [85] to analytically calculate the PDF. In [85], the distribution of the distance between the vertex of a triangle and a random point within the triangle was proposed. Since the rectangle can be divided into several triangles with the same vertex, we can analytically calculate the PDF of the distance in a rectangular region using the idea proposed by the work [85]. The analytical results of the PDF $f_{R_\mathrm{t}}(r|\mathbf{v})$ is given in Lemma 1.

Lemma 1. *The conditional PDF of the random variable R_t is given by*

$$f_{R_\mathrm{t}}(r|\mathbf{v}) = \sum_{k=1}^{8} \frac{\omega_k r}{LW}, \tag{3.8}$$

where

$$\omega_k = \begin{cases} \theta_k, & r < D_k, \\ \theta_k - \arccos\left(\frac{D_k}{r}\right), & D_k \leq r < \frac{D_k}{\cos(\theta_k)}, \\ 0, & r \geq \frac{D_k}{\cos(\theta_k)}. \end{cases} \tag{3.9}$$

If $\mathbf{v}$ *is represented by a Cartesian coordinate* (x,y)*, the values of the array* D_k *and* θ_k *are provided in Table 3.1.*

Proof. According to the relationship between the PDF and the CDF, when $\mathrm{d}r \to 0$, we have

$$f_{R_\mathrm{t}}(r|\mathbf{v}) = \frac{F_{R_\mathrm{t}}(r+\mathrm{d}r|\mathbf{v}) - F_R(r|\mathbf{v})}{\mathrm{d}r}, \tag{3.10}$$

where $F_{R_\mathrm{t}}(r|\mathbf{v})$ is the CDF of the random variable R_t when the receiver $\mathbf{v}_0$ is located at $\mathbf{v}$. This CDF is equivalent to the probability that the transmitter is deployed in the circular region with $\mathbf{v}$ as the center and r as the radius. We denote this circular region as $\mathbf{b}(\mathbf{v},r)$. The overlapping region between the circle $\mathbf{b}(\mathbf{v},r)$ and the region $\mathbb{B}$ can be defined as $\mathscr{A}\{\mathbf{b}(\mathbf{v},r),\mathbb{B}\} = \mathbf{b}(\mathbf{v},r) \cap \mathbb{B}$.

The area of the overlapping region $\mathscr{A}\{\mathbf{b}(\mathbf{v},r),\mathbb{B}\}$ can be represented by $S_{\mathscr{A}\{\mathbf{b}(\mathbf{v},r),\mathbb{B}\}}$. The CDF $F_{R_\mathrm{t}}(r|\mathbf{v})$ is further derived as

$$F_{R_\mathrm{t}}(r|\mathbf{v}) = \frac{S_{\mathscr{A}\{\mathbf{b}(\mathbf{v},r),\mathbb{B}\}}}{LW}. \tag{3.11}$$

The shape of $\mathscr{A}\{\mathbf{b}(\mathbf{v},r),\mathbb{B}\}$ differs with different $\mathbf{v}$ and the value of r. In order to calculate $S_{\mathscr{A}\{\mathbf{b}(\mathbf{v},r),\mathbb{B}\}}$, we divide the region $\mathbb{B}$ into 8 triangles based on the location $\mathbf{v}$ as shown in Fig. 3.2. Triangular regions are denoted by B_k for $k = 1,2,\ldots,8$. The angle with $\mathbf{v}$ as the vertex of triangle B_k is denoted by θ_k in rad while the length of the right-angled edge ending at $\mathbf{v}$ of B_k is D_k. Similarly, we denote the overlapping area between $\mathbf{b}(\mathbf{v},r)$ and B_k as $\mathscr{A}\{\mathbf{b}(\mathbf{v},r),B_k\}$. Accordingly, the CDF $F_{R_\mathrm{t}}(r)$ is given by

$$F_{R_\mathrm{t}}(r|\mathbf{v}) = \frac{1}{LW}\sum_{k=1}^{8} S_{\mathscr{A}\{\mathbf{b}(\mathbf{v},r),B_k\}}. \tag{3.12}$$

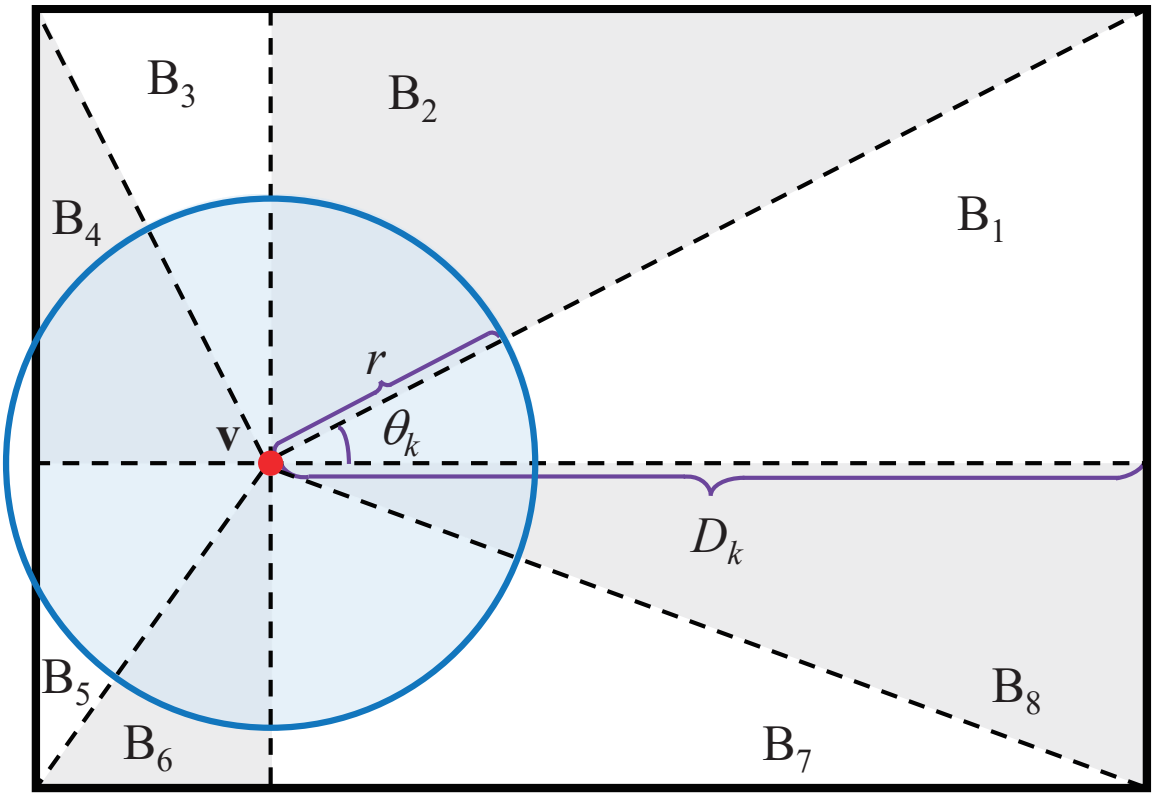

Fig. 3.2 The rectangular region $\mathbb{B}$ is divided into 8 parts, centered at the receiver $\mathbf{v}$.

By substituting (3.12) into (3.10), the PDF of variable R_t is defined as

$$f_{R_t}(r|\mathbf{v}) = \frac{1}{LW}\sum_{k=1}^{8}\frac{S_{\mathscr{A}\{\mathbf{b}(\mathbf{v},r+\mathrm{d}r),B_k\}} - S_{\mathscr{A}\{\mathbf{b}(\mathbf{v},r),B_k\}}}{\mathrm{d}r}. \tag{3.13}$$

As shown in Fig. 3.2, according to the location $\mathbf{v}$ and the value of r, $\mathscr{A}\{\mathbf{b}(\mathbf{v},r),B_k\}$ might have two types of shapes: sector (such as B_1) or non-sector (such as B_4). Since $\mathrm{d}r \to 0$, shapes of $\mathscr{A}\{\mathbf{b}(\mathbf{v},r),B_k\}$ are same as corresponding $\mathscr{A}\{\mathbf{b}(\mathbf{v},r+\mathrm{d}r),B_k\}$. Thus, we discuss different cases separately.

Case 1: When $0 < r < D_k$, shapes of $\mathscr{A}\{\mathbf{b}(\mathbf{v},r),B_k\}$ and $\mathscr{A}\{\mathbf{b}(\mathbf{v},r+\mathrm{d}r),B_k\}$ are sectors, we have

$$\frac{S_{\mathscr{A}\{\mathbf{b}(\mathbf{v},r+\mathrm{d}r),B_k\}} - S_{\mathscr{A}\{\mathbf{b}(\mathbf{v},r),B_k\}}}{\mathrm{d}r} = \frac{\mathrm{d}}{\mathrm{d}r}\frac{\theta_k \pi r^2}{2\pi} = \theta_k r. \tag{3.14}$$

Case 2: When $D_k \leq r < \frac{D_k}{\cos(\theta_k)}$, shapes of $\mathscr{A}\{\mathbf{b}(\mathbf{v},r),B_k\}$ and $\mathscr{A}\{\mathbf{b}(\mathbf{v},r+\mathrm{d}r),B_k\}$ are non-sectors, we can obtain

$$\begin{aligned}
&\frac{S_{\mathscr{A}\{\mathbf{b}(\mathbf{v},r+\mathrm{d}r),B_k\}} - S_{\mathscr{A}\{\mathbf{b}(\mathbf{v},r),B_k\}}}{\mathrm{d}r} \\
&= \frac{\mathrm{d}}{\mathrm{d}r}\left\{\frac{1}{2\pi}\left[\left(\theta_k - \arccos\left(\frac{D_k}{r}\right)\right)\right]\pi r^2 + \frac{1}{2}D_k\sqrt{r^2 - D_k^2}\right\} \\
&= \left(\theta_k - \arccos\left(\frac{D_k}{r}\right)\right) r.
\end{aligned} \tag{3.15}$$

Therefore, the conditional PDF of the random variable R_t is given by (3.8) □

Since interfering devices are deployed based on PPP, locations of interfering devices inside the room are independent and uniformly distributed, which are same as $\mathbf{v}_\mathrm{t}$. The random variable R_i for $i \in \Phi_\mathrm{in}$ and R_t are independent and identically distributed (i.i.d.). Thus, the distribution of R_i, denoted by $f_{R_i}(r|\mathbf{v})$, is equal to the PDF $f_{R_\mathrm{t}}(r|\mathbf{v})$. With the PDF $f_{R_\mathrm{t}}(r|\mathbf{v})$ and $f_{R_i}(r|\mathbf{v})$, we can derive $\mathscr{P}_{\mathrm{I},\mathbf{v},r}$ and $\mathscr{P}_{\mathrm{O},\mathbf{v},r}$.

3.3.2 SACP of indoor scenario

In the indoor scenario, out-of-room interference is totally blocked, hence we only analyze intra-room interfering devices. Since locations of interfering devices are modeled by PPP Φ of intensity λ, the number of interfering devices inside the room N follows Poisson distribution with mean λLW. Hence, we have the PMF of the random variable N as

$$\mathbb{P}(N=n) = \frac{e^{-\lambda LW}(\lambda LW)^n}{n!}. \tag{3.16}$$

With the PMF obtained from (3.16), the conditional coverage probability $\mathscr{P}_{\mathrm{I},\mathbf{v},r}$ can be derived as

$$\mathscr{P}_{\mathrm{I},\mathbf{v},r} = \sum_{n=0}^{\infty} \frac{e^{-\lambda LW}(\lambda LW)^n}{n!}\mathbb{P}\left\{\mathrm{SINR}_\mathrm{I} \geq \tau | \mathbf{v}, R_\mathrm{t} = r, N = n\right\}, \tag{3.17}$$

where the conditional probability $\mathbb{P}\left\{\mathrm{SINR}_\mathrm{I} \geq \tau | \mathbf{v}, R_\mathrm{t} = r, N = n\right\}$ is equivalent to the coverage probability with n intra-room interfering devices.

The calculation of the conditional probability $\mathbb{P}\{\mathrm{SINR_I} \geq \tau | \mathbf{v}, R_\mathrm{t} = r, N = n\}$ can be conducted with the BPP model [86]. In the BPP model, a fixed number of nodes are uniformly and independently deployed in a finite region. BPP models can capture the non-stationary and non-isotropic features of most practical wireless networks, which are not characterized by PPP models. With the BPP model, the coverage probability of an arbitrarily-located reference receiver within a circular region has been derived under both uniform association policy and k-th nearest association policy in prior works [87, 88]. By adopting the calculation approach of the coverage probability mentioned in the work [87], we derive the conditional coverage probability $\mathscr{P}_{\mathrm{I},\mathbf{v},r}$, which is shown in Theorem 1.

Theorem 1. *The conditional coverage probability $\mathscr{P}_{\mathrm{I},\mathbf{v},r}$ is given by*

$$\begin{aligned}\mathscr{P}_{\mathrm{I},\mathbf{v},r} = \sum_{n=0}^{\infty} \frac{e^{-\lambda LW}(\lambda LW)^n}{n!} e^{-\tau r^\alpha \hat{n}} \Bigg\{ \frac{1}{LW} \sum_{k=1}^{8} \Bigg\{ \left(\theta_k - \frac{\pi}{2}\right) G\left(\frac{D_k}{\cos(\theta_k)}\right) \\ + \frac{\pi}{2} G(D_k) + \sum_{l=0}^{\infty} \frac{(2l)!}{2^{2l}(l!)^2} \frac{(D_k)^{2l+1}}{2l+1} \left[H(l, D_k) - H\left(l, \frac{D_k}{\cos(\theta_k)}\right) \right] \Bigg\} \Bigg\}^n ,\end{aligned} \tag{3.18}$$

where the function $G(X)$ and $H(l,Y)$ are defined as

$$G(X) = \frac{r^{-\alpha} X^{\alpha+2}}{(\alpha+2)\tau} {}_2F_1\left(1, 1+\frac{2}{\alpha}, 2+\frac{2}{\alpha}, -\frac{r^{-\alpha}X^\alpha}{\tau}\right), \tag{3.19}$$

$$H(l,Y) = \frac{Y^{1-2l}}{2l-1} {}_2F_1\left(1, \frac{2l-1}{\alpha}, 1+\frac{2l-1}{\alpha}, -\tau\left(\frac{r}{Y}\right)^\alpha\right), \tag{3.20}$$

where l is a natural number, and the function ${}_2F_1(\cdot)$ is the Gauss hypergeometric function.

Proof. Due to the definition of the SINR given by (3.4), the conditional coverage probability given in (3.17) is derived as

$$\begin{aligned}&\mathbb{P}\{\mathrm{SINR_I} \geq \tau | v, R_\mathrm{t} = r, N = n\} \\ &= \mathbb{P}\left\{ \frac{g_\mathrm{t} R_\mathrm{t}^{-\alpha}}{I_\mathrm{in} + \hat{n}} \geq \tau | v, R_\mathrm{t} = r, N = n \right\} \\ &= \mathbb{P}\left\{ g_t \geq \tau R_\mathrm{t}^{-\alpha} (I_\mathrm{in} + \hat{n}) | v, R_t = r, N = n \right\}.\end{aligned} \tag{3.21}$$

As mentioned in the Section 3.2, the channel coefficient g_{t} follows the exponential distribution. Thus, (3.21) can be further derived as

$$\begin{aligned}
&\mathbb{P}\left\{g_{\mathrm{t}} \geq \tau R_{\mathrm{t}}^{-\alpha}\left(I_{\mathrm{in}}+\hat{n}\right)|v, R_{\mathrm{t}}=r, N=n\right\} \\
&=\mathbb{E}_{I_{\mathrm{in}}}\left[e^{-\tau r^{\alpha}\left(I_{\mathrm{in}}+\hat{n}\right)}|r, v\right] \\
&=e^{-\tau r^{\alpha} \hat{n}} \mathscr{L}_{I_{\mathrm{in}}}\left(\tau r^{\alpha}\right),
\end{aligned} \tag{3.22}$$

where $\mathscr{L}_{I_{\mathrm{in}}}\left(\tau r^{\alpha}\right)$ is the Laplace transform of the random variable I_{in}. It is given by

$$\begin{aligned}
\mathscr{L}_{I_{\mathrm{in}}}\left(\tau r^{\alpha}\right) &= \mathbb{E}_{I_{\mathrm{in}}}\left[e^{-\tau r^{\alpha} I_{\mathrm{in}}}\right]=\mathbb{E}_{R_i, g_i}\left[e^{-\tau r^{\alpha} \sum_{i=1}^{n} g_i R_i^{-\alpha}}\right] \\
&=\mathbb{E}_{R_i, g_i}\left[\prod_{i=1}^{n} e^{-\tau r^{\alpha} g_i R_i^{-\alpha}}\right] \overset{(a)}{=} \mathbb{E}_{R_i}\left[\prod_{i=1}^{n} \mathbb{E}_g\left[e^{-\tau r^{\alpha} g R_i^{-\alpha}}\right]\right] \\
&\overset{(b)}{=}\left(\int_0^{\infty} \mathbb{E}_g\left[e^{-\tau r^{\alpha} g R^{-\alpha}}\right] f_{R_i}(R|\mathbf{v})\,\mathrm{d}R\right)^n,
\end{aligned} \tag{3.23}$$

where (a) follows the independence of g_i and R_i and the i.i.d. distribution of g_i, and (b) follows from the i.i.d. distribution of R_i.

The expectation $\mathbb{E}_g\left[e^{-\tau r^{\alpha} g R^{-\alpha}}\right]$ can be obtained as

$$\mathbb{E}_g\left[e^{-\tau r^{\alpha} g R^{-\alpha}}\right]=\int_0^{\infty} e^{-\tau r^{\alpha} g R^{-\alpha}} e^{-g}\mathrm{d}g=\frac{R^{\alpha}}{R^{\alpha}+\tau r^{\alpha}}, \tag{3.24}$$

and the Laplace transform $\mathscr{L}_{I_{\mathrm{in}}}(\tau r^{\alpha})$ is

$$\mathscr{L}_{I_{\mathrm{in}}}(\tau r^{\alpha})=\left(\int_0^{\infty} \frac{R^{\alpha}}{R^{\alpha}+\tau r^{\alpha}} f_{R_i}(R|\mathbf{v})\,\mathrm{d}R\right)^n. \tag{3.25}$$

According to (3.8), the integral $\int_0^{\infty} \frac{R^{\alpha}}{R^{\alpha}+\tau r^{\alpha}} f_{R_i}(R|\mathbf{v})\,\mathrm{d}R$ can be expressed as

$$\begin{aligned}
&\int_0^{\infty} \frac{R^{\alpha}}{R^{\alpha}+\tau r^{\alpha}} f_{R_i}(R|\mathbf{v})\,\mathrm{d}R \\
&=\int_0^{D_k} \frac{R^{\alpha+1}}{R^{\alpha}+\tau r^{\alpha}} \theta_k \mathrm{d}R+\int_{D_k}^{\frac{D_k}{\cos(\theta_k)}} \frac{R^{\alpha+1}}{R^{\alpha}+\tau r^{\alpha}}\left(\theta_k-\arccos\left(\frac{D_k}{R}\right)\right)\mathrm{d}R \\
&=\int_0^{\frac{D_k}{\cos(\theta_k)}} \frac{R^{\alpha+1}}{R^{\alpha}+\tau r^{\alpha}} \theta_k \mathrm{d}R-\int_{D_k}^{\frac{D_k}{\cos(\theta_k)}} \frac{R^{\alpha+1}}{R^{\alpha}+\tau r^{\alpha}} \arccos\left(\frac{D_k}{R}\right)\mathrm{d}R.
\end{aligned} \tag{3.26}$$

Among the two integrals of (3.26), the integral $\int_0^{\frac{D_k}{\cos(\theta_k)}} \frac{R^{\alpha+1}}{R^\alpha+\tau r^\alpha}\theta_k \mathrm{d}R$ can be derived as

$$\int_0^{\frac{D_k}{\cos(\theta_k)}} \frac{R^{\alpha+1}}{R^\alpha+\tau r^\alpha}\theta_k \mathrm{d}R = G\left(\frac{D_k}{\cos(\theta_k)}\right), \tag{3.27}$$

where the function $G(X)$ is given by (3.19). We then derive $\int_{D_k}^{\frac{D_k}{\cos(\theta_k)}} \frac{R^{\alpha+1}}{R^\alpha+\tau r^\alpha}\arccos\left(\frac{D_k}{R}\right)\mathrm{d}R$ using the infinite series $\arccos(x) = \frac{\pi}{2} - \sum_{l=0}^{\infty} \frac{(2l)!}{2^{2l}(l!)^2}\frac{x^{2l+1}}{2l+1}$ as

$$\begin{aligned}&\int_{D_k}^{\frac{D_k}{\cos(\theta_k)}} \frac{R^{\alpha+1}}{R^\alpha+\tau r^\alpha}\arccos\left(\frac{D_k}{R}\right)\mathrm{d}R \\ &= \frac{\pi}{2}\left[G\left(\frac{D_k}{\cos(\theta_k)}\right) - G(D_k)\right] - \sum_{l=0}^{\infty}\frac{(2l)!}{2^{2l}(l!)^2}\frac{(D_k)^{2l+1}}{2l+1}\int_{D_k}^{\frac{D_k}{\cos(\theta_k)}}\frac{R^{\alpha-2l}}{R^\alpha+\tau r^\alpha}\mathrm{d}R.\end{aligned} \tag{3.28}$$

The integral $\int_{D_k}^{\frac{D_k}{\cos(\theta_k)}} \frac{R^{\alpha-2l}}{R^\alpha+\tau r^\alpha}\mathrm{d}R$ is derived as

$$\int_{D_k}^{\frac{D_k}{\cos(\theta_k)}} \frac{R^{\alpha-2l}}{R^\alpha+\tau r^\alpha}\mathrm{d}R = H(l, D_k) - H\left(l, \frac{D_k}{\cos(\theta_k)}\right), \tag{3.29}$$

where the function $H(l,Y)$ is given by (3.20). Thus, we obtain the conditional coverage probability $\mathscr{P}_{\mathrm{I},\mathbf{v},r}$, which is given by (3.18). □

By substituting (3.18) into (3.2) and (3.7), we can obtain the analytical results of the SACP $\mathscr{P}_{\mathrm{I}}$.

3.3.3 SACP of open space scenario

In the open space scenario, both intra-room interference and out-of-room interference are received without room wall blockage, we can calculate the SACP of the open space scenario based on the SINR given by (3.5).

Theorem 2. *The conditional coverage probability $\mathscr{P}_{\mathrm{O},\mathbf{v},r}$ is given by*

$$\mathscr{P}_{\mathrm{O},\mathbf{v},r} = \exp\left\{-\tau r^\alpha \hat{n} - \frac{2\pi^2\lambda}{\alpha}(\tau r^\alpha)^{\frac{2}{\alpha}}\csc\left(\frac{2\pi}{\alpha}\right)\right\}. \tag{3.30}$$

Proof. With the SINR given by (3.5), we have the conditional coverage probability $\mathscr{P}_{\mathrm{O},\mathbf{v},r}$ as

$$\begin{aligned}\mathscr{P}_{\mathrm{O},\mathbf{v},r} &= \mathbb{P}\left\{g_t \geq \tau R_t^{\alpha(I+\hat{n})} | \mathbf{v}, R_{\mathrm{t}} = r\right\} \\ &= \mathbb{E}_I\left[e^{-\tau r^{\alpha}(I+\hat{n})}\right] \\ &= e^{-\tau r^{\alpha}\hat{n}}\mathscr{L}_I\left(\tau r^{\alpha}\right),\end{aligned} \tag{3.31}$$

where $\mathscr{L}_I\left(\tau r^{\alpha}\right)$ is the Laplace transform of the random variable I. It is defined as

$$\begin{aligned}\mathscr{L}_I\left(\tau r^{\alpha}\right) &= \mathbb{E}_I\left[e^{-\tau r^{\alpha} I}\right] \\ &= \mathbb{E}_{g_m,\Phi}\left[e^{-\tau r^{\alpha}\sum_{m\in\Phi} g_m R_m^{-\alpha}}\right] \\ &\overset{(c)}{=} \mathbb{E}_{\Phi}\left[\prod_{m\in\Phi}\mathbb{E}_g\left[e^{-\tau r^{\alpha} g R_m^{-\alpha}}\right]\right] \\ &\overset{(d)}{=} \exp\left(-2\pi\lambda\int_0^{\infty}\left(1-\frac{u^{\alpha}}{u^{\alpha}+\tau r^{\alpha}}\right)u\mathrm{d}u\right) \\ &= \exp\left(-2\pi\lambda\tau r^{\alpha}\int_0^{\infty}\frac{u}{u^{\alpha}+\tau r^{\alpha}}\mathrm{d}u\right),\end{aligned} \tag{3.32}$$

where (c) follows from the i.i.d. distribution of variable g_m and the independence from the point process Φ, and (d) follows (3.24) and the probability generating functional (PGFL) of PPP, which is given by [89]. The integral $\int_0^{\infty}\frac{u}{u^{\alpha}+\tau r^{\alpha}}\mathrm{d}u$ is derived as

$$\int_0^{\infty}\frac{u}{u^{\alpha}+\tau r^{\alpha}}\mathrm{d}u = \frac{\left(\tau r^{\alpha}\right)^{\frac{2}{\alpha}-1}\pi\csc\left(\frac{2\pi}{\alpha}\right)}{\alpha}. \tag{3.33}$$

Accordingly, the conditional coverage probability $\mathscr{P}_{\mathrm{O},\mathbf{v},r}$ can be calculated according to (3.30). □

Similar to $\mathscr{P}_{\mathrm{I}}$, by substituting (3.30) into (3.2) and (3.7), we can analytically calculate $\mathscr{P}_{\mathrm{O}}$.

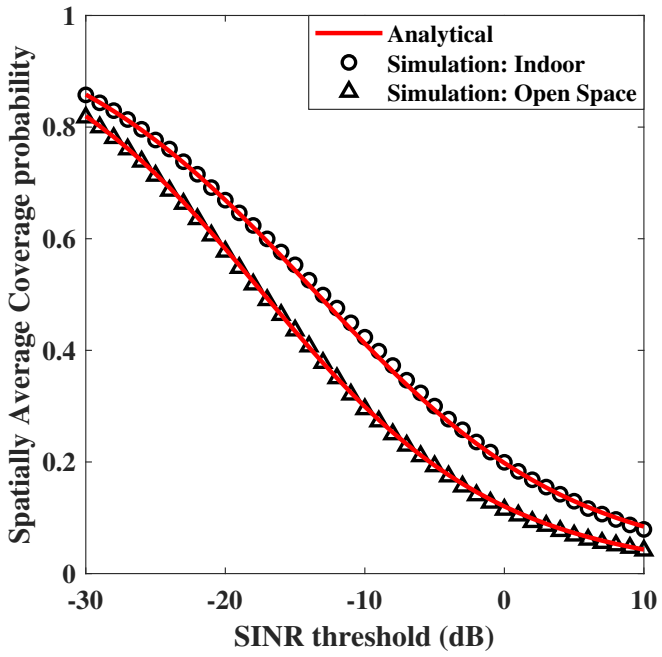

Fig. 3.3 The validation of $\mathscr{P}_{\mathrm{I}}$ and $\mathscr{P}_{\mathrm{O}}$ through Monte Carlo simulations.

Table 3.2 Simulation parameters

Parameter	Description	Value
A	Area of the room	40 m^2
AR	AR of the room	0.8
λ	Density of interfering devices	0.1 devices/m^2
β	Wall penetration loss	10 dB
τ	SINR threshold	-30 dB $\sim$ 10 dB
α	Path-loss exponent	4
$\hat{n}$	Normalized noise power	-30 dB

3.3.4 Validation

We validate $\mathscr{P}_{\mathrm{I}}$ and $\mathscr{P}_{\mathrm{O}}$ obtained in Section 3.3.2 and Section 3.3.3 by Monte Carlo simulations. The comparison between the analytical results and simulation results of $\mathscr{P}_{\mathrm{I}}$ and $\mathscr{P}_{\mathrm{O}}$ are shown in Fig. 3.3. The simulation parameters we adopt in this chapter are summarized in Table 3.2. As shown in Fig. 3.3, the analytical results of $\mathscr{P}_{\mathrm{I}}$ and $\mathscr{P}_{\mathrm{O}}$ match corresponding simulation results closely, which validates our derived results.

3.4 Empirical formulas of SACP and blockage gain

In this section, we obtain the empirical formulas of the $\mathscr{P}_{\mathrm{G}}$ and the blockage gain G_{B} by function fitting, aiming at conveniently evaluating BWP for rooms under design. In this approach, $\mathscr{P}_{\mathrm{G}}$ is approximately calculated by the function fitting method with the aid of $\mathscr{P}_{\mathrm{I}}$ and $\mathscr{P}_{\mathrm{O}}$, which are derived and validated in Section 3.3.

According to the definition of the three scenarios mentioned in Section 3.2, the SACP $\mathscr{P}_{\mathrm{I}}$ and $\mathscr{P}_{\mathrm{O}}$ are also the upper and lower bounds of $\mathscr{P}_{\mathrm{G}}$ regarding the wall penetration loss β. To simplify the process of function fitting, we define η as the relative position of $\mathscr{P}_{\mathrm{G}}$ between its upper and lower bounds, which is given by

$$\eta = \frac{\mathscr{P}_{\mathrm{G}} - \mathscr{P}_{\mathrm{O}}}{\mathscr{P}_{\mathrm{I}} - \mathscr{P}_{\mathrm{O}}}. \tag{3.34}$$

To fit $\mathscr{P}_{\mathrm{G}}$ into a simple function, we obtain simulation data of $\mathscr{P}_{\mathrm{G}}$ by Monte Carlo simulations. With simulation data of $\mathscr{P}_{\mathrm{G}}$, the simulation results of η can be calculated by (3.34). Fig. 3.4 shows the trends of η changing with five main variables which impact the coverage performance of the indoor D2D network. Compared with wall penetration loss, we can observe that the change in η caused by the other four variables does not exceed 15%. Accordingly, we can ignore the impact of the room AR, the room area, the interfering device density λ, and the SINR threshold τ on η in our empirical model. This can reduce the complexity of our empirical formula but will not significantly decrease the accuracy. Thus, η

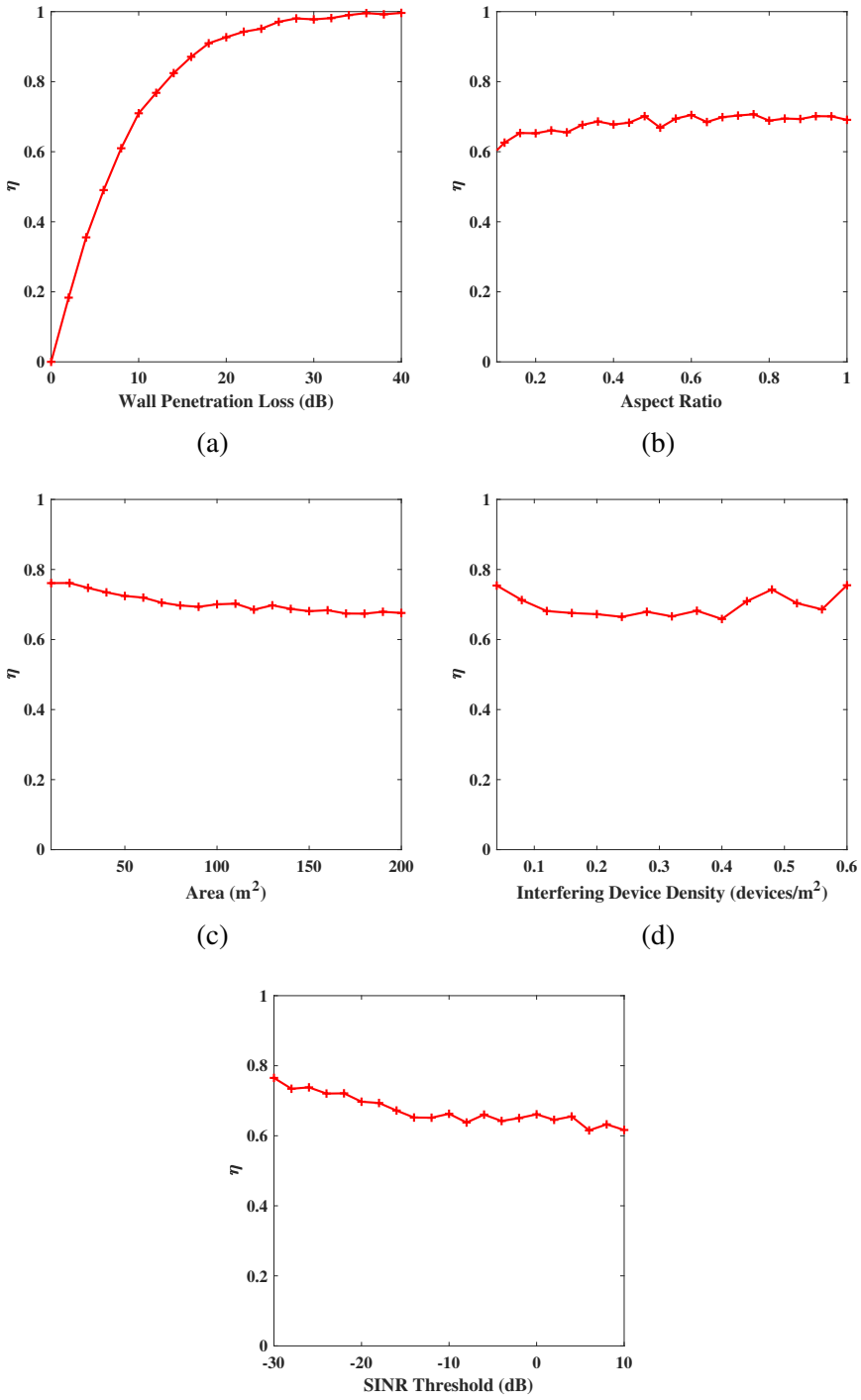

Fig. 3.4 Variation trends of η with other four main variables: room AR, room area, interfering device density, and SINR threshold.

can be approximately equivalent to a single variable function of variable β, which is given by

$$\eta \approx f(\beta). \tag{3.35}$$

The function trend shown in Fig. 3.4(a) has the following characteristics: 1) the range of the function is $[0,1]$; 2) the function rises monotonically; 3) the slope of the function decreases monotonically; 4) the value of $f(0)$ is 0 and $f(\beta)$ approaches to 1 when $\beta \to \infty$. Only exponential functions can satisfy all the above characteristics among the elementary functions. We establish the fitting function model as

$$\eta = 1 - e^{-a\beta}. \tag{3.36}$$

By the least-square method, the parameter a is calculated to be 0.121. The goodness of fit is 0.9680, which is very close to 1. This means that the empirical formula $\eta = 1 - e^{-0.121\beta}$ is acceptable. Fig. 3.5 presents the comparison between the empirical formula and the simulation results of η. It is shown that the fitting function of η can match the simulation results closely, which further validates the acceptance of the empirical formula. Based on the definition of η given by (3.34), the SACP $\mathscr{P}_{\mathrm{G}}$ can be approximately calculated using the equation

$$\mathscr{P}_{\mathrm{G}} = \eta \mathscr{P}_{\mathrm{I}} + (1-\eta)\mathscr{P}_{\mathrm{O}}, \tag{3.37}$$

where $\mathscr{P}_{\mathrm{I}}$ and $\mathscr{P}_{\mathrm{O}}$ can be calculated by (3.18), (3.30), (3.2), and (3.7).

Comparison between the approximate results and simulation results of $\mathscr{P}_{\mathrm{G}}$ is exhibited in Fig. 3.6. The figure reveals that the approximate results of $\mathscr{P}_{\mathrm{G}}$ match the simulation results closely for both $\lambda = 0.1$ devices/m^2 and $\lambda = 0.2$ devices/m^2, which can validates the approximate results of $\mathscr{P}_{\mathrm{G}}$. We can also obtain the approximate results of the blockage gain G_{B} with $\mathscr{P}_{\mathrm{G}}$ as

$$G_{\mathrm{B}} = \mathscr{P}_{\mathrm{G}} - \mathscr{P}_{\mathrm{O}} = \eta\left(\mathscr{P}_{\mathrm{I}} - \mathscr{P}_{\mathrm{G}}\right). \tag{3.38}$$

The term $\mathscr{P}_{\mathrm{I}} - \mathscr{P}_{\mathrm{O}}$ given by (3.38) is the upper bound of the blockage gain, denoted by $G_{\mathrm{B,upp}}$. According to (3.18) and (3.30), both $\mathscr{P}_{\mathrm{I}}$ and $\mathscr{P}_{\mathrm{I}}$ are not influenced by the wall

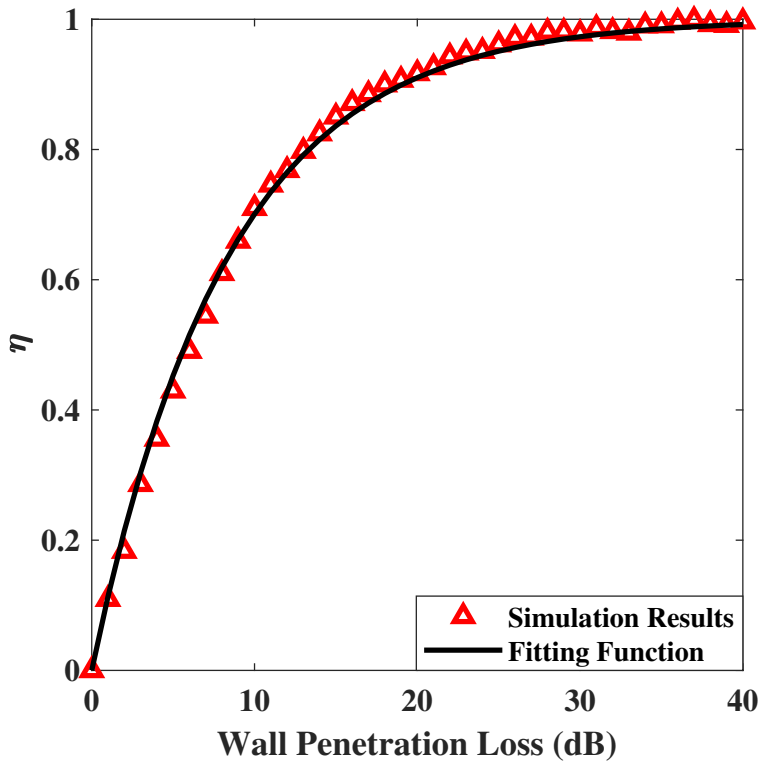

Fig. 3.5 Comparison between the fitting function $\eta = 1 - e^{-0.121\beta}$ and the simulation results of η.

penetration loss β, we can conclude that $G_{\mathrm{B,upp}}$ is independent of wall penetration loss. In contrast, η is only determined by the wall penetration loss according to (3.35). Therefore, $G_{\mathrm{B,upp}}$ represents the impact of building layouts on the blockage gain, and η represents the impact of building materials, and the impact of building materials and that of building layouts on the blockage gain can be decoupled. We can refer to $G_{\mathrm{B,upp}} = \mathscr{P}_{\mathrm{I}} - \mathscr{P}_{\mathrm{O}}$ as building layout blockage gain, denoted by G_{L}, and η as building material blockage gain, denoted by G_{M}, and we have

$$G_{\mathrm{B}} = G_{\mathrm{M}} G_{\mathrm{L}}. \tag{3.39}$$

Because of the decoupling of G_{M} and G_{L}, the blockage gain can be evaluated in terms of building materials and layouts separately. Architects can quickly and accurately identify which factor has a higher impact on the blockage gain in the building design. Thus, the efficiency of the building design can be significantly improved.

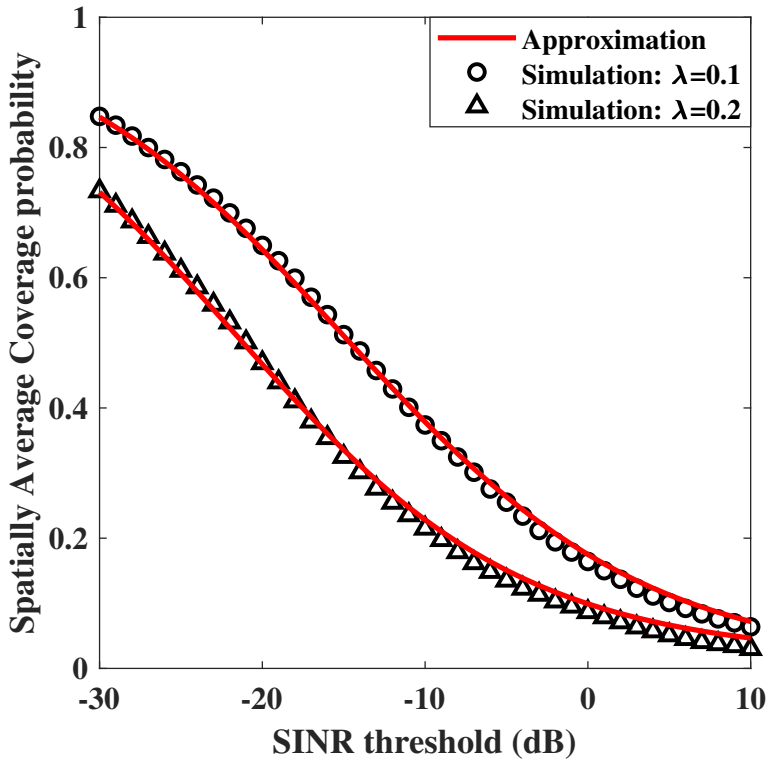

Fig. 3.6 Comparison between the approximate results and simulation results of the SACP of the general scenario for $\lambda = 0.1$ devices/m^2 and $\lambda = 0.2$ devices/m^2.

3.5 Numerical results

In this section, numerical results are provided to evaluate the performance of the indoor D2D network. We analyze the impact of different parameters on the SACP and the blockage gain.

3.5.1 Analysis of the SACP

In Fig. 3.7, we exhibit the SACP of different scenarios versus the AR with the interfering device density being 0.1 devices/m^2 and 0.3 devices/m^2, respectively. As mentioned in Section 3.2, the SACP of the indoor D2D network is determined by both the network parameters and the building. From the perspective of the network, the SACP is mainly determined by the interfering device density. With a high interfering device density, the receiver suffers a high interference power, which results in a low SACP. From the perspective

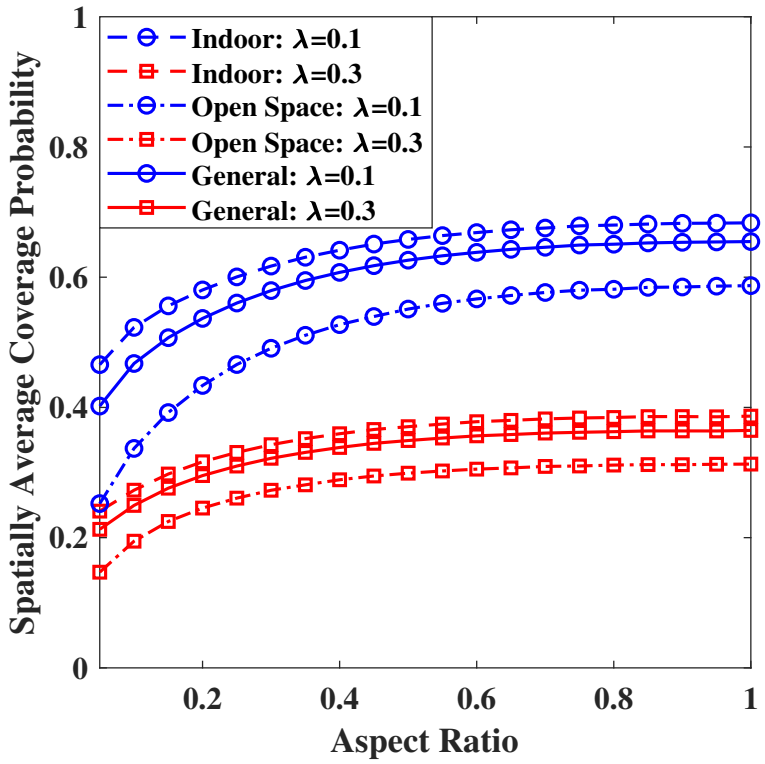

Fig. 3.7 The impact of AR on the SACP with the interfering device density being 0.1 devices/m^2, and 0.3 devices/m^2.

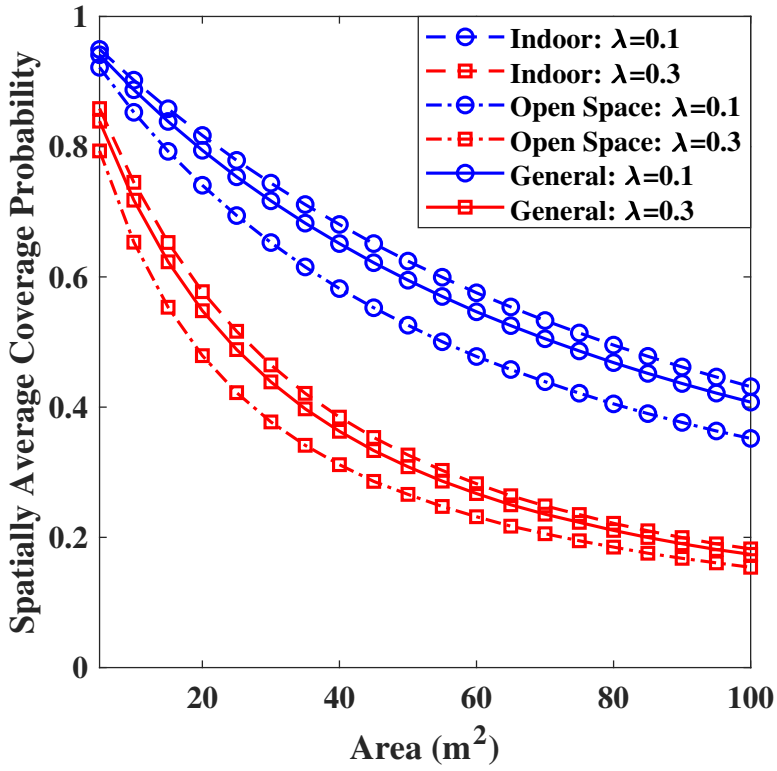

Fig. 3.8 The impact of the room area on the SACP with the interfering device density being 0.1 devices/m^2 and 0.3 devices/m^2.

of the building, it is shown in Fig. 3.7 that the SACP increases with the room AR for different interfering device densities. The main reason is that the spatial distribution of the transmitter is more limited on the width dimension, and the transmitter is thus less likely to be distributed close to the receiver in a narrow and long cavity, e.g., a corridor.

Fig. 3.8 shows the SACP with the increasing room area for different interfering device densities. We observe that both $\mathscr{P}_{\mathrm{O}}$ and $\mathscr{P}_{\mathrm{I}}$ decline with the increasing room area A. Although $\mathscr{P}_{\mathrm{O}}$ and $\mathscr{P}_{\mathrm{I}}$ have the same trend, the reasons are different. In the indoor scenario, the coverage performance of the D2D network mainly depends on the number of interfering devices deployed inside the room, which is determined by both the room area A and the interfering device density λ. The average number of intra-room interfering devices is equal to the expectation of the Poisson distribution, which is given by $N = \lambda A$. However, in the open space scenario, both intra-room interference and out-of-room interference are received

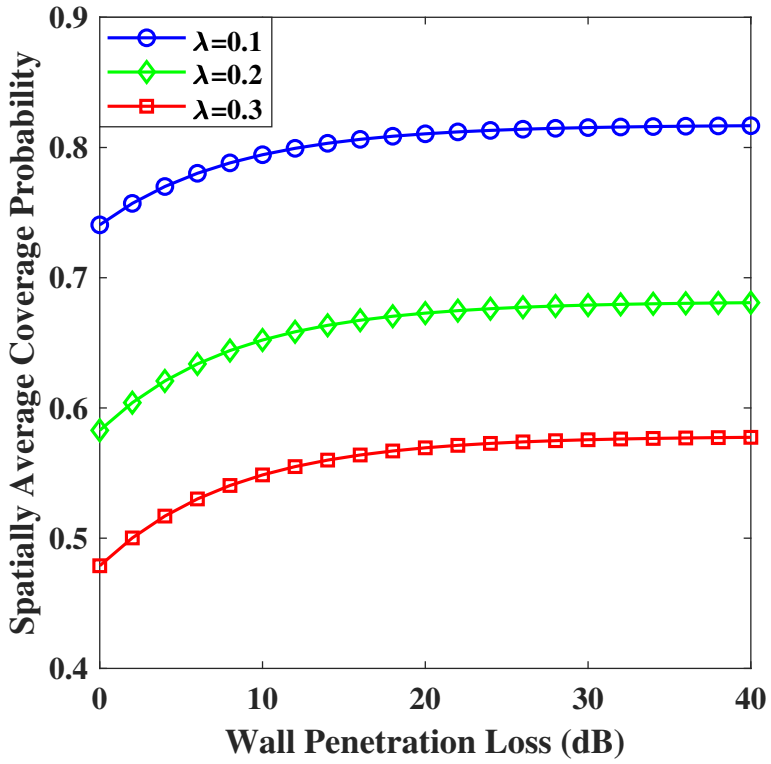

Fig. 3.9 The impact of the wall penetration loss of the room on the SACP.

without wall blockage, thus the received interference power does not depend on the room area. The room area only determines the deployment region of the transmitter and the receiver, and further influences the distance between them. Thus, in the open space scenario, the room area impacts the intended signal power, instead of the interference power.

The impact of wall penetration loss on the SACP is shown in Fig. 3.9. Since $\mathscr{P}_{\mathrm{I}}$ and $\mathscr{P}_{\mathrm{O}}$ are not affected by β, we only exhibit the SACP of the general scenario in this figure. It can be observed that with the increase of the wall penetration loss, the coverage performance of the indoor D2D network is improved. The blockage effect of walls on out-of-room interference can effectively reduce the received interference power, thereby enhancing the SINR. The trend of the SACP is similar to $\eta = 1 - e^{-0.121\beta}$ which is shown in Fig. 3.5.

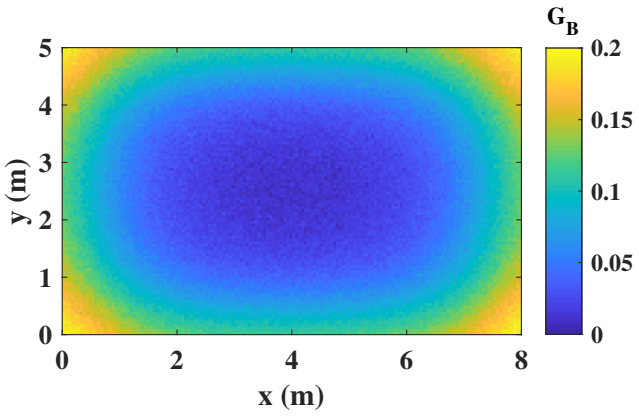

Fig. 3.10 The spatial distribution of the blockage gain within a room.

3.5.2 Analysis of the blockage gain

In this subsection, we first analyze the spatial distribution of the blockage gain within a room, as shown in Fig. 3.10. Fig. 3.10 shows that the blockage gain is lower in the room center region than at the edges and corners. This is because in the room center region, interfering devices close to the user, which dominates the received interference due to the path loss, are not blocked by walls. As a result, the received interference does not change significantly, and the SACP has no noticeable improvement due to the room. However, at the edges or corners of the room, some interfering devices close to the user are blocked by the wall, and the user receives less interference as a result, leading to a higher SACP improvement. Furthermore, we can observe that the blockage gain is higher at corners than at edges. This is because the surrounding interfering devices can be blocked by more walls when the user is at corners. The room brings a better blockage effect of out-of-room interference at corners than edges, and the SACP improvement is higher.

Then, as shown in (3.39), the blockage gain can be decoupled into the building material blockage gain and the building layout blockage gain. Since the building material blockage

gain is mainly determined by the wall penetration loss and can be represented by a simple function $G_{\mathrm{M}} = 1 - e^{-0.121\beta}$, we only analyze the impact of building layout on G_{L} in the rest of the subsection.

Fig. 3.11 displays the impact of the room area on the building layout blockage gain. It is illustrated that G_{L} increases first and then decreases. The main reason behind the non-monotonic behavior is that the SINR transfers from signal-dominated to interference-dominated with the growing room area. When the room area approaches 0, the intended signal power is considerably larger than the interference power due to the small distance between the transmitter and the receiver. In this case, the interference can be ignored, and the received SINR is approximately equal to the signal-to-noise ratio (SNR). Whether the room walls block the out-of-room interference has almost no influence on the SACP. Then, with the increase of the room area, the intended signal power declines while more interfering devices are accommodated inside the room. The SINR is gradually dominated by interference power. The blockage of out-of-room interference has an increasing impact on the SACP, and the building layout blockage gain thus grows. However, the impact of interfering nodes far from the receiver on the total interference power is neglectable due to the path-loss. When the room area enlarges, only blocking far interfering devices does not impact the SACP, thus the building layout blockage gain decreases and finally approaches 0.

We can observe from Fig. 3.11 that the maximal value of G_{L} is independent of the interfering device density. Fig. 3.11 also shows that the maximal value of G_{L} decreases with growing AR, and finally converges to 0.1. Meanwhile, we observe that when the maximal building layout blockage gain is achieved, the product of the corresponding room area and the interfering device density is a constant value, which is 3 for $\mathrm{AR} = 0.3$, 4 for $\mathrm{AR} = 0.5$, and 5 for $\mathrm{AR} = 0.8$. Therefore, it can be concluded from the analysis that when the product of the room area and the interfering device density is a specific value, which is determined by AR, the SACP of the indoor D2D network can obtain the highest improvement (by at least 0.1).

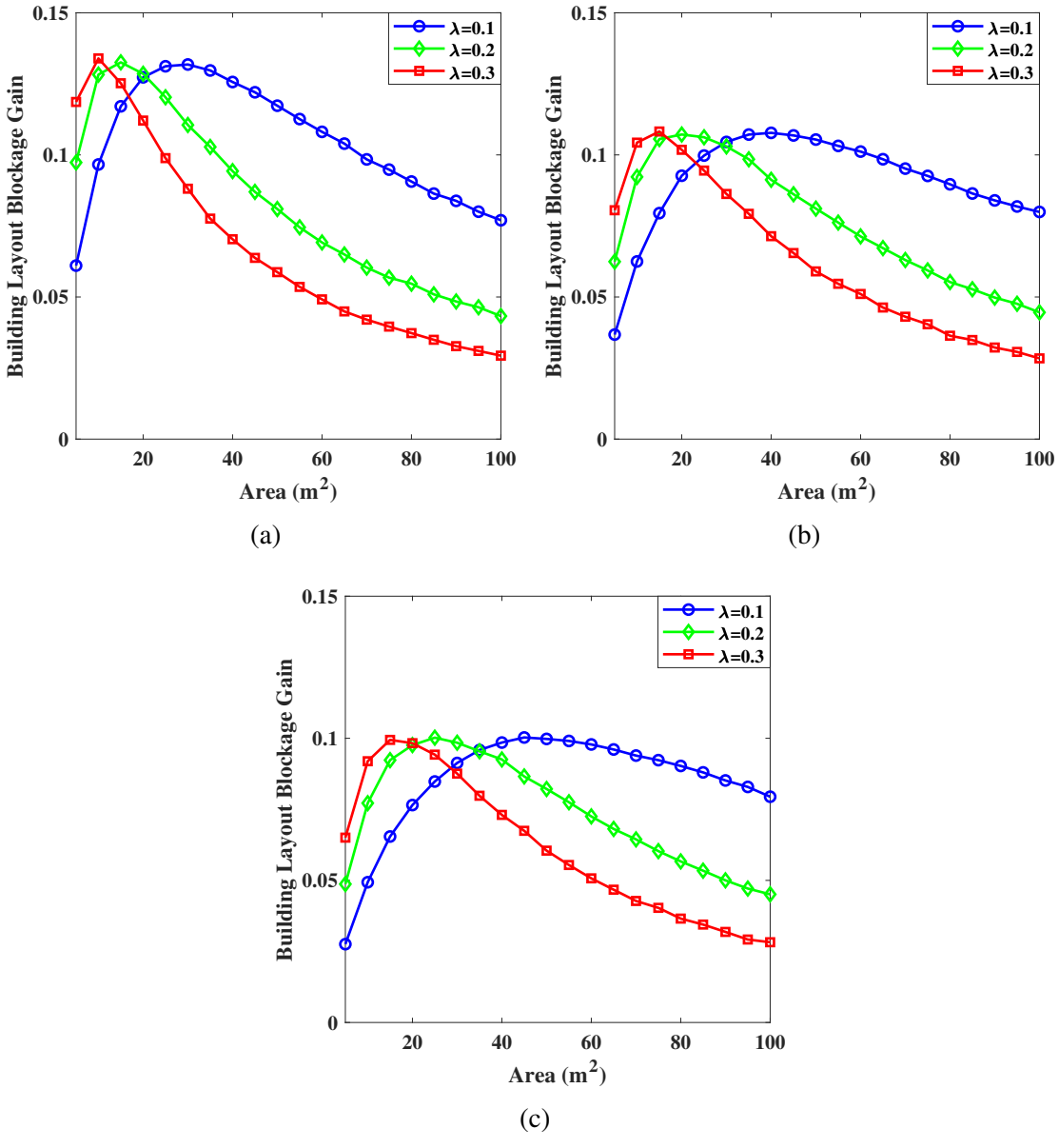

Fig. 3.11 The impact of room area and AR on the building layout blockage gain.

It should be noted that the primary purpose of the blockage gain is providing a new reference for building design. Architects should also consider other building requirements in the building design, e.g., water and electricity supply, the comfort of residents, etc.

3.6 Summary

In this paper, we have proposed a BWP evaluation approach for indoor D2D networks. We created the blockage gain as the performance metric to evaluate the BWP. The empirical formulas of the SACP and the blockage gain have been obtained for the convenient BWP evaluation. We have observed that the impacts of building layouts and materials on the blockage gain can be decoupled, which allows architects to quickly and accurately identify which factor has a higher impact on the blockage gain in the building design. Numerical results show that the maximal building layout blockage gain can be achieved when the product of the room area and the interfering device density is a specific value. The maximal blockage gain is determined by the room AR. In this case, the SACP of the network can be improved by at least 0.1 compared with the open space scenario. This work can provide guidance for architects to design wireless-friendly buildings for indoor D2D networks. In future works, the analysis will be extended to a 3-dimensional building space to better approximate practical scenarios. Moreover, a multi-story building model will be considered, and for this purpose, a multi-story indoor D2D network model will be used to incorporate the building's story height and number of stories into the BWP evaluation considerations.

Chapter 4

BWP evaluation for indoor ELAA networks

Overview

The emerging ELAA systems are expected to serve indoor users with higher data rate, area throughput, and coverage performance in the future. The performance of indoor ELAA systems is significantly constrained by the VR which is determined by building layouts and the placement of indoor blockages. For a higher network performance, buildings should be designed and constructed to be wireless-friendly to indoor ELAA networks. Therefore, a BWP evaluation approach is proposed for indoor ELAA networks for the design of future wireless-friendly buildings in this chapter. The achievable power gain is adopted as the primary metric for the BWP evaluation and an algorithm to calculate the achievable power gain for an arbitrary building layout and placement of indoor blockages is proposed. With an example room for the BWP evaluation and analysis, a room modification scheme based on the BWP evaluation is provided. The room modification scheme can effectively enhance the performance of indoor ELAA networks.

4.1 Introduction

ELAAs are expected to be widely deployed indoors to provide higher data rate, area throughput, and coverage performance in the future [11, 90, 91]. However, the wireless performance of indoor ELAA networks is significantly constrained by the indoor wireless propagation environment which is determined by the building layout and the placement of indoor blockages, especially when signals are propagated in mmWave frequencies with a high reflection loss and penetration loss [92]. This issue will become increasingly acute because the indoor data traffic demand is predicted to increase by at least 1000$\times$ in the next decade [75]. To solve this looming problem, future indoor ELAA networks should actively provide guidance on building design instead of passively adapting to the built environment. This requires the evaluation of the BWP for indoor ELAA networks.

The constraint imposed by the indoor wireless propagation environment will become a significant bottleneck hindering the indoor ELAA network performance improvement. Basically, indoor ELAAs must be deployed on interior walls, otherwise ELAA-equipped BSs will be physically large and occupy most of the room space, rendering the basic room functions unusable [93, 94]. The performance of such wall-integrated ELAAs is constrained by the indoor wireless propagation environment for two main reasons. On the one hand, the performance of a user terminal is limited by the terminal's VR. The VR is the portion of the array where most of the signal energy from the terminal is focused, and it is impacted by indoor blockages, such as walls, human bodies and pillars [12]. On the other hand, the array dimension and the wireless performance of wall-integrated ELAAs are limited by the size of the walls. Thus, if ELAAs are deployed in unsuitable rooms or buildings, indoor ELAA networks cannot provide satisfactory performance.

Designing and constructing buildings that are wireless-friendly to indoor ELAA networks can fundamentally solve the constraint, and the wireless friendliness of buildings should be evaluated. Our previous works provide the theoretical basis for achieving this goal. The work [8] has proposed the concept of BWP to measure how buildings are wireless-friendly to indoor wireless networks quantitatively. Then, some related works have also proposed BWP evaluation methods for different types of wireless networks [9, 68, 69, 39]. By evaluating

BWP and optimizing the building under design, architects can design buildings that are more wireless-friendly to indoor ELAA networks.

BWP evaluation should capture characteristics of different building layouts, which can be embodied by the sizes, shapes, and positions of major indoor blockages. Accordingly, the BWP evaluation for indoor ELAA networks mainly faces following challenges: 1) existing single-shaped blockage models, such as [95, 1], are limited in evaluating the BWP with various shaped indoor blockages; 2) commonly used stochastic channel models cannot capture the impact of different building layouts [48]; 3) there exists a high computational complexity which reduces the efficiency of the BWP evaluation and the building design if conventional deterministic channel models, such as geometry-optical methods [48], are employed to evaluate the BWP for indoor ELAA networks because ELAAs usually consist of a large number of antennas, especially in mmWave frequencies.

Motivated by these challenges, we propose the first BWP evaluation approach for indoor ELAA networks. We adopt the achievable power gain first proposed by [8] as the primary metric to evaluate the BWP, then provide an algorithm to calculate the achievable power gain for an arbitrary building layout and indoor blockage placement. This algorithm can effectively avoid the high computational complexity by incorporating the ELAA as an entirety into the calculation. We also provide a specific building layout as an example to show the process of the BWP evaluation and building design optimization. It should be noted that there are very diverse types of building layouts, and the building design should also consider various building requirements, including but not limited to wireless friendliness. We cannot analyze all types of building layouts and requirements in just one paper. Hence, we focus on the BWP evaluation on arbitrary specific building layouts, while the more concrete building design optimization based on BWP should be undertaken by architects based on the practical building requirements.

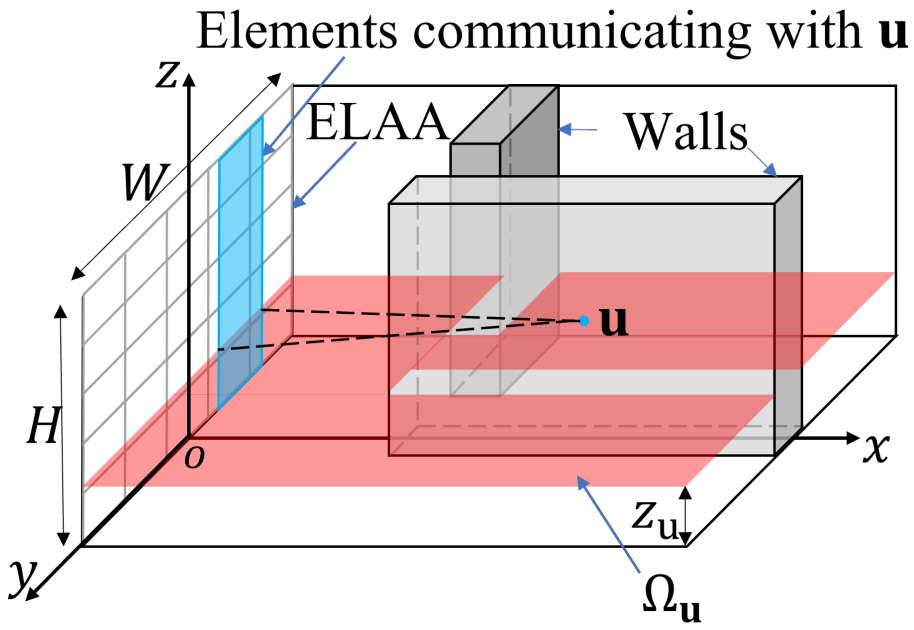

Fig. 4.1 An example of an arbitrary room where the ELAA is deployed on a wall.

4.2 System model

Indoor blockages heavily reduce the power the user receives from the ELAA at the mmWave frequency due to the weak penetration and reflection ability. Accordingly, we employ the achievable power gain to measure the impact of indoor blockages on the user's received power and adopt it as the primary metric for the BWP evaluation. We consider a single-user downlink scenario and define the achievable power gain as the ratio of the user's received powers when the user is impacted and not impacted by indoor blockages, respectively. We use $P_{\mathrm{B}}(\mathbf{u})$ and $P_{\mathrm{O}}(\mathbf{u})$ to denote the total powers received by the user at the location $\mathbf{u}$ when we consider and ignore indoor blockages, respectively. Since both $P_{\mathrm{B}}(\mathbf{u})$ and $P_{\mathrm{O}}(\mathbf{u})$ are impacted by the path loss and change with the roughly same trend, the gap between their values is the impact of indoor blockages. The achievable power gain at the location $\mathbf{u}$ can be obtained by

$$g_{\mathrm{P}}(\mathbf{u}) = \frac{P_{\mathrm{B}}(\mathbf{u})}{P_{\mathrm{O}}(\mathbf{u})}. \tag{4.1}$$

The achievable power gain $g_{\mathrm{P}}(\mathbf{u})$ is within the range of $[0,1]$ because $P_{\mathrm{B}}(\mathbf{u}) \leq P_{\mathrm{O}}(\mathbf{u})$. Higher power gain means that the user suffers less impact of indoor blockages at the location $\mathbf{u}$.

Then, we denote the region where the user may be located as Ω_{u}, and we can obtain the spatially averaged power gain within Ω_{u} as

$$\mathbb{E}\left[g_{\mathrm{P}}\left(\Omega_{\mathrm{u}}\right)\right] = \mathbb{E}_{\mathbf{u}\in\Omega_{\mathrm{u}}}\left[g_{\mathrm{P}}\left(\mathbf{u}\right)\right]. \tag{4.2}$$

The term Ω_{u} is determined by both the building layout and the placement of indoor blockages, and $\mathbb{E}\left[g_{\mathrm{P}}\left(\Omega_{\mathrm{u}}\right)\right]$ can represent the impact of specific building layout and placement of indoor blockages on the user's received power throughout the whole interior space.

We present the system model below for the BWP evaluation. We undertake the BWP evaluation for a room with an arbitrary shape, which is exemplified by Fig. 4.1. In this room, the ELAA is deployed on a rectangular wall with the size of $W \times H$, and we assume that the ELAA fills the whole wall to obtain the maximal ELAA performance. We construct the spatial coordinate system, as shown in Fig. 4.1, where the wall deployed by the ELAA is the yOz-plane and the intersection of the central axis with the bottom edge of the ELAA is the origin. The location of the user terminal can be represented by $\mathbf{u} = (x_{\mathrm{u}}, y_{\mathrm{u}}, z_{\mathrm{u}})$. For simplicity, we assume that the user has an invariable height, and we have Ω_{u} as a 2-dimensional planar region. Nevertheless, our BWP evaluation approach can also be employed in 3-dimensional spaces. Then, we represent indoor blockages with a set $\mathbb{B}$, whose elements $\mathbf{b} = (x_{\mathrm{B}}, y_{\mathrm{B}}, z_{\mathrm{B}})$ are the 3-D coordinates of the discrete points constituting indoor blockages. This method can effectively represent the indoor blockage size, position, and shape. Similarly, the ELAA can be represented by the set $\mathbb{A}$, whose elements have 3-D coordinates of $\mathbf{a} = (x_{\mathrm{a}}, y_{\mathrm{a}}, z_{\mathrm{a}})$.

We assume that the ELAA has M elements, which are arranged as a uniform rectangular array (URA). The user terminal has an isotropic and lossless antenna. We only consider LoS links since the indoor mmWave channel is dominated by LoS components [63, 96]. In addition, small-scale fading is neglected because fading is not significant in LoS mmWave links [63, 97]. Hence, the user's received power from the k-th ELAA element can be obtained by Friis' equation [98] as

$$P_{\mathrm{r}}\left(\mathbf{u}, k\right) = \frac{A_k^{\mathrm{eff}}}{4\pi {d_k}^2} P_{\mathrm{t}}, \tag{4.3}$$

where the k-th element has the transmitted power P_{t}, the effective area A_k^{eff} and the distance d_k to the user. The effective area of antennas is equal to the antenna area perpendicular to the signal propagation direction, and it is $A_k^{\mathrm{eff}} \leq \lambda^2/4\pi$, where λ is the signal wavelength.

According to the law of the conservation of energy, if we ignore indoor blockages, the total power received by the user from the ELAA is given by

$$P_{\mathrm{O}}(\mathbf{u}) = \sum_{k=1}^{M} \frac{A_k^{\mathrm{eff}}}{4\pi {d_k}^2} P_{\mathrm{t}}. \tag{4.4}$$

The sizes of indoor blockages are usually smaller than the spatial dimension of ELAAs, thus indoor blockages usually cannot completely block the communication links from all array elements, such as the user $\mathbf{u}$ in Fig. 4.1. In this case, we use $\mathbb{M}_{\mathrm{b}}$ to denote the set of the index of all elements that cannot establish LoS links with the users. Then, the total power received from the ELAA impacted by indoor blockages is given by

$$P_{\mathrm{B}}(\mathbf{u}) = \sum_{k \notin \mathbb{M}_{\mathrm{b}}} \frac{A_k^{\mathrm{eff}}}{4\pi {d_k}^2} P_{\mathrm{t}}, \tag{4.5}$$

The equations (4.4) and (4.5) are obtained by assuming the phase-derivations of received signals are negligible [99].

4.3 Performance analysis

To address the challenges mentioned in previous sections, we present a method in this section to calculate $g_{\mathrm{P}}(\mathbf{u})$ and $\mathbb{E}[g_{\mathrm{P}}(\Omega_{\mathrm{u}})]$ for an arbitrary building layout and indoor blockage placement. This method can obtain the user's received power under the impact of a specific indoor blockage by projecting the entire ELAA onto a sphere. We can preserve the characteristics of the indoor blockage by the projection, while projecting the entire ELAA can avoid the high computational complexity.

We first refer to (4.3), it is evident that the channel gain is determined by the factor $\frac{A_k^{\mathrm{eff}}}{{d_k}^2}$. This means that a large-sized antenna with a further distance and a small-sized antenna located at a nearer distance can receive the same power as long as they have the same value

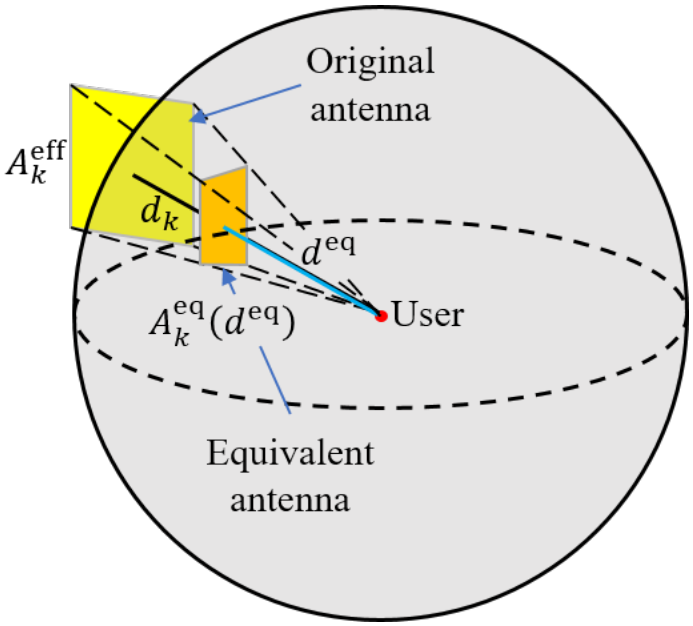

Fig. 4.2 The equivalent antenna which is perpendicular to the signal propagation direction and has the area $A_k^{\text{eq}}(d^{\text{eq}})$ at the transmission distance d^{eq}.

of $\frac{A_k^{\text{eff}}}{{d_k}^2}$. Accordingly, we can calculate $P_{\text{r}}(\mathbf{u},k)$ by calculating the received power from the equivalent antenna, which has an area perpendicular to the signal propagation direction and a distance convenient for the received power calculation. As shown in Fig. 4.2, the original antenna with the effective area A_k^{eff} and the transmission distance d_k has an equivalent antenna at the transmission distance d^{eq}. The area of the equivalent antenna is given by

$$A_k^{\text{eq}}(d^{\text{eq}}) = \left(\frac{d^{\text{eq}}}{d_k}\right)^2 A_k^{\text{eff}}. \tag{4.6}$$

The area of the equivalent antenna $A_k^{\text{eq}}(d^{\text{eq}})$ is determined by the transmission distance we set, we thus denote $A_k^{\text{eq}}(d^{\text{eq}})$ as a function of the distance d^{eq}.

Then, we can normalize d_k in (4.5) by obtaining the equivalent antennas of elements not in $\mathbb{M}_{\text{b}}$ at an identical transmission distance 1 m. In this case, all equivalent antennas are compactly arranged on a spherical surface with the radius 1 m, as shown in Fig 4.3. We can obtain $P_{\text{B}}(\mathbf{u})$ as

$$P_{\text{B}}(\mathbf{u}) = \frac{\sum_{k\notin\mathbb{M}_{\text{b}}} A_k^{\text{eq}}(1)}{4\pi} P_{\text{t}}. \tag{4.7}$$

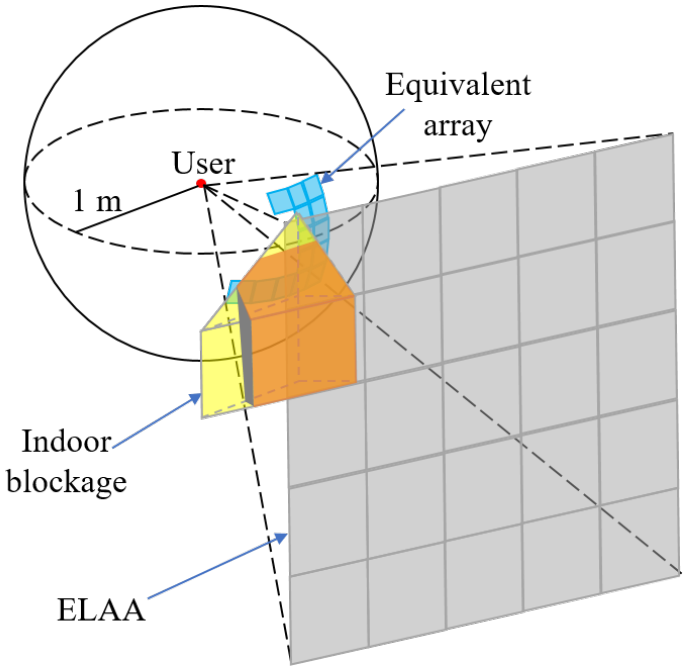

Fig. 4.3 Equivalent antennas of all array element not being blocked by indoor blockages are compactly arranged on a spherical surface with the radius 1 m.

The factor $\sum_{k\notin\mathbb{M}_\mathrm{b}} A_k^{\mathrm{eq}}(1)$ is approximately equal to the projected area of the ELAA region consisting of elements in $\mathbb{M}_\mathrm{b}$ on the spherical surface according to the projection principle, and we have

$$P_\mathrm{B}(\mathbf{u}) \approx \frac{S_\mathrm{p}}{4\pi} P_\mathrm{t}, \tag{4.8}$$

where S_p is the projected area. The equation (4.8) can also be utilized to calculate $P_\mathrm{O}(\mathbf{u})$, and S_p is the projected area of the whole ELAA on the spherical surface. Note that the approximation holds when the ELAA has a large number of elements with small physical sizes. MmWave can satisfy this condition because the effective area of antennas is $A = \lambda^2/4\pi$, where λ is the wavelength of the transmitted signal. In this case, equivalent antennas can tightly fit the spherical surface, and the approximation holds. With this method, we can consider the array as an entirety to calculate the total received power instead of independently calculating each element's effective area and transmission distance as equation (4.5) shows.

Based on above analysis, we provide an algorithm to quickly obtain $g_\mathrm{P}(\mathbf{u})$ and $\mathbb{E}[g_\mathrm{P}(\Omega_\mathrm{u})]$ as presented by Algorithm 1. We project discrete points in $\mathbb{B}$ and $\mathbb{A}$ on the spherical surface, then we can obtain the area S_p of the region consisting of these projected points by convex

hulls [100]. Firstly, some parts of the indoor blockages may not block the signal propagation, hence we should exclude the impact of these parts of the indoor blockages. We can project $\mathbb{B}$ on the yOz-plane to eliminate the points in $\mathbb{B}$ whose projected points are not in the ELAA region. The point $\mathbf{b} \in \mathbb{B}$, its projected point on the the yOz-plane $\mathbf{p} = \left(x_{\mathrm{p}}, y_{\mathrm{p}}, z_{\mathrm{p}}\right)$, and the user $\mathbf{u}$ are collinear, we can thus obtain the coordinates of the projected point as

$$\mathbf{p} = \alpha \mathbf{b} + (1-\alpha)\mathbf{u}, \tag{4.9}$$

where the coefficient α is given by

$$\alpha = \frac{x_{\mathrm{p}} - x_{\mathrm{u}}}{x_{\mathrm{B}} - x_{\mathrm{u}}}. \tag{4.10}$$

When $x_{\mathrm{p}} = 0$, $\alpha = \frac{x_{\mathrm{u}}}{x_{\mathrm{u}} - x_{\mathrm{B}}}$. The coefficient α is the relative distance of the point $\mathbf{b}$ between the user and the ELAA. Since the size of the ELAA is $W \times H$, we only remain points $\mathbf{b} \in \mathbb{B}$ whose projected points are within the region $x \in \left[-\frac{W}{2}, \frac{W}{2}\right], z \in [0, H]$ and we obtain the set $\mathbb{B}_{\mathrm{C}}$ consisting of these remained points.

We can then project discrete points in $\mathbb{B}_{\mathrm{C}}$ and $\mathbb{A}$ on the spherical surface. To carry out the spherical projection, we can construct a spherical coordinate system with $\mathbf{u}$ as the origin. The coordinates of the point $\mathbf{b}$ can be presented by the spherical coordinate $(d\sin\theta\cos\phi, d\sin\theta\sin\phi, d\cos\theta)$, where the angle θ and ϕ are given by

$$\theta = \arccos\left(\frac{z_{\mathrm{b}} - z_{\mathrm{u}}}{d}\right), \phi = \arctan\left(\frac{y_{\mathrm{b}} - y_{\mathrm{u}}}{x_{\mathrm{b}} - x_{\mathrm{u}}}\right), \tag{4.11}$$

and d is the distance of the point $\mathbf{b}$ to the user. All projected points on the spherical surface have the same distance to the user, and the angles θ and ϕ of each original point are the same as its projected point. Hence, the coordinates of the projected point can be obtained by replacing d to 1, then the coordinates of the projected point of the point $\mathbf{b}$ on the spherical surface is $\mathbf{b}_{\mathrm{p}} = (\sin\theta\cos\phi, \sin\theta\sin\phi, \cos\theta)$. By converting the spherical coordinates of the projected point into Cartesian coordinates, the coordinates of the projected point $\mathbf{b}_{\mathrm{p}}$ are given

Algorithm 1: The Achievable Power Gain Calculation Algorithm

Require: Ω_{u}: the region where the user may be located;
$\mathbb{B}$: the coordinates of points consisting indoor blockages;
$\mathbb{A}$: the coordinates of points consisting the ELAA;
Ensure: $\mathbb{E}\left[g_{\mathrm{P}}\left(\Omega_{\mathrm{u}}\right)\right]$: the achievable spatially averaged power gain;

```
for Different user location u do
    if the user is within the region of indoor blockages then
        Skip;
    else
        Project points in 𝔹 on the yOz-plane using (4.9);
        Remain the points in 𝔹 whose projected point is within the ELAA region and
        obtain 𝔹_C;
        Project points in 𝔹_C and 𝔸 on the spherical surface using (4.12) to obtain 𝔸_P and
        𝔹_P;
        Compute V_array and V_blockage by computing the convex hulls of 𝔸_P and 𝔹_P;
        Calculate P_B(u) and P_O(u) using equations (4.13) and (4.14);
        Calculate g_P(u) using equation (4.1)
    end if
end for
Calculate 𝔼[g_P(Ω_u)] using equation (4.2);
```

by

$$\mathbf{b}_{\mathrm{p}}=\left(\frac{x_{\mathrm{b}}-x_{\mathrm{u}}}{d}+x_{\mathrm{u}},\frac{y_{\mathrm{b}}-y_{\mathrm{u}}}{d}+y_{\mathrm{u}},\frac{z_{\mathrm{b}}-z_{\mathrm{u}}}{d}+z_{\mathrm{u}}\right). \tag{4.12}$$

We thus obtain the set of the coordinates of points projected by indoor blockages on the spherical surface, which is denoted by $\mathbb{B}_{\mathrm{P}}$. With the same method, we can obtain the set of the coordinates of points projected from $\mathbb{A}$, and we denote the set as $\mathbb{A}_{\mathrm{P}}$.

Then, we can obtain the projected area S_{p} by computing the convex hulls of $\mathbb{A}_{\mathrm{P}}$ and $\mathbb{B}_{\mathrm{P}}$ if $\mathbb{A}_{\mathrm{P}}$ and $\mathbb{B}_{\mathrm{P}}$ are convex sets. Computing the convex hull is an effective way to obtain the area of a planar region occupied by a series of 2-dimensional discrete points or the volume of a cavity occupied by a series of 3-dimensional discrete points [100]. The convex hull of a set of discrete points is the convex polygon with the minimum volume containing all these points, and it can be computed by many algorithms, such as [101, 102]. We denote the area of projected regions corresponding to the ELAA and indoor blockages as A_{p} and B_{p}, and the projected area can be obtained by $S_{\mathrm{p}}=A_{\mathrm{p}}-B_{\mathrm{p}}$ with the impact of indoor blockages and $S_{\mathrm{p}}=A_{\mathrm{p}}$ without the impact of indoor blockages. Since points in $\mathbb{A}_{\mathrm{P}}$ or $\mathbb{B}_{\mathrm{P}}$ are not on the

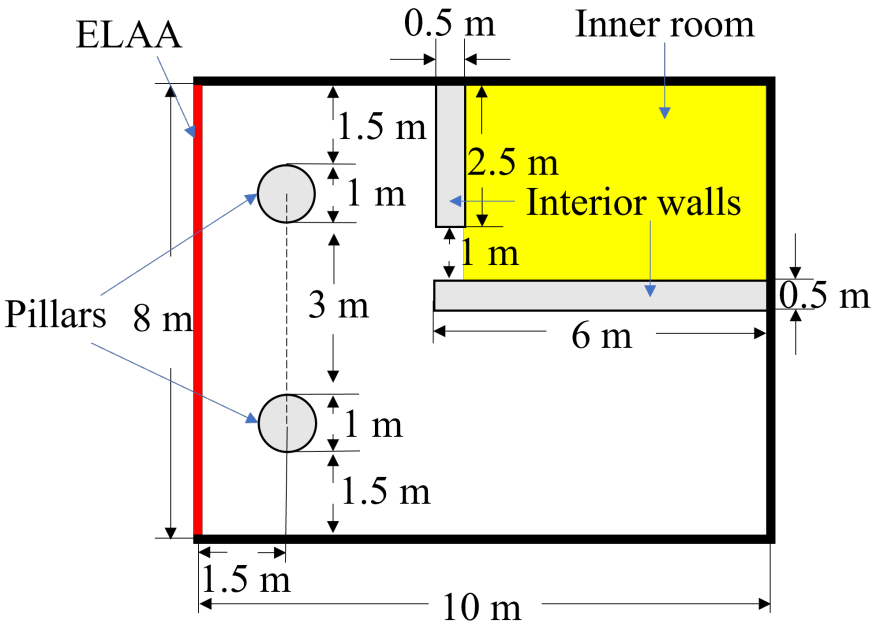

Fig. 4.4 Floor plan 1: The example room for the BWP evaluation.

same plane, we cannot directly obtain the area of the region consisting of these points by convex hulls. One effective method is to add the coordinates of the user into the set $\mathbb{A}_{\mathrm{P}}$ or $\mathbb{B}_{\mathrm{P}}$ and compute the volume of the spherical cones corresponding to different projected regions. The volume of each spherical cone is denoted by V_{array} and V_{blockage}, respectively. According to the relationships between the superficial area and the volume of a sphere, the total power received from the ELAA in different scenarios can be calculated by the equations

$$P_{\mathrm{B}}(\mathbf{u}) = \frac{3\left(V_{\mathrm{array}} - V_{\mathrm{blockage}}\right)}{4\pi} P_{\mathrm{t}}, \tag{4.13}$$

$$P_{\mathrm{O}}(\mathbf{u}) = \frac{3V_{\mathrm{array}}}{4\pi} P_{\mathrm{t}}. \tag{4.14}$$

Then, we can calculate $g_{\mathrm{P}}(\mathbf{u})$ and $\mathbb{E}\left[g_{\mathrm{P}}(\Omega_{\mathrm{u}})\right]$ using equations (4.1) and (4.2). The process of obtaining the achievable power gain is presented in Algorithm 1.

4.4 Results

In this section, we provide a specific room layout and placement of indoor blockages as an example for the BWP evaluation and analysis. We consider a rectangular room whose floor plan is shown in Fig. 4.4. In this room, a rectangular inner room is formed by two interior walls, and we have two round pillars as indoor blockages. The heights of pillars and interior walls are the same as the room's height, which is $H = 3$ m, and the height of the user is $z_{\mathrm{u}} = 1.5$ m. We set the transmitted power as $P_{\mathrm{t}} = 1$ W.

We first analyze the impact of the dimension of the ELAA on $g_{\mathrm{P}}(\mathbf{u})$. The ELAA has the same height as the room, so that the ELAA width can represent the ELAA dimension. The total power transmitted from the ELAA keeps invariable, hence the transmitted power per unit area decreases with the increasing ELAA width inverse proportionally. We can obtain the spatial distribution of $g_{\mathrm{P}}(\mathbf{u})$ shown by Fig. 4.5 and the empirical cumulative distribution function (ECDF) of $g_{\mathrm{P}}(\mathbf{u})$ with different ELAA widths shown by Fig. 4.6. We can observe that with a small-sized ELAA, $g_{\mathrm{P}}(\mathbf{u})$ is distributed bipolarly within the range of $[0,1]$. The reason is that the sizes of pillars are comparable to or larger than the ELAA dimension, if the user cannot fully receive the power transmitted by the ELAA, the signal received by the user will be completely blocked by indoor blockages. With the increase of the ELAA width, the region where the user is completely blocked is shrinking and the power gain is distributed more uniformly within the range of $[0,1]$. This is because the user can receive signals from a wider range of the angle of view (AoV) with the increasing array width and the sizes of indoor blockages are smaller than the AoV range, it is more difficult for indoor blockages to completely block the signal transmitted to the user. Meanwhile, as shown in Fig. 4.5, there is always a region where the user cannot receive the signal due to the inner wall regardless of the ELAA width. The results indicate that ELAAs outperform small-scale antenna arrays in resisting the negative impact of small-sized indoor blockages, such as pillars and human bodies, but have a limited effect facing large-sized indoor blockages, such as walls.

We also analyze the impact of the indoor blockage separation and the distance to the ELAA of small-sized indoor blockages on $\mathbb{E}[g_{\mathrm{P}}(\Omega_{\mathrm{u}})]$. To avoid inaccuracy caused by the influence of the inner room, we only consider two pillars in an empty rectangular room, as

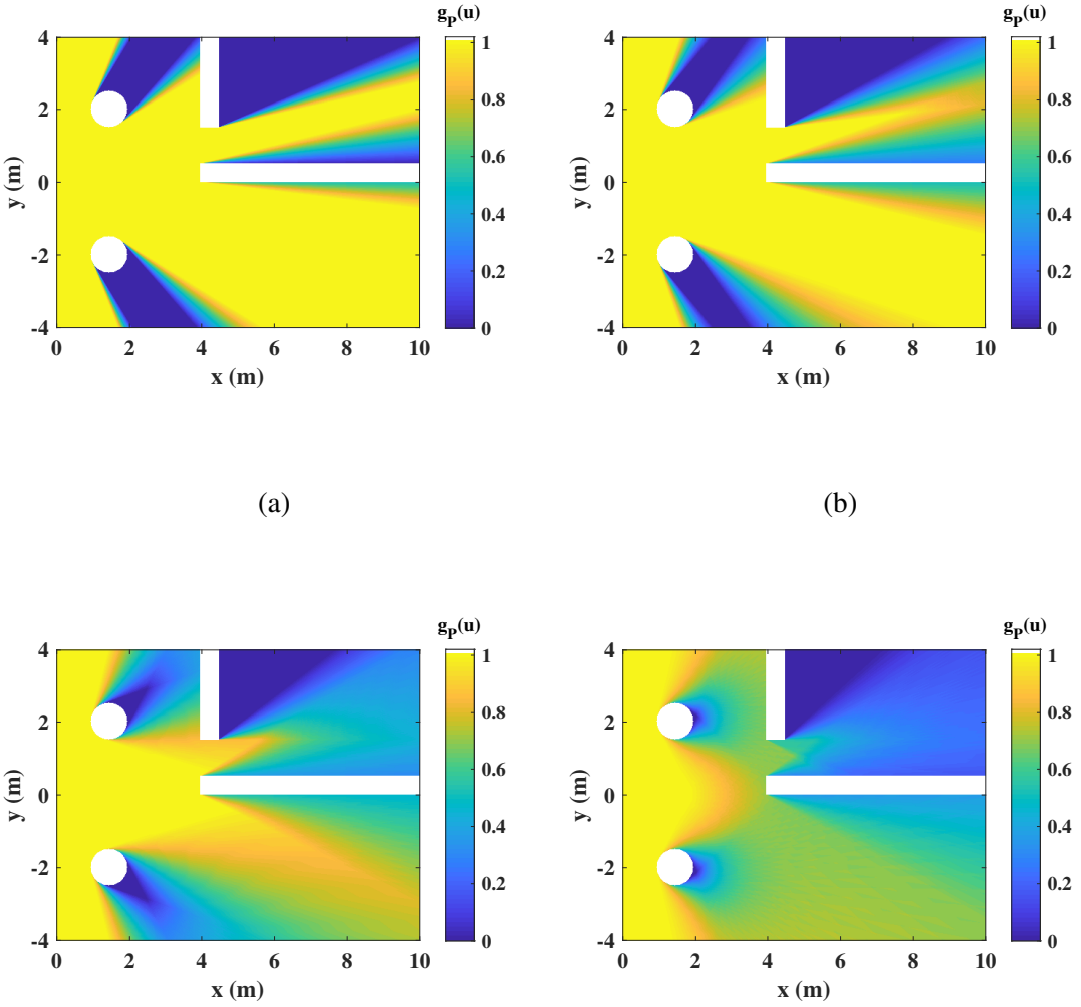

Fig. 4.5 The spatial distribution of $g_{\mathrm{P}}(\mathbf{u})$ with different ELAA widths based on Floor plan 1: (a) The ELAA width is 1 m; (b) The ELAA width is 2 m; (c) The ELAA width is 4 m; (d) The ELAA width is 8 m.

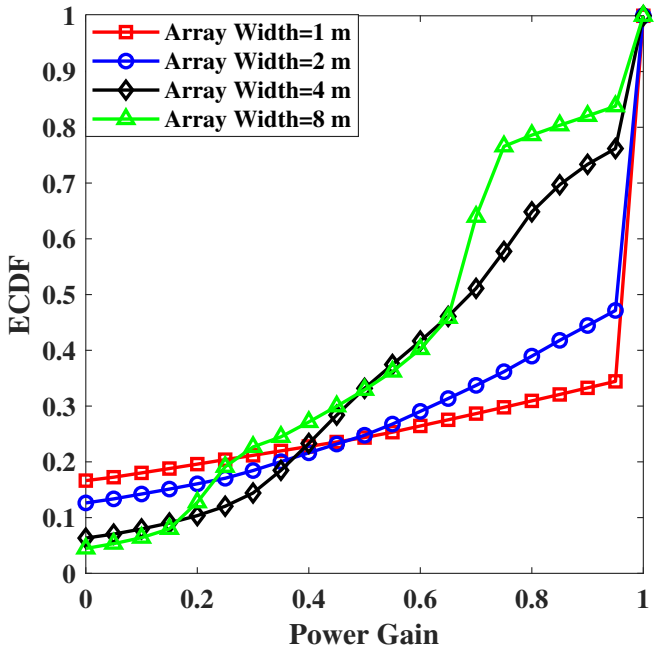

Fig. 4.6 The ECDFs of the power gain with different ELAA widths based on Floor plan 1.

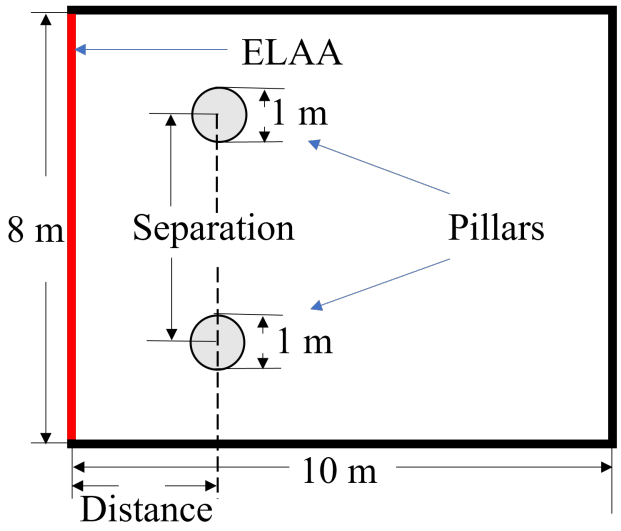

Fig. 4.7 Floor plan 2: Two round pillars are placed in an empty room for the analysis of impact of the distance to the ELAA and the separation between pillars.

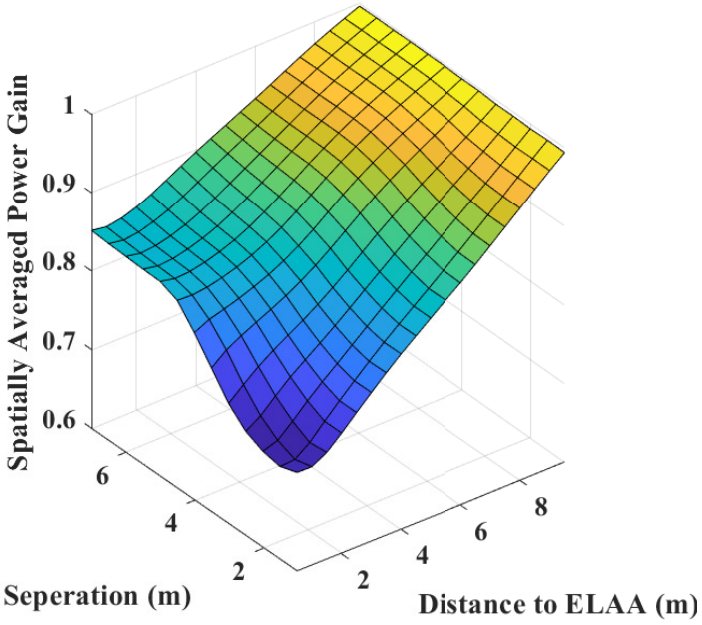

Fig. 4.8 The analysis of the impact of the distance of indoor blockages to the ELAA and the indoor blockage separation on the spatially averaged power gain based on Floor plan 2.

shown in Fig. 4.7. Fig. 4.8 shows $\mathbb{E}\left[g_{\mathrm{P}}\left(\Omega_{\mathrm{u}}\right)\right]$ with the increasing indoor blockage separation and the distance to the ELAA. The results show that a higher $\mathbb{E}\left[g_{\mathrm{P}}\left(\Omega_{\mathrm{u}}\right)\right]$ can be achieved as indoor blockages moving further away from the ELAA because the user's received power is less likely to be reduced by indoor blockages. In addition, $\mathbb{E}\left[g_{\mathrm{P}}\left(\Omega_{\mathrm{u}}\right)\right]$ increases with the increase of the indoor blockage separation, which reveals that small-sized indoor blockages placed sparsely have less impact on the user's received power from the ELAA. A higher power gain can be achieved by moving small-sized indoor blockages away from the ELAA compared to sparsely placing small-sized indoor blockages.

Based on the above results, we place pillars more sparsely and deploy the ELAA on the wall away from the pillars as shown in Fig. 4.9. In this case, the ELAA can directly serve users in the inner room without the blockage of walls. To obtain a higher power gain, we analyze the impact of the AR of the inner room on the power gain with the area of the inner room keeping unchanged. Fig. 4.10 shows $\mathbb{E}\left[g_{\mathrm{P}}\left(\Omega_{\mathrm{u}}\right)\right]$ with the increasing inner room AR, and we also compare $\mathbb{E}\left[g_{\mathrm{P}}\left(\Omega_{\mathrm{u}}\right)\right]$ of different inner room ARs with $\mathbb{E}\left[g_{\mathrm{P}}\left(\Omega_{\mathrm{u}}\right)\right]$ of the

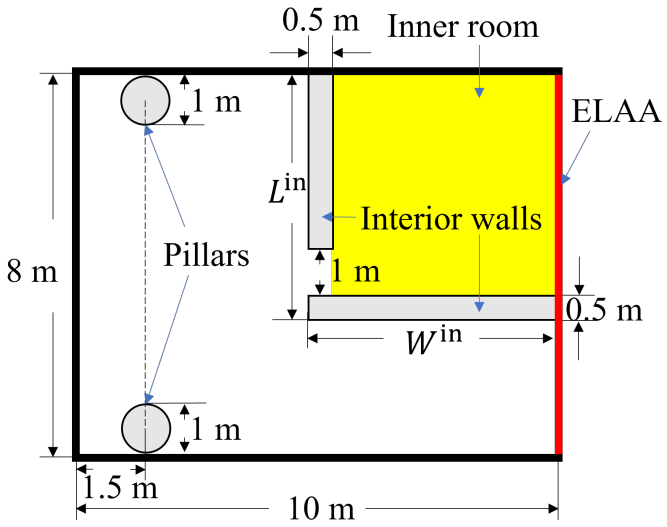

Fig. 4.9 Floor plan 3: The ELAA is deployed on the wall away from the pillars and the impact of the AR of the inner room on the power gain can be analyzed.

original room design. The results show that the average value of the achievable power gain can be monotonically improved by increasing the AR of the inner room. We can accordingly provide a room modification scheme as shown in Fig. 4.11. Compared to the original room design with a $\mathbb{E}\left[g_{\text{P}}\left(\Omega_{\text{u}}\right)\right]$ of 0.5897, our room modification scheme can improve spatially averaged power gain to 0.6664, achieving a performance improvement of 13%.

4.5 Summary

In this chapter, a BWP evaluation approach based on indoor ELAA networks is proposed for the design of future wireless-friendly buildings, so that architects can optimize the building design based on the BWP of the building under design. A room modification scheme is exemplified for an example room based on the analysis. Numerical results show that the room modification scheme can achieve a 13% spatially averaged power gain improvement, which can demonstrate the potential of BWP evaluation and optimization. Three main suggestions for the design of future wireless-friendly buildings based on the analysis: 1) indoor blockages should be placed sparsely and away from the ELAA; 2) moving indoor blockages away from the ELAA can achieve a higher BWP compared with placing indoor blockages more sparsely;

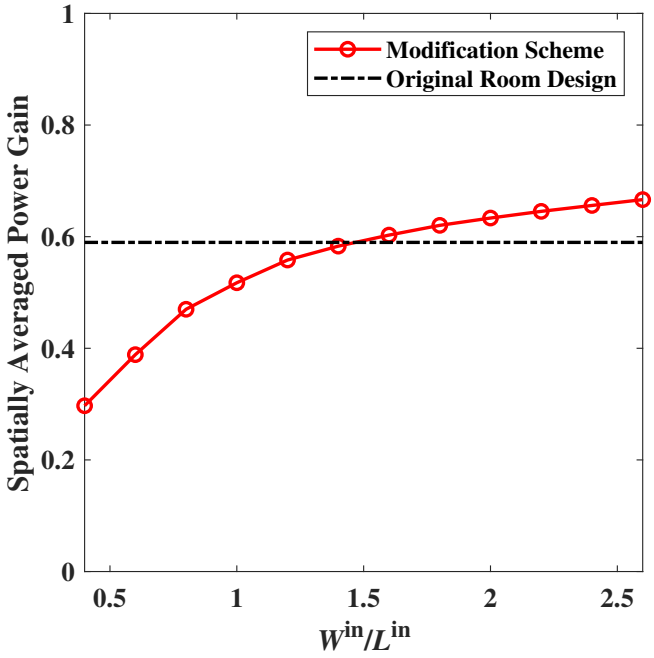

Fig. 4.10 The spatially averaged power gain with the increasing inner room AR for the room modification scheme and the comparison to the spatially averaged power gain of the original room under design.

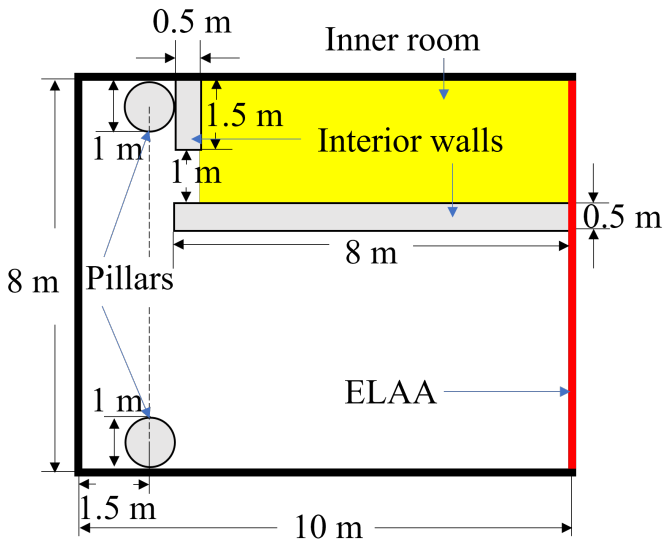

Fig. 4.11 Floor plan 4: The room modification scheme.

3) a portion of the ELAA should be deployed in the inner rooms when inner rooms exist in the room under design, and in this case, inner rooms should be designed narrower and longer from the view of the ELAA.

Chapter 5

BWP evaluation with joint consideration of indoor ELAA networks and D2D communication

Overview

As two key wireless communication technologies, D2D communication and ELAAs are likely to serve indoor users jointly. Considering the cooperative signal transmission of these two technologies, an ELAA network assisted by D2D relays architecture is proposed in this chapter to extend the coverage range of ELAA systems in indoor scenarios. Besides, a BWP evaluation method based on such networks is proposed. The spatially averaged coverage rate is adopted as the metric for the BWP evaluation, and the corresponding computation method is provided. By analyzing the impact of building parameters on the spatially averaged coverage rate, it is illustrated that the loss of spatially averaged coverage rate due to unsuitable building design exceeds 34%, which demonstrates the significance of the wireless-friendly buildings.

5.1 Introduction

As two key technologies in the B5G and sixth generation (6G) era, ELAA systems and D2D networks are likely to be deployed indoors to serve indoor mobile users jointly in the future. On the one hand, ELAAs are expected to be deployed indoors to provide higher data rate and coverage performance to indoor users because of the larger array dimension than massive MIMO networks. On the other hand, as an essential technology of IoT, D2D technology can also be widely applied indoors to enable direct connections between indoor smart devices for lower indoor network load and transmission latency. Consequently, it is crucial to consider the signal cooperative transmission achieved by these two types of wireless networks.

We have observed in the previous chapter that when ELAAs operate in mmWave, ELAAs have a limited effect in resisting the negative impact of large-sized indoor blockages, such as walls. In this case, there are always regions where users cannot receive signals from the ELAA due to indoor blockages. To solve this problem, D2D communications can provide relays to compensate for these uncovered regions and provide higher coverage and received power for indoor mobile users [27].

Similar to indoor D2D networks discussed in Chapter 3 and indoor ELAA networks discussed in Chapter 4, the performance of such indoor ELAA networks assisted by D2D relays is also significantly impacted by the indoor wireless propagation environment. The reasons can be summarized as follows: 1) the performance of such indoor relay-assisted ELAA network depends on the coverage performance provided to relay nodes by ELAAs, which is impacted by the building layout and has been analyzed in the previous chapter; 2) operating in mmWave, signals transmitted by relays can be blocked by indoor blockages, which is impacted by the placement of indoor blockages [92]; 3) the building layout impacts the density of relays around the user, further determining the coverage extension ability of D2D relays [29].

The BWP should be evaluated based on indoor relay-assisted ELAA networks for the design and construction of future wireless-friendly buildings. The corresponding evaluation approaches are necessary because the BWP can quantitatively measure how buildings are wireless-friendly to indoor relay-assisted ELAA networks. The BWP evaluation approach

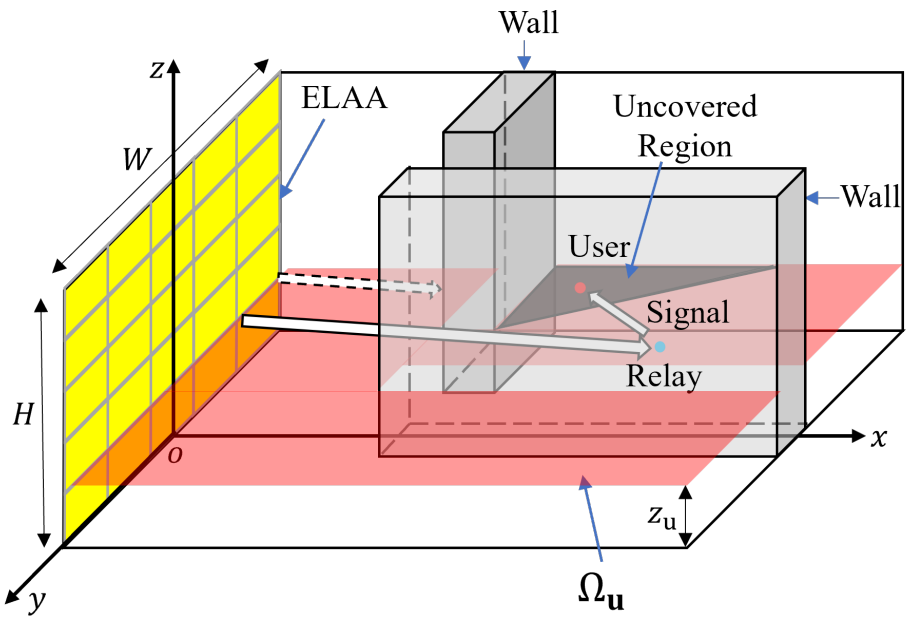

Fig. 5.1 The system model of the indoor relay-assisted ELAA network within an example building layout.

for indoor relay-assisted ELAA networks can provide architects with an intuitive value as a reference to optimize the building under design to wireless-friendly buildings. The BWP evaluation approach should satisfy two main requirements: 1) the BWP evaluation approach should be applied to various building layouts and indoor blockage shapes; 2) the approach should quickly calculate the BWP, otherwise, the building design will be inefficient. To satisfy the above requirements, we design a BWP evaluation approach for indoor relay-assisted ELAA networks in this chapter.

5.2 System model

In this chapter, we mainly focus on the coverage performance of the indoor relay-assisted ELAA network and adopt the coverage rate as the primary metric for the BWP evaluation. Similar to the previous chapter, we consider a single-user downlink scenario and evaluate the BWP from the user's view. Considering the wireless network operating in mmWave, we focus more on LoS links between the ELAA, relays and the user. In this case, the user may not receive the signal from the ELAA or relays because of indoor blockages, such as walls,

furniture and human bodies. Thus, the coverage rate is an important metric to measure how the building is suitable to the indoor relay-assisted ELAA network.

We denote the region where the user terminal and D2D relays may be located as Ω_{u}. Ω_{u} is determined by both the building layout and the placement of indoor blockages. The power received from the ELAA or relays by the user at the location $\mathbf{u}$ can be denoted by $P_{\mathrm{r}}(\mathbf{u})$. Then, we can define the coverage rate when the user is located at $\mathbf{u}$ as the probability that the received power $P_{\mathrm{r}}(\mathbf{u})$ is higher than the received power threshold T. The coverage rate is given by

$$R_{\mathrm{c}}(\mathbf{u}) = \mathbb{P}\left[P_{\mathrm{r}}(\mathbf{u}) \geq T\right]. \tag{5.1}$$

The threshold T can be treated as the lowest power can be detected by the receiver. We can also obtain the spatially averaged coverage rate within Ω_{u} as

$$R_{\mathrm{c}}(\Omega_{\mathrm{u}}) = \mathbb{E}_{\mathbf{u}\in\Omega_{\mathrm{u}}}\left[R_{\mathrm{c}}(\mathbf{u})\right]. \tag{5.2}$$

The spatially averaged coverage rate $R_{\mathrm{c}}(\Omega_{\mathrm{u}})$ can also be defined as the proportion of the region where the user can receive a power greater than the threshold T within Ω_{u}. The term Ω_{u} is determined by both the building layout and the placement of the indoor blockages. $R_{\mathrm{c}}(\Omega_{\mathrm{u}})$, which is a function of Ω_{u}, can represent the QoS can be provided to the user by the indoor relay-assisted ELAA network in a specific building.

To obtain the coverage rate, we present the system model below. We undertake the BWP evaluation in a rectangular room with an arbitrary layout, which is exemplified in Fig 5.1. We assume that the room has a size of $L \times W \times H$. To avoid indoor BSs equipped with ELAA occupying the most of the room space, rendering the basic room functions unusable, we deploy the ELAA on an interior wall with the size of $W \times H$. Then, we take the wall deployed by the ELAA as the yOz-plane and the intersection of the central axis with the bottom edge of the ELAA as the origin to construct the spatial coordinate system, as shown in Fig. 5.1. The location of the user terminal can be represented by $\mathbf{u} = (x_{\mathrm{u}}, y_{\mathrm{u}}, z_{\mathrm{u}})$. For simplicity, we assume that the user has an invariable height, i.e., z_{u} is unchanged, and we have Ω_{u} as the

2-dimensional red plane in Fig. 5.1. Nevertheless, our BWP evaluation approach can be employed in a 3-dimensional space.

We consider an indoor ELAA network assisted by D2D relays which is deployed inside the room under evaluation. The setup of the ELAA is the same as that of the previous chapter and we denote the power received from the ELAA by the user at the location $\mathbf{u}$ as $P_{\mathrm{r,ELAA}}(\mathbf{u})$. On the other hand, the D2D part of the network includes N_{relay} potential relays. In this chapter, we call all devices in the network as potential relays because each device has the probability of relaying signals to the user, depending on their locations. Potential relays are randomly distributed within Ω_{u} waiting to forward signals to the user when the user is not covered by the ELAA. Potential relays that do not forward the signal to the user will be inactive to save energy. We denote the locations of potential relays as $\mathbf{r}_j$ for $j = 1, ..., N_{\mathrm{relay}}$. Since the transmission is operated in mmWave, we only consider the path-loss and ignore the small-scale fading. We assume that each potential relay has the same transmit power, which is denoted by $P_{\mathrm{t,relay}}$. If the j-th potential relay can act as a relay, the user can receive the power from the j-th potential relay at the location $\mathbf{u}$ which is represented as

$$P_{\mathrm{r,relay}}\left(\mathbf{u}, \mathbf{r}_j\right) = P_{\mathrm{t,relay}} ||\mathbf{u} - \mathbf{r}_j||^{-2}; \tag{5.3}$$

where $||\mathbf{u} - \mathbf{r}_j||$ is the distance between the user and the j-th potential relay.

Depending on whether the user is covered by the ELAA or the relays, the user may be in three cases, which are summarized as follows.

1) Case 1: When the user is in Case 1, the user can receive the signal from the ELAA with a power higher than the threshold T. We can obtain $P_{\mathrm{r,ELAA}}(\mathbf{u})$ by Algorithm 1, and we have

$$P_{\mathrm{r}}(\mathbf{u}) = P_{\mathrm{r,ELAA}}(\mathbf{u}) \geq T. \tag{5.4}$$

2) Case 2: In this case, the user cannot receive the signal from the ELAA due to indoor blockages or severe path loss, i.e., $P_{\mathrm{r,ELAA}}(\mathbf{u}) < T$, and the user should receive the signal via relays. The primary condition for the j-th potential relay to forward the signal to the user is that the j-th potential relay can be covered by the ELAA, i.e., the j-th potential relay receives

a power from the ELAA higher than the threshold, which is given by $P_{\mathrm{r,ELAA}}\left(\mathbf{r}_j\right) \geq T$. We use $\mathbb{Q}$ to denote the set of the index of all potential relays whose received power from the ELAA are higher than the threshold T. Among all potential relays in the set $\mathbb{Q}$, the user select the potential relay which can provide the highest received power which is higher than the threshold T to receive the forwarded signal. The user's received power from relays is given by

$$P_{\mathrm{r}}\left(\mathbf{u}\right) = \max\left\{P_{\mathrm{r,relay}}\left(\mathbf{u},\mathbf{r}_k\right)\right\} \geq T, k \in \mathbb{Q}. \tag{5.5}$$

3) Case 3: In this case, the user is not covered by both the ELAA and the relays. The reason may be that both $P_{\mathrm{r,ELAA}}\left(\mathbf{u}\right)$ and $\max\left\{P_{\mathrm{r,relay}}\left(\mathbf{u},\mathbf{r}_k\right)\right\}$ for $k \in \mathbb{Q}$ are lower than the power threshold T, or that $\mathbb{Q}$ is an empty set.

When the user is randomly located within Ω_{u}, the probabilities of these three cases are determined by building layouts. We can define the probabilities that the user is in different cases as $p_{\mathrm{case1}}\left(\Omega_{\mathrm{u}}\right)$, $p_{\mathrm{case2}}\left(\Omega_{\mathrm{u}}\right)$ and $p_{\mathrm{case3}}\left(\Omega_{\mathrm{u}}\right)$, respectively. Our aim is to improve $p_{\mathrm{case1}}\left(\Omega_{\mathrm{u}}\right)$ and $p_{\mathrm{case2}}\left(\Omega_{\mathrm{u}}\right)$ by optimizing the building layout. It should noted that in Case 2, the employment of potential relays can lead a higher cost compared with the scenario where only the ELAA is deployed indoors.

5.3 Performance analysis

In this section, we present an approach to quickly obtain the spatially averaged coverage rate $R_{\mathrm{c}}\left(\Omega_{\mathrm{u}}\right)$ for the BWP evaluation.

Before we begin obtaining $R_{\mathrm{c}}\left(\Omega_{\mathrm{u}}\right)$, we need to calculate the spatial distribution of the user's received power from the ELAA within Ω_{u} by Algorithm 1. Then, we can obtain the coverage region in the building based on the spatial distribution of the user's received power. Since the power $P_{\mathrm{r,ELAA}}\left(\mathbf{u}\right)$ is a deterministic value, the coverage rate $R_{\mathrm{C}}\left(\mathbf{u}\right)$ equals to 1 when $P_{\mathrm{r,ELAA}}\left(\mathbf{u}\right) \geq T$. This not only helps us identify whether the user is in Case 1, but can also help us determine which potential relay is in $\mathbb{Q}$.

If the user is not covered by the ELAA, i.e., $P_{\mathrm{r,ELAA}}\left(\mathbf{u}\right) < T$, we need to calculate the probability that the user can be covered by relays, which represents $R_{\mathrm{C}}\left(\mathbf{u}\right)$. We use the Monte

Carlo method to obtain $R_{\mathrm{c}}(\mathbf{u})$. In the Monte Carlo method, we calculate the probability that the user is covered by relays within a specific building from experimental results obtained by a large number of random trails. The probability is approximately equal to the frequency of the coverage in random trails according to the law of large numbers.

The signal propagation in D2D links might be completely blocked by indoor blockages when operating in mmWave, unlike that in indoor ELAA networks where the blockage effect on the signal propagation is only reduced due to the large ELAA dimension. Thus, $R_{\mathrm{c}}(\mathbf{u})$ is significantly determined by indoor blockages. However, it is hard to calculate the probability distribution of the distance between the user and the relays within different building layouts by a uniform model due to the variety of building layouts. Facing this issue, we use the Monte Carlo method to obtain $R_{\mathrm{c}}(\mathbf{u})$. We randomly obtain the locations of N_{relay} potential relays in each random trial, represented by the set $\mathbf{D} = \left\{\mathbf{r}_1, \mathbf{r}_2, ..., \mathbf{r}_{N_{\mathrm{relay}}}\right\}$. Then we judge whether the user is covered in this random trial by judging whether there is a potential relay in $\mathbf{D}$ can cover the user.

For the j-th potential relay, whether it can cover the user should achieve following three conditions simultaneously: 1) the j-th potential relay is covered by the ELAA; 2) there is no indoor blockages between the user and the potential relay because in the mmWave band, when the link between the user and the potential relay is blocked, the user will not be able to receive the signal from the potential relay; 3) the user receives a power higher than the power threshold from the potential relay. We provide the judgment methods for each of the three conditions below.

Condition 1: the j-th potential relay is covered by the ELAA

When the j-th potential relay can be covered by the ELAA, its received power from ELAA is greater than the threshold T. The received power can be obtained by Algorithm 1. When the j-th potential relay has $P_{\mathrm{r,ELAA}}\left(\mathbf{r}_j\right) \geq T$, it achieves Condition 1.

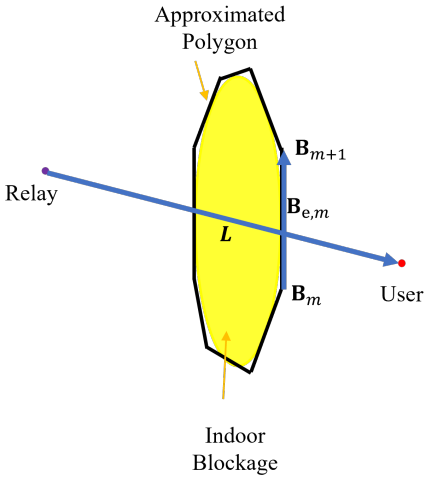

Fig. 5.2 Judging whether the j-th potential relay achieves Condition 2 by judging whether the line segment with the user and the j-th potential relay as endpoints intersects the space occupied by indoor blockages.

Condition 2: there is no indoor blockages between the user and the j-th potential relay

The core idea of judging whether the j-th potential relay achieves Condition 2 is to judge whether the line segment with the user and the j-th potential relay as endpoints intersects the space occupied by indoor blockages by the cross product method, as shown by Fig. 5.2. For an arbitrarily shaped indoor blockage, we approximate its shape as a polyhedron. If the height of the indoor blockage equals to the room height, the region occupied by the indoor blockage can be approximated to a polygon. Whether the line segment intersects the indoor blockage is determined by whether the line segment intersects any edge of the polyhedron or the polygon. We construct the vectors $\mathbf{L} = \mathbf{u} - \mathbf{r}_j$. We take the polygon case as an example here, and denote each vertex of the polygon as $\mathbf{B}_m$ for $m = 1, ..., M$ clockwise (or anticlockwise), where M is the number of the vertex of the polygon. Then, we can obtain vectors

$$\mathbf{B}_{\mathrm{e},m} = \mathbf{B}_{m+1} - \mathbf{B}_m, \tag{5.6}$$

for $m = 1, ..., M-1$, and the vector

$$\mathbf{B}_{\mathrm{e},M} = \mathbf{B}_1 - \mathbf{B}_M. \tag{5.7}$$

Meanwhile, we can also obtain vectors

$$\mathbf{B}_{\mathrm{u},m} = \mathbf{u} - \mathbf{B}_m, \quad \mathbf{B}_{\mathrm{r},m} = \mathbf{r}_j - \mathbf{B}_m. \tag{5.8}$$

For the edge vector $\mathbf{B}_{\mathrm{e},m}$, when we have

$$(\mathbf{L} \times \mathbf{B}_{\mathrm{u},m}) \cdot (\mathbf{L} \times \mathbf{B}_{\mathrm{u},m+1}) < 0, (\mathbf{B}_{\mathrm{u},m} \times \mathbf{B}_{\mathrm{e},m}) \cdot (\mathbf{B}_{\mathrm{r},m} \times \mathbf{B}_{\mathrm{e},m}) < 0, \tag{5.9}$$

the line segment intersects the edge $\mathbf{B}_{\mathrm{e},m}$.

By judging whether the line segment does not intersect with all the edges, we can judge whether there is an indoor blockage between the user and the j-th relay, and we can judge whether the j-th relay achieves Condition 2.

Condition 3: the user receives a power higher than the power threshold from the j-th potential relay

Based on (5.3), if the received power from the j-th potential relay is higher than the power threshold, we have

$$||\mathbf{u} - \mathbf{r}_j|| \leq \sqrt{\frac{P_{\mathrm{t,relay}}}{T}}. \tag{5.10}$$

Thus, once the distance between the user and the j-th potential relay is lower than the distance threshold $\sqrt{\frac{P_{\mathrm{t,relay}}}{T}}$, the j-th potential relay achieves Condition 3.

In summary, if there exists any potential relay achieving the above three conditions simultaneously, we consider the user is covered by relays in this random trail. Then, we can calculate the coverage probability $R_{\mathrm{c}}(\mathbf{u})$ and the spatial distribution of $R_{\mathrm{c}}(\mathbf{u})$ within the building Ω_{u}.

With the spatial distribution of $R_{\mathrm{c}}(\mathbf{u})$, we can calculate the spatially averaged coverage rate of the indoor relay-assisted ELAA network within the building by (5.2). The process to obtain the spatially averaged coverage rate is summarized in Algorithm 2.

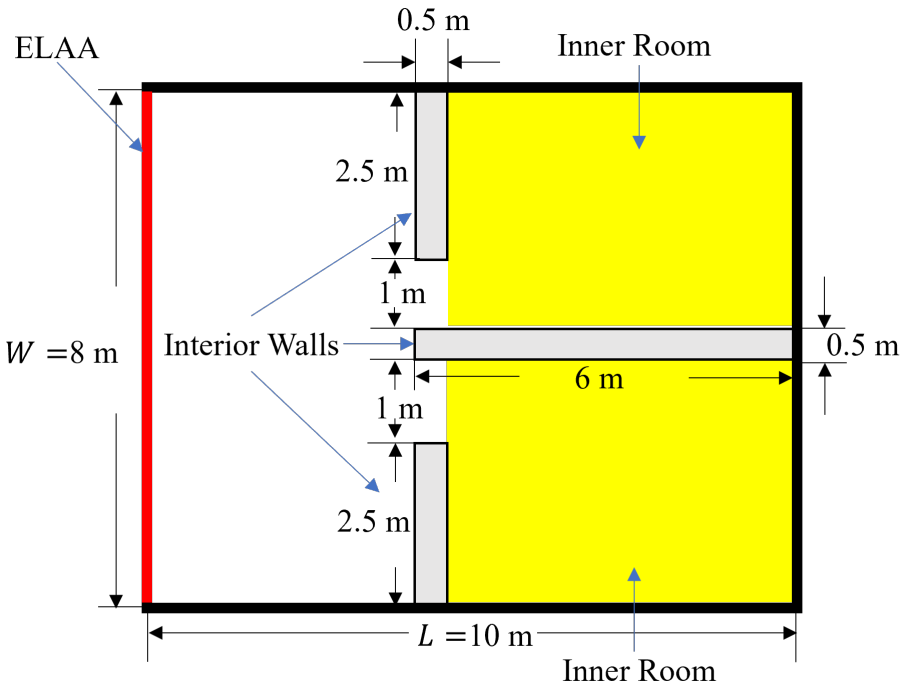

Fig. 5.3 An example room for the BWP evaluation with the indoor relay-assisted ELAA network.

5.4 Numerical results

In this section, we deploy the relay-assisted ELAA network in a specific room under design which is exemplified by the floor plan in Fig. 5.3. The room is rectangular and two inner rooms are formed by three interior walls in the room under design. We assume that the height of the ELAA is equal to the room's height, which is $H = 3$ m, so that we can represent the dimension of the ELAA by the ELAA's width. The total power transmitted from the ELAA keeps invariable, hence the transmitted power per unit area decreases with the increasing ELAA width inverse proportionally. As the height of the user is unchanged, we set it as $z_{\mathrm{u}} = 1.5$ m. Then, we can initially set the transmit power of the ELAA and devices as $P_{\mathrm{t,ELAA}} = 30$ dBm and $P_{\mathrm{t,relay}} = 20$ dBm, respectively. The received power threshold is set as $T = -30$ dBm for the analysis of the coverage rate $R_{\mathrm{c}}(\Omega_{\mathrm{u}})$ [29].

We first analyze the impact of the ELAA dimension on the coverage rate. In our setup, there are 10 devices may act as relays. Fig.5.4 shows $p_{\mathrm{case1}}(\Omega_{\mathrm{u}})$, $p_{\mathrm{case2}}(\Omega_{\mathrm{u}})$, $p_{\mathrm{case3}}(\Omega_{\mathrm{u}})$ and

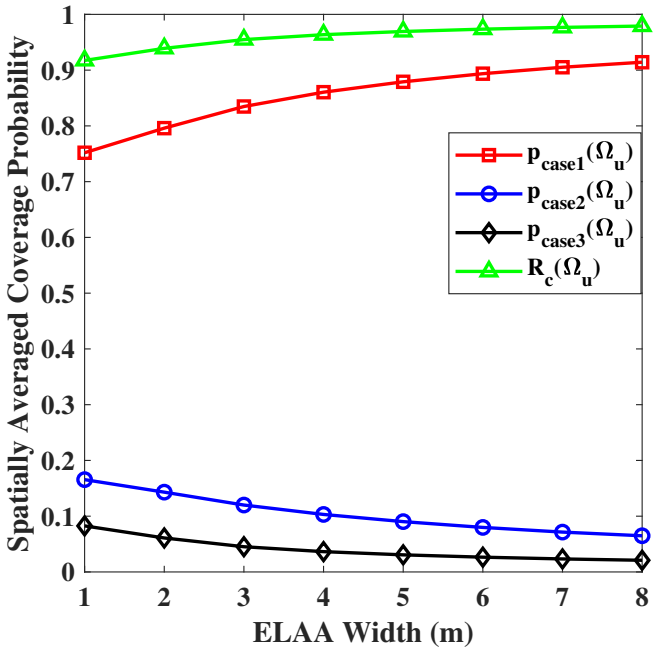

Fig. 5.4 The spatially averaged coverage rate with the increasing width of the ELAA.

$R_{\mathrm{c}}(\Omega_{\mathrm{u}})$ with different ELAA widths in the building under design. According to the definition of $p_{\mathrm{case1}}(\Omega_{\mathrm{u}})$, $p_{\mathrm{case2}}(\Omega_{\mathrm{u}})$ and $p_{\mathrm{case3}}(\Omega_{\mathrm{u}})$, we have $R_{\mathrm{c}}(\Omega_{\mathrm{u}}) = p_{\mathrm{case1}}(\Omega_{\mathrm{u}}) + p_{\mathrm{case2}}(\Omega_{\mathrm{u}})$. We can observe from Fig. 5.4 that $p_{\mathrm{case1}}(\Omega_{\mathrm{u}})$ increases with the increase of the ELAA width. Based on the results we obtain in the previous chapter, ELAAs with a large dimension can effectively resist the negative influence of indoor blockages on the signal propagation, hence the ELAA can provide higher coverage rate with the increasing width. Meanwhile, $p_{\mathrm{case2}}(\Omega_{\mathrm{u}})$ reduces with the increase of the ELAA width. In the indoor relay-assisted network, the user is given a higher priority to connect to ELAA, and the user connects to D2D relays only if the user cannot be covered by the ELAA. The reduction of $p_{\mathrm{case2}}(\Omega_{\mathrm{u}})$ is mainly due to the improvement of $p_{\mathrm{case1}}(\Omega_{\mathrm{u}})$. In addition, the increase of the coverage rate illustrates that the coverage rate of the indoor relay-assisted ELAA network is mainly provided by the ELAA.

To obtain an appropriate configuration of D2D relays in the network, we analyze the impact of the transmit power and the number of devices on $R_{\mathrm{c}}(\Omega_{\mathrm{u}})$, as shown in Fig. 5.5. In the analysis, we set the width of the ELAA to be 1 m to obtain an environment with

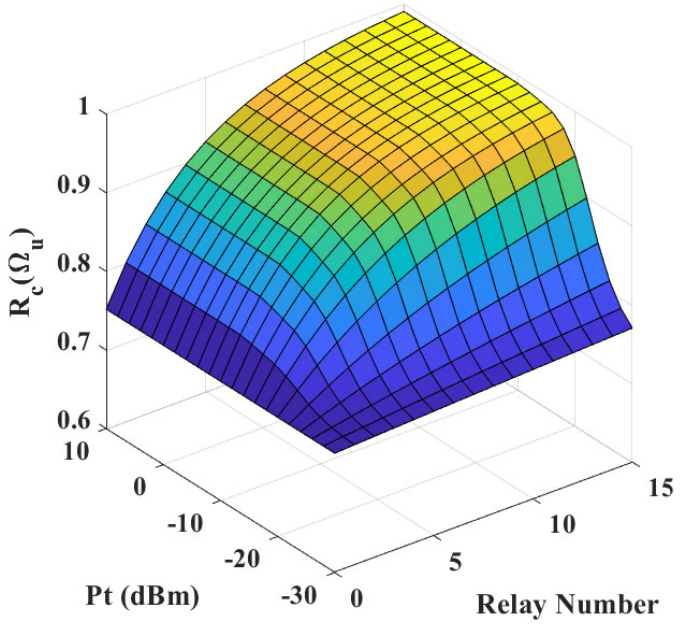

Fig. 5.5 $R_c\,(\Omega_u)$ versus the device transmit power and the number of devices.

a poor ELAA coverage. In this case, the effect of relays can be shown more clearly. We can observe from the figure that a higher $R_c\,(\Omega_u)$ can be achieved by both increasing the transmit power or the number of potential relays. When the transmit power exceeds the received power threshold less than about 25 dB, increasing the number of devices brings a slow increase of $R_c\,(\Omega_u)$. The reason is that low transmit power leads to an insufficient coverage capability of D2D relays. In this case, only when relays are located close to the user can they cover the user, and increasing the number of devices cannot effectively improve the coverage rate. In contrast, the improvement in $R_c\,(\Omega_u)$ achieved by increasing the transmit power saturates when the transmit power exceeds the received power threshold above 25 dB, which is much lower compared to general transmit power of D2D communications [29]. This is because limited by the size of the building we analyze, the coverage range of relays is beyond the building region in this case, and increasing the transmit power cannot further improve $R_c\,(\Omega_u)$. The coverage capability of relays is enhanced and the benefits brought by increasing the number of devices will exceed increasing the transmit power. Thanks to this

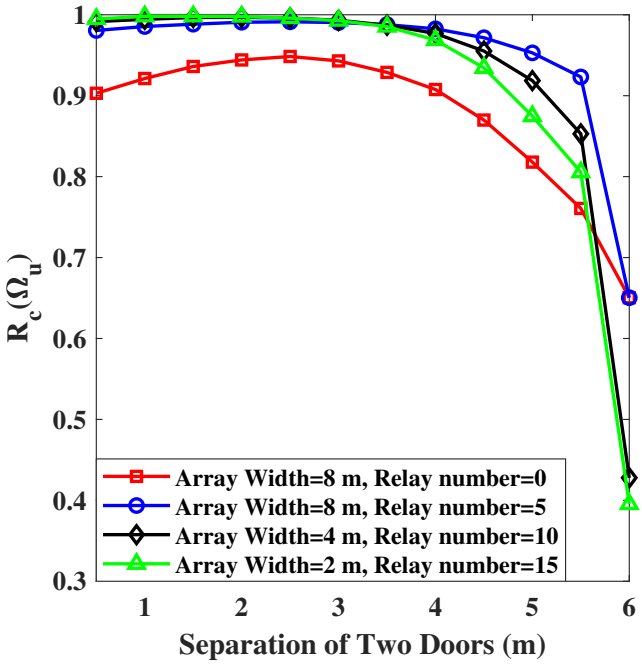

Fig. 5.6 The impact of the separation between two doors on the spatially averaged coverage rate under four network configurations.

short-range transmission, the devices do not need transmit with a high power, which reduces the energy consumption of each device and can extend the life of device batteries.

We also analyze the impact of building layout parameters, such as the positions of the doors of the two inner rooms shown in Fig. 5.3, on the spatially averaged coverage rate. We consider the separation between the two doors as the primary building layout parameter, analyze $R_{\mathrm{c}}(\Omega_{\mathrm{u}})$ with different door separations under four network configurations. The separation is defined as the closest distance between two doors. We can observe from Fig. 5.6 that as two doors moving toward the edges of the room, $R_{\mathrm{c}}(\Omega_{\mathrm{u}})$ of different configuration all decreases. This indicates that the best position of the door should be the center of the entire room rather than the center of each inner room. When the doors are placed near the edges of the room, the maximum spatially averaged coverage rate is 0.65 with the ELAA width as 8 m. Compared to the case where the doors are placed in the center of the room and $R_{\mathrm{c}}(\Omega_{\mathrm{u}})$ is 0.99, the loss of $R_{\mathrm{c}}(\Omega_{\mathrm{u}})$ exceed 34%. This demonstrates that performance of indoor wireless networks will suffer a great loss in unsuitable buildings.

5.5 Summary

In this chapter, an indoor relay-assisted ELAA network architecture was proposed to enhance the coverage performance of indoor ELAA networks, and the coverage rate was adopted as the metric for the BWP evaluation. To obtain the coverage rate of the network in a given building, a BWP evaluation approach was proposed based on the Monte Carlo method. Numerical results show that the coverage rate is determined by the ratio between the area of the ELAA and the wall instead of the absolute dimension of the ELAA. Besides, it has been observed that only a very low transmit power is required for D2D relays to provide sufficient coverage rate, and in this case, increasing the number of potential relays can achieve a higher coverage rate than increasing the D2D transmit power. By analyzing the impact of building layouts on the spatially averaged coverage rate, it is illustrated that the loss of spatially averaged coverage rate due to unsuitable building design exceeds 34%, which demonstrates that the performance of indoor wireless networks will suffer a great loss in unsuitable buildings.

Algorithm 2: The Achievable Spatially Averaged Coverage Rate Calculation Algorithm

Require: Ω_{u}: the region where the user may be located;
$\mathbb{B}$: the coordinates of points consisting indoor blockages;
$\mathbb{A}$: the coordinates of points consisting the ELAA;
N_{relay}: the number of potential relays;
S: the number of random trails;

Ensure: $R_{\mathrm{c}}(\Omega_{\mathrm{u}})$: the spatially averaged coverage rate;

Apply Algorithm 1 to obtain the spatial distribution of $P_{\mathrm{r,ELAA}}(\mathbf{u})$ within Ω_{u};
for Different user location **u do**
  if $P_{\mathrm{r,ELAA}}(\mathbf{u}) \geq T$ **then**
    $R_{\mathrm{c}}(\mathbf{u}) = 1$;
  else
    for Each random trail **do**
      Randomly generate N_{relay} locations within Ω_{u} for potential relays;
      Determine whether each potential relay can be covered by the ELAA based on $P_{\mathrm{r,ELAA}}(\mathbf{r}) \geq T$;
      Determine whether there is no indoor blockages between each potential relay and the user **u**;
      Determine whether each potential relay satisfies the condition $||\mathbf{u}-\mathbf{r}|| \leq \sqrt{\frac{P_{\mathrm{t,relay}}}{T}}$;
      if There exists potential relay satisfy the above three conditions **then**
        The user can be covered by relays in this random trail;
      else
        The user cannot be covered;
      end if
    end for
    Count the times the user is covered in S random trails and obtain the $R_{\mathrm{c}}(\mathbf{u})$;
  end if
end for
Calculate the spatially averaged coverage rate using equation (5.2);

Chapter 6

Conclusions and future work

6.1 Conclusions

This thesis mainly investigates the BWP evaluation based on several wireless communication networks that are likely to be widely deployed in indoor scenarios in the 6G era. By investigating the relationship between building layouts and in-building wireless networks, several BWP evaluation methods are proposed. Facing the conception of wireless-friendly buildings, which is still in its infancy, and the theoretical system of BWP in the early stage, this research promotes the perfection of BWP-related theories. This research is expected to provide guidance for architects to design and construct wireless-friendly buildings in the future.

In Chapter 3, the first systematic BWP evaluation approach for indoor D2D networks has been proposed. Considering that room walls can block out-of-room interference to improve the SINR and coverage performance, the blockage gain was adopted as the performance metric to evaluate the BWP. The blockage gain was defined as the SACP improvement due to the out-of-room interference blockage by the room walls and this metric takes into account the influence of both building layouts and building materials on indoor network performance. To calculate the blockage gain, three scenarios were defined: indoor scenario, open space scenario and general scenario. The SACP was derived for both the indoor scenario and outdoor scenario, respectively. Then, by analyzing the impact of five main parameters, i.e.,

wall penetration loss, aspect ratio, area, interfering device density and SINR threshold, on the blockage gain, the empirical formulas of the SACP in the general scenario and the blockage gain have been obtained for the fast calculation. It has been observed that the impacts of building layouts and materials on the blockage gain can be decoupled, which allows architects to quickly and accurately identify which factor has a higher impact on the blockage gain in the building design. Numerical results show that the maximal building layout blockage gain can be achieved when the product of the room area and the interfering device density is a specific value. The maximal blockage gain is determined by the building AR. In this case, the SACP of the network can be improved by at least 0.1 compared with the open space scenario.

In Chapter 4, a BWP evaluation approach was proposed for indoor ELAA networks. The performance of ELAA systems is mainly determined by VRs, which is determined by blockages in indoor scenarios. Hence, the concept of achievable power gain, which was proposed in [8], was improved to suit indoor ELAA networks and adopted as the primary metric to evaluate the BWP. The achievable power gain can measure the impact of indoor blockages on the total power received by the user from the ELAA. To calculate the achievable power gain of a given building, an algorithm based on convex hull was proposed. Different from conventional indoor blockage models which are limited by single building layout and indoor blockage shape, the proposed algorithm can quickly calculate the achievable power gain with arbitrary building layouts and placement of indoor blockages as the input. The BWP evaluation approach was applied for an example room and a room modification scheme was provided for a higher BWP. Numerical results show that the room modification scheme can achieve a 12.4 % spatially averaged power gain improvement. The analysis can provide three main suggestions for the design of future wireless-friendly buildings: 1) indoor blockages should be placed sparsely and away from the ELAA; 2) moving indoor blockages away from the ELAA can achieve a higher BWP compared with placing indoor blockages more sparsely; 3) a portion of the ELAA should be deployed in the inner rooms when inner rooms exist in the room under design, and in this case, inner rooms should be designed narrower and longer from the view of the ELAA.

In Chapter 5, a BWP evaluation approach was proposed for indoor relay-assisted ELAA networks. It has been observed in Chapter 4 that ELAAs have a limited effect in resisting negative impact of large-sized indoor blockages, such as walls, especially when ELAAs operate in mmWave. To solve this problem, indoor ELAA networks can be combined with D2D technology. Hence, in this research, an indoor relay-assisted ELAA network architecture was proposed to enhance the coverage performance of indoor ELAA networks, and the coverage rate was adopted as the metric for the BWP evaluation. To obtain the coverage rate of the network in a given building, a BWP evaluation approach was proposed based on the Monte Carlo method. Numerical results show that the coverage rate is determined by the ratio between the area of the ELAA and the wall instead of the absolute dimension of the ELAA. Besides, it has been observed that only a very low transmit power is required for D2D relays to provide sufficient coverage rate, and in this case, increasing the number of potential relays can achieve a higher coverage rate than increasing the D2D transmit power. By analyzing the impact of building layouts on the spatially averaged coverage rate, it is illustrated that the loss of spatially averaged coverage rate due to unsuitable building design exceeds 34%, which demonstrates that the performance of indoor wireless networks will suffer a great loss in unsuitable buildings.

6.2 Future work

In this section, the challenges and issues with future research directions of BWP evaluation systems are discussed.

- **Multiple wall penetration model**

  The BWP evaluation approaches investigated in this thesis are carried out in a single room. For the convenience of architects, BWP of the overall building interior layout and building external size should be evaluated. An inevitable problem in the BWP evaluation for the room layout within the building is multiple wall penetration. When the transmitter and receiver of a signal are distributed in different rooms, the signal may be propagated through multiple walls. Additionally, depending on the distance

and relative angle between these two rooms, the number of walls penetrated by the signal will also vary. This involves the probability distribution of the number of walls penetrated by the signal based on the building layout, which should be considered in the evaluation of indoor network performance. Multiple attenuation of signal strength due to the multiple wall penetration affects the evaluation of indoor network performance, and affect the accuracy of BWP evaluation. Thus, multiple wall penetration should be investigated in the future works.

- **3-dimensional (3D) multi-story building model**

  Existing BWP evaluation approaches are conducted in single-story buildings and ignore the height of the building. This model can simplify the BWP evaluation, but cannot take the building's storey height into the account of building design. Existing BWP evaluation approaches cannot help architects determine the building's story height. Therefore, the analysis should be extended to 3D building space to better approximate practical scenarios, and the multi-layer indoor network model can be adopted to incorporate the number of building stories into the BWP evaluation considerations.

- **BWP evaluation based on user behaviors**

  Existing BWP evaluation works assume that the user receives wireless communication services at all locations with the equal probability, hence, the user's location is assumed to be uniformly distributed in the 2D plane. However, the frequencies that users receive wireless communication services at different indoor locations vary significantly in practical scenarios, depending on the users' life habits and the functions arranged for different region in the building. Thus, users's behaviors should be considered in BWP evaluation to design wireless-friendly buildings where networks deployed can provide users higher QoS. Users' behaviors can be analyzed by fitting the user's indoor behavioral data, and the approximate probability distribution of users receiving wireless communication services at different locations can be obtained. The approximate probability distribution can be employed in future BWP evaluation.

References

[1] M. K. Müller, M. Taranetz, and M. Rupp, "Analyzing wireless indoor communications by blockage models," *IEEE Access*, vol. 5, pp. 2172–2186, 2016.

[2] Ericsson, "Ericsson mobility report," 2023, available: https://www.ericsson.com/en/reports-and-papers/mobility-report/reports/june-2023.

[3] M. Series, "Imt vision–framework and overall objectives of the future development of imt for 2020 and beyond," *Recommendation ITU*, vol. 2083, no. 0, 2015.

[4] K. Samdanis and T. Taleb, "The road beyond 5g: A vision and insight of the key technologies," *IEEE Network*, vol. 34, no. 2, pp. 135–141, 2020.

[5] Cisco, "Cisco vision: 5g-thriving indoors," *Cisco White Paper*, 2017.

[6] H. Obeidat, A. Alabdullah, E. Elkhazmi, W. Suhaib, O. Obeidat, M. Alkhambashi, M. Mosleh, N. Ali, Y. Dama, Z. Abidin *et al.*, "Indoor environment propagation review," *Computer Science Review*, vol. 37, p. 100272, 2020.

[7] M. Xiao, S. Mumtaz, Y. Huang, L. Dai, Y. Li, M. Matthaiou, G. K. Karagiannidis, E. Björnson, K. Yang, I. Chih-Lin *et al.*, "Millimeter wave communications for future mobile networks," *IEEE Journal on Selected Areas in Communications*, vol. 35, no. 9, pp. 1909–1935, 2017.

[8] J. Zhang, A. A. Glazunov, W. Yang, and J. Zhang, "Fundamental wireless performance of a building," *IEEE wireless communications*, vol. 29, no. 1, pp. 186–193, 2021.

[9] Y. Zhang, C. Chen, S. Yang, J. Zhang, X. Chu, and J. Zhang, "How friendly are building materials as reflectors to indoor los mimo communications?" *IEEE Internet of Things Journal*, vol. 7, no. 9, pp. 9116–9127, 2020.

[10] Y. Zhou, Y. Shao, J. Zhang, and J. Zhang, "Wireless performance evaluation of building materials integrated with antenna arrays," *IEEE Communications Letters*, vol. 26, no. 4, pp. 942–946, 2022.

[11] E. Björnson, L. Sanguinetti, H. Wymeersch, J. Hoydis, and T. L. Marzetta, "Massive mimo is a reality—what is next?: Five promising research directions for antenna arrays," *Digital Signal Processing*, vol. 94, pp. 3–20, 2019.

[12] E. De Carvalho, A. Ali, A. Amiri, M. Angjelichinoski, and R. W. Heath, "Non-stationarities in extra-large-scale massive mimo," *IEEE Wireless Communications*, vol. 27, no. 4, pp. 74–80, 2020.

[13] A. Asadi, Q. Wang, and V. Mancuso, "A survey on device-to-device communication in cellular networks," *IEEE Communications Surveys & Tutorials*, vol. 16, no. 4, pp. 1801–1819, 2014.

[14] R. I. Ansari, C. Chrysostomou, S. A. Hassan, M. Guizani, S. Mumtaz, J. Rodriguez, and J. J. Rodrigues, "5g d2d networks: Techniques, challenges, and future prospects," *IEEE Systems Journal*, vol. 12, no. 4, pp. 3970–3984, 2017.

[15] P. Gandotra, R. K. Jha, and S. Jain, "A survey on device-to-device (d2d) communication: Architecture and security issues," *Journal of Network and Computer Applications*, vol. 78, pp. 9–29, 2017.

[16] P. Janis, V. Koivunen, C. Ribeiro, J. Korhonen, K. Doppler, and K. Hugl, "Interference-aware resource allocation for device-to-device radio underlaying cellular networks," in *VTC Spring 2009-IEEE 69th Vehicular Technology Conference*, 2009, pp. 1–5.

[17] T. Peng, Q. Lu, H. Wang, S. Xu, and W. Wang, "Interference avoidance mechanisms in the hybrid cellular and device-to-device systems," in *2009 IEEE 20th international symposium on personal, indoor and mobile radio communications*, 2009, pp. 617–621.

[18] R. Zhang, X. Cheng, L. Yang, and B. Jiao, "Interference-aware graph based resource sharing for device-to-device communications underlaying cellular networks," in *2013 IEEE wireless communications and networking conference (WCNC)*, 2013, pp. 140–145.

[19] A. Memmi, Z. Rezki, and M.-S. Alouini, "Power control for d2d underlay cellular networks with channel uncertainty," *IEEE Transactions on Wireless Communications*, vol. 16, no. 2, pp. 1330–1343, 2016.

[20] S. Selmi and R. Bouallegue, "Interference and power management algorithm for d2d communications underlay 5g cellular network," in *2019 International Conference on Wireless and Mobile Computing, Networking and Communications (WiMob)*, 2019, pp. 1–8.

[21] B. Kaufman and B. Aazhang, "Cellular networks with an overlaid device to device network," in *2008 42nd Asilomar conference on signals, systems and computers*, 2008, pp. 1537–1541.

[22] N. Golrezaei, P. Mansourifard, A. F. Molisch, and A. G. Dimakis, "Base-station assisted device-to-device communications for high-throughput wireless video networks," *IEEE Transactions on Wireless Communications*, vol. 13, no. 7, pp. 3665–3676, 2014.

[23] Q. Wang and B. Rengarajan, "Recouping opportunistic gain in dense base station layouts through energy-aware user cooperation," in *2013 IEEE 14th International Symposium on" A World of Wireless, Mobile and Multimedia Networks"(WoWMoM)*, 2013, pp. 1–9.

[24] H. Dou, X. Yu, B. Kang, M. Chen, L. Wang, and B. Zheng, "Robust resource allocation for indoor self-blockage millimeter wave device-to-device communications," *IEEE Open Journal of the Communications Society*, 2022.

[25] S. AG and T. R. Rao, "Sinr based association algorithm for indoor device-to-device communication networks," *Peer-to-Peer Networking and Applications*, vol. 13, no. 6, pp. 1921–1930, 2020.

[26] Y. Orlov, D. Zenyuk, A. K. Samuylov, D. Moltchanov, S. Andreev, O. N. Romashkova, Y. Gaidamaka, and K. E. Samouylov, "Time-dependent sir modeling for d2d communications in indoor deployments." in *ECMS*, 2017, pp. 726–731.

[27] P. Mach and Z. Becvar, "Device-to-device relaying: Optimization, performance perspectives, and open challenges towards 6g networks," *IEEE Communications Surveys & Tutorials*, vol. 24, no. 3, pp. 1336–1393, 2022.

[28] S. Wen, X. Zhu, Y. Lin, Z. Lin, X. Zhang, and D. Yang, "Achievable transmission capacity of relay-assisted device-to-device (d2d) communication underlay cellular networks," in *2013 IEEE 78th vehicular technology conference (VTC Fall)*, 2013, pp. 1–5.

[29] S. Wu, R. Atat, N. Mastronarde, and L. Liu, "Improving the coverage and spectral efficiency of millimeter-wave cellular networks using device-to-device relays," *IEEE Transactions on Communications*, vol. 66, no. 5, pp. 2251–2265, 2017.

[30] D. Singh and S. C. Ghosh, "Network-assisted d2d relay selection under the presence of dynamic obstacles," in *2019 IEEE 44th Conference on Local Computer Networks (LCN)*, 2019, pp. 129–132.

[31] T. L. Marzetta and H. Q. Ngo, *Fundamentals of massive MIMO*. Cambridge University Press, 2016.

[32] E. Björnson, J. Hoydis, L. Sanguinetti *et al.*, "Massive mimo networks: Spectral, energy, and hardware efficiency," *Foundations and Trends® in Signal Processing*, vol. 11, no. 3-4, pp. 154–655, 2017.

[33] T. L. Marzetta, "Noncooperative cellular wireless with unlimited numbers of base station antennas," *IEEE transactions on wireless communications*, vol. 9, no. 11, pp. 3590–3600, 2010.

[34] E. Björnson, J. Hoydis, and L. Sanguinetti, "Massive mimo has unlimited capacity," *IEEE Transactions on Wireless Communications*, vol. 17, no. 1, pp. 574–590, 2017.

[35] X. Gao, F. Tufvesson, and O. Edfors, "Massive mimo channels—measurements and models," in *2013 Asilomar conference on signals, systems and computers*, 2013, pp. 280–284.

[36] À. O. Martínez, E. De Carvalho, and J. Ø. Nielsen, "Towards very large aperture massive mimo: A measurement based study," in *2014 IEEE Globecom Workshops (GC Wkshps)*, 2014, pp. 281–286.

[37] A. Yaghjian, "An overview of near-field antenna measurements," *IEEE Transactions on antennas and propagation*, vol. 34, no. 1, pp. 30–45, 1986.

[38] A. Ali, E. De Carvalho, and R. W. Heath, "Linear receivers in non-stationary massive mimo channels with visibility regions," *IEEE Wireless Communications Letters*, vol. 8, no. 3, pp. 885–888, 2019.

[39] X. Yang, F. Cao, M. Matthaiou, and S. Jin, "On the uplink transmission of extra-large scale massive mimo systems," *IEEE Transactions on Vehicular Technology*, vol. 69, no. 12, pp. 15 229–15 243, 2020.

[40] Y. Han, S. Jin, C.-K. Wen, and X. Ma, "Channel estimation for extremely large-scale massive mimo systems," *IEEE Wireless Communications Letters*, vol. 9, no. 5, pp. 633–637, 2020.

[41] A. Amiri, M. Angjelichinoski, E. De Carvalho, and R. W. Heath, "Extremely large aperture massive mimo: Low complexity receiver architectures," in *2018 IEEE Globecom Workshops (GC Wkshps)*, 2018, pp. 1–6.

[42] J. C. Marinello, T. Abrão, A. Amiri, E. De Carvalho, and P. Popovski, "Antenna selection for improving energy efficiency in xl-mimo systems," *IEEE Transactions on Vehicular Technology*, vol. 69, no. 11, pp. 13 305–13 318, 2020.

[43] H. Obeidat, A. Alabdullah, E. Elkhazmi, W. Suhaib, O. Obeidat, M. Alkhambashi, M. Mosleh, N. Ali, Y. Dama, Z. Abidin *et al.*, "Indoor environment propagation review," *Computer Science Review*, vol. 37, p. 100272, 2020.

[44] S. S. Ghassemzadeh, R. Jana, C. W. Rice, W. Turin, and V. Tarokh, "Measurement and modeling of an ultra-wide bandwidth indoor channel," *IEEE Transactions on Communications*, vol. 52, no. 10, pp. 1786–1796, 2004.

[45] G. Retscher and T. Tatschl, "Indoor positioning using wi-fi lateration—comparison of two common range conversion models with two novel differential approaches," in *2016 Fourth International Conference on Ubiquitous Positioning, Indoor Navigation and Location Based Services (UPINLBS)*, 2016, pp. 1–10.

[46] P. E. Mogensen and J. Wigard, "Cost action 231: Digital mobile radio towards future generation system, final report." in *Section 5.2: On antenna and frequency diversity in GSM. Section 5.3: Capacity study of frequency hopping GSM network*, 1999.

[47] J. Meinilä, P. Kyösti, T. Jämsä, and L. Hentilä, "Winner ii channel models," in *Radio Technologies and Concepts for IMT-Advanced*, 2009.

[48] D. He, B. Ai, K. Guan, L. Wang, Z. Zhong, and T. Kürner, "The design and applications of high-performance ray-tracing simulation platform for 5g and beyond wireless communications: A tutorial," *IEEE Communications Surveys & Tutorials*, vol. 21, no. 1, pp. 10–27, 2018.

[49] K. L. Virga and Y. Rahmat-Samii, "Efficient wide-band evaluation of mobile communications antennas using [z] or [y] matrix interpolation with the method of moments," *IEEE Transactions on Antennas and Propagation*, vol. 47, no. 1, pp. 65–76, 1999.

[50] J. Song, C.-C. Lu, and W. C. Chew, "Multilevel fast multipole algorithm for electromagnetic scattering by large complex objects," *IEEE transactions on antennas and propagation*, vol. 45, no. 10, pp. 1488–1493, 1997.

[51] K. Ito and Y. Hotta, "Signal path loss simulation of human arm for galvanic coupling intra-body communication using circuit and finite element method models," in *2015 IEEE Twelfth International Symposium on Autonomous Decentralized Systems*, 2015, pp. 230–235.

[52] K. S. Kunz and R. J. Luebbers, *The finite difference time domain method for electromagnetics*. CRC press, 1993.

[53] S. Loredo, L. Valle, and R. P. Torres, "Accuracy analysis of go/utd radio-channel modeling in indoor scenarios at 1.8 and 2.5 ghz," *IEEE Antennas and Propagation Magazine*, vol. 43, no. 5, pp. 37–51, 2001.

[54] G. German, Q. Spencer, L. Swindlehurst, and R. Valenzuela, "Wireless indoor channel modeling: statistical agreement of ray tracing simulations and channel sounding measurements," in *2001 IEEE International Conference on Acoustics, Speech, and Signal Processing. Proceedings (Cat. No. 01CH37221)*, vol. 4, 2001, pp. 2501–2504.

[55] E. C. Lai, M. J. Neve, and A. G. Williamson, "Identification of dominant propagation mechanisms around corners in a single-floor office building," in *2008 IEEE Antennas and Propagation Society International Symposium*, 2008, pp. 1–4.

[56] A. O. Kaya, L. J. Greenstein, and W. Trappe, "Characterizing indoor wireless channels via ray tracing combined with stochastic modeling," *IEEE Transactions on Wireless Communications*, vol. 8, no. 8, pp. 4165–4175, 2009.

[57] L. Azpilicueta, F. Falcone, and R. Janaswamy, "A hybrid ray launching-diffusion equation approach for propagation prediction in complex indoor environments," *IEEE Antennas and Wireless Propagation Letters*, vol. 16, pp. 214–217, 2016.

[58] Z. Yun, S. Lim, and M. F. Iskander, "An integrated method of ray tracing and genetic algorithm for optimizing coverage in indoor wireless networks," *IEEE Antennas and Wireless Propagation Letters*, vol. 7, pp. 145–148, 2008.

[59] W. Khawaja, O. Ozdemir, Y. Yapici, I. Guvenc, M. Ezuma, and Y. Kakishimay, "Indoor coverage enhancement for mmwave systems with passive reflectors: Measurements and ray tracing simulations," *arXiv preprint arXiv:1808.06223*, 2018.

[60] C. Chen, J. Zhang, X. Chu, and J. Zhang, "On the optimal base-station height in mmwave small-cell networks considering cylindrical blockage effects," *IEEE Transactions on Vehicular Technology*, vol. 70, no. 9, pp. 9588–9592, 2021.

[61] W. Yang, J. Zhang, and J. Zhang, "On evaluation of indoor to outdoor communications using neighbourhood small cells," *IEEE Transactions on Vehicular Technology*, vol. 69, no. 7, pp. 8045–8050, 2020.

[62] Y. Wang, H. Zheng, C. Chen, and X. Chu, "The effect of wall blockages on indoor small cell networks with los/nlos user association strategies," in *2021 IEEE 93rd Vehicular Technology Conference (VTC2021-Spring)*, 2021, pp. 1–6.

[63] Z. Li, H. Hu, J. Zhang, and J. Zhang, "Impact of wall penetration loss on indoor wireless networks," *IEEE Antennas and Wireless Propagation Letters*, vol. 20, no. 10, pp. 1888–1892, 2021.

[64] M. R. Akdeniz, Y. Liu, M. K. Samimi, S. Sun, S. Rangan, T. S. Rappaport, and E. Erkip, "Millimeter wave channel modeling and cellular capacity evaluation," *IEEE journal on selected areas in communications*, vol. 32, no. 6, pp. 1164–1179, 2014.

[65] H. Zheng, J. Zhang, H. Li, Q. Hong, H. Hu, and J. Zhang, "Exact line-of-sight probability for channel modeling in typical indoor environments," *IEEE Antennas and Wireless Propagation Letters*, vol. 17, no. 7, pp. 1359–1362, 2018.

[66] W. Yang, J. Zhang, and J. Zhang, "Machine learning based indoor line-of-sight probability prediction," in *2019 International Symposium on Antennas and Propagation (ISAP)*, 2019, pp. 1–3.

[67] W. Yang, J. Zhang, A. A. Glazunov, and J. Zhang, "Line-of-sight probability for channel modeling in 3-d indoor environments," *IEEE Antennas and Wireless Propagation Letters*, vol. 19, no. 7, pp. 1182–1186, 2020.

[68] J. Zhang, A. A. Glazunov, and J. Zhang, "Wireless energy efficiency evaluation for buildings under design based on analysis of interference gain," *IEEE transactions on vehicular technology*, vol. 69, no. 6, pp. 6310–6324, 2020.

[69] ——, "Wireless performance evaluation of building layouts: Closed-form computation of figures of merit," *IEEE Transactions on Communications*, vol. 69, no. 7, pp. 4890–4906, 2021.

[70] W. Yang, J. Zhang, H. Song, and J. Zhang, "Partition-based analytic evaluation of building wireless performance," *IEEE Transactions on Vehicular Technology*, vol. 70, no. 9, pp. 9036–9049, 2021.

[71] Y. Zhang, J. Zhang, X. Chu, and J. Zhang, "Lower-bound capacity-based wireless friendliness evaluation for walls as reflectors," *IEEE Transactions on Broadcasting*, vol. 67, no. 4, pp. 917–924, 2021.

[72] I. O. Sanusi, K. M. Nasr, and K. Moessner, "Radio resource management approaches for reliable device-to-device (d2d) communication in wireless industrial applications," *IEEE transactions on cognitive communications and networking*, vol. 7, no. 3, pp. 905–916, 2020.

[73] J. Guo, W. Yu, and J. Yuan, "Enhancing cellular performance through device-to-device distributed mimo," *IEEE Transactions on Communications*, vol. 66, no. 12, pp. 6096–6109, 2018.

[74] M. Hamra and S. Joshi, "Indoor propagation effects in d2d communication: 5g applications and coverage analysis," in *2021 IEEE 94th Vehicular Technology Conference (VTC2021-Fall)*, 2021, pp. 1–5.

[75] X. Ge, S. Tu, G. Mao, C.-X. Wang, and T. Han, "5g ultra-dense cellular networks," *IEEE Wireless Communications*, vol. 23, no. 1, pp. 72–79, 2016.

[76] D. J. MacKay and R. M. Neal, "Near shannon limit performance of low density parity check codes," *Electronics letters*, vol. 33, no. 6, pp. 457–458, 1997.

[77] X. Wang, T. Taleb, Z. Han, S. Xu, and V. C. Leung, "Content-centric collaborative edge caching in 5g mobile internet," *IEEE Wireless Communications*, vol. 25, no. 3, pp. 10–11, 2018.

[78] C. Chen, Y. Zhang, J. Zhang, X. Chu, and J. Zhang, "On the performance of indoor multi-story small-cell networks," *IEEE Transactions on Wireless Communications*, vol. 20, no. 2, pp. 1336–1348, 2020.

[79] G. George, R. K. Mungara, and A. Lozano, "An analytical framework for device-to-device communication in cellular networks," *IEEE Transactions on Wireless Communications*, vol. 14, no. 11, pp. 6297–6310, 2015.

[80] J. Guo, S. Durrani, X. Zhou, and H. Yanikomeroglu, "Device-to-device communication underlaying a finite cellular network region," *IEEE Transactions on Wireless Communications*, vol. 16, no. 1, pp. 332–347, 2016.

[81] M. Mozaffari, W. Saad, M. Bennis, and M. Debbah, "Unmanned aerial vehicle with underlaid device-to-device communications: Performance and tradeoffs," *IEEE Transactions on Wireless Communications*, vol. 15, no. 6, pp. 3949–3963, 2016.

[82] M. Afshang and H. S. Dhillon, "Optimal geographic caching in finite wireless networks," in *2016 IEEE 17th International Workshop on Signal Processing Advances in Wireless Communications (SPAWC)*. IEEE, 2016, pp. 1–5.

[83] Z. Khalid and S. Durrani, "Distance distributions in regular polygons," *IEEE Transactions on Vehicular Technology*, vol. 62, no. 5, pp. 2363–2368, 2013.

[84] F. Tong and J. Pan, "Random distances associated with arbitrary polygons: An algorithmic approach between two random points," *arXiv preprint arXiv:1602.03407*, 2016.

[85] M. Ahmadi and J. Pan, "Random distances associated with arbitrary triangles: A recursive approach with an arbitrary reference point," Tech. Rep., 2013.

[86] S. Srinivasa and M. Haenggi, "Distance distributions in finite uniformly random networks: Theory and applications," *IEEE Transactions on Vehicular Technology*, vol. 59, no. 2, pp. 940–949, 2009.

[87] M. Afshang and H. S. Dhillon, "Fundamentals of modeling finite wireless networks using binomial point process," *IEEE Transactions on Wireless Communications*, vol. 16, no. 5, pp. 3355–3370, 2017.

[88] V. V. Chetlur and H. S. Dhillon, "Downlink coverage analysis for a finite 3-d wireless network of unmanned aerial vehicles," *IEEE Transactions on Communications*, vol. 65, no. 10, pp. 4543–4558, 2017.

[89] J. G. Andrews, F. Baccelli, and R. K. Ganti, "A tractable approach to coverage and rate in cellular networks," *IEEE Transactions on communications*, vol. 59, no. 11, pp. 3122–3134, 2011.

[90] L. Sanguinetti, E. Björnson, and J. Hoydis, "Toward massive mimo 2.0: Understanding spatial correlation, interference suppression, and pilot contamination," *IEEE Transactions on Communications*, vol. 68, no. 1, pp. 232–257, 2019.

[91] G. Gui, M. Liu, F. Tang, N. Kato, and F. Adachi, "6g: Opening new horizons for integration of comfort, security, and intelligence," *IEEE Wireless Communications*, vol. 27, no. 5, pp. 126–132, 2020.

[92] J. G. Andrews, T. Bai, M. N. Kulkarni, A. Alkhateeb, A. K. Gupta, and R. W. Heath, "Modeling and analyzing millimeter wave cellular systems," *IEEE Transactions on Communications*, vol. 65, no. 1, pp. 403–430, 2016.

[93] K. Haneda, L. Tian, H. Asplund, J. Li, Y. Wang, D. Steer, C. Li, T. Balercia, S. Lee, Y. Kim *et al.*, "Indoor 5g 3gpp-like channel models for office and shopping mall environments," in *2016 IEEE international conference on communications workshops (ICC)*, 2016, pp. 694–699.

[94] S. K. Yoo, L. Zhang, S. L. Cotton, H. Q. Ngo, and W. G. Scanlon, "Ceiling-or wall-mounted access points: An experimental evaluation for indoor millimeter wave communications," in *2019 13th European Conference on Antennas and Propagation (EuCAP)*, 2019, pp. 1–5.

[95] M. Gapeyenko, A. Samuylov, M. Gerasimenko, D. Moltchanov, S. Singh, E. Aryafar, S.-p. Yeh, N. Himayat, S. Andreev, and Y. Koucheryavy, "Analysis of human-body blockage in urban millimeter-wave cellular communications," in *2016 IEEE International Conference on Communications (ICC)*, 2016, pp. 1–7.

[96] P. Liu, M. Di Renzo, and A. Springer, "Line-of-sight spatial modulation for indoor mmwave communication at 60 ghz," *IEEE Transactions on Wireless Communications*, vol. 15, no. 11, pp. 7373–7389, 2016.

[97] Y. Zhu, L. Wang, K.-K. Wong, and R. W. Heath, "Secure communications in millimeter wave ad hoc networks," *IEEE Transactions on Wireless Communications*, vol. 16, no. 5, pp. 3205–3217, 2017.

[98] H. T. Friis, "A note on a simple transmission formula," *Proceedings of the IRE*, vol. 34, no. 5, pp. 254–256, 1946.

[99] E. Björnson and L. Sanguinetti, "Power scaling laws and near-field behaviors of massive mimo and intelligent reflecting surfaces," *IEEE Open Journal of the Communications Society*, vol. 1, pp. 1306–1324, 2020.

[100] d. B. Mark, C. Otfried, v. K. Marc, and O. Mark, *Computational geometry algorithms and applications*. Spinger, 2008.

[101] R. L. Graham, "An efficient algorithm for determining the convex hull of a finite planar set," *Info. Pro. Lett.*, vol. 1, pp. 132–133, 1972.

[102] W. F. Eddy, "A new convex hull algorithm for planar sets," *ACM Transactions on Mathematical Software (TOMS)*, vol. 3, no. 4, pp. 398–403, 1977.